INVESTIGATING THE PERFORMANCES OF PHOTOVOLTAIC MODULES/SYSTEMS FOR CENTRAL ANATOLIA USING A THERMAL MODELING APPROACH

A THESIS SUBMITTED TO
THE GRADUATE SCHOOL OF NATURAL AND APPLIED SCIENCES
OF
MIDDLE EAST TECHNICAL UNIVERSITY

BY

BİLGE TUNÇEL

IN PARTIAL FULFILLMENT OF THE REQUIREMENTS
FOR
THE DEGREE OF MASTER OF SCIENCE
IN
PHYSICS

SEPTEMBER 2019

Approval of the thesis:

INVESTIGATING THE PERFORMANCES OF PHOTOVOLTAIC MODULES/SYSTEMS FOR CENTRAL ANATOLIA USING A THERMAL MODELING APPROACH

submitted by **BİLGE TUNÇEL** in partial fulfillment of the requirements for the degree of **Master of Science in Physics Department, Middle East Technical University** by,

Prof. Dr. Halil Kalıpçılar
Dean, Graduate School of **Natural and Applied Sciences** _____

Prof. Dr. Altuğ Özpineci
Head of Department, **Physics** _____

Prof. Dr. Bülent G. Akınoğlu
Supervisor, **Physics, METU** _____

Assoc. Prof. Dr.Robert S. Balog
Co-Supervisor, **Electrical&Computer Eng., Texas A&M Uni.** _____

Examining Committee Members:

Assist. Prof. Dr.Özgür Selimoğlu
Energy Engineering, Ankara University _____

Prof. Dr. Bülent G. Akınoğlu
Physics, METU _____

Assist. Prof. Dr. Selçuk Yerci
Electrical & Electronics Engineering, METU _____

Date: 09.09.2019

I hereby declare that all information in this document has been obtained and presented in accordance with academic rules and ethical conduct. I also declare that, as required by these rules and conduct, I have fully cited and referenced all material and results that are not original to this work.

Name, Surname :Bilge Tunçel

Signature:

ABSTRACT

INVESTIGATING THE PERFORMANCES OF PHOTOVOLTAIC MODULES/SYSTEMS FOR CENTRAL ANATOLIA USING A THERMAL MODELING APPROACH

Tunçel, Bilge
M.Sc., Department of Physics
Supervisor: Prof. Dr. Bülent G. Akınoğlu
Co-Supervisor: Assoc. Prof. Dr. Robert S. Balog

September 2019, 115 pages

Effective use and performance enhancement of the renewable energy systems are becoming increasingly important as climate change is widely recognized as one of the most crucial problems for the Earth. Turkey, a country within the solar belt, has an abundance of solar energy potential. Economical, environmental and physical investigations are needed to ensure effective utilization of this potential. In this thesis, using the meteorological parameters of the Central Anatolia and parameters of photovoltaic (PV) modules, a thermal analysis is carried out. The aim of the thermal analysis is to accurately estimate the temperatures and performances of the modules to be able to determine the feasibility of the solar PV systems

The thermal model uses the geographic location information, PV module/system parameters, and meteorological data including insolation, wind speed and direction, ambient temperature and dew point temperatures as inputs. In this thesis, the transient behavior of the weather along with wind direction, which is often neglected in similar studies, are taken into consideration. The model was run for a one-year interval and the results verified against measured outdoor performance data of a photovoltaic (PV) module. The thermal model was shown to accurately estimate hourly electrical output

of the PV module with a root mean square deviation of 3.08 W/m2 and PV module temperature with a root mean square deviation of 2.43ºC.

Keywords: Solar Panels, Thermal Modeling, Module Temperature, Module Performance

ÖZ

FOTOVOLTAİK MODÜLLERİN/SİSTEMLERİN PERFORMANSLARININ İÇ ANADOLU BÖLGESİ İÇİN TERMAL MODELLEME YÖNTEMİYLE ANALİZLERİ

Tunçel, Bilge
Yüksek Lisans, Fizik Bölümü
Tez Danışmanı: Prof. Dr. Bülent. G. Akınoğlu
Ortak Tez Danışmanı: Doç. Dr. Robert S. Balog

Eylül 2019, 115 sayfa

İklim değişikliğinin dünya gündeminde olduğu bu günlerde, alternatif enerji kaynaklarının etkin kullanımı ve veriminin artırılması gittikçe önem kazanmaktadır. Türkiye dünya üzerindeki konumu itibariyle özellikle güneş enerjisinde büyük bir potansiyele sahiptir. Bu potansiyelin en verimli şekilde kullanımı için ülkenin çeşitli bölgelerinde ekonomik, çevresel ve fiziki incelemelerin yapılması gerekmektedir. Bu çalışmada İç Anadolu bölgesinin meteorolojik verileri, modül parametreleri ve modül konum verileri kullanılarak fotovoltaik (FV) panel sistemlerinin termal analizleri gerçekleştirilmiştir. Bu analizlerin amacı FV sistemlerin kurulmasının planlandığı bölgelerde güneş panellerinin sıcaklıklarını ve buna bağlı performanslarını hassas bir şekilde tahmin etmektir.

Termal model, bölgenin konum bilgileri, güneşlenme, rüzgâr hızı ve yönü, çevre sıcaklığı ve çiy noktası sıcaklığı gibi meteorolojik verileri ve FV modül/sistem parametrelerini girdi olarak kullanmaktadır. Bu tezde, meteorolojik verilerin zamana bağlı değişkenliği ve özellikle benzer çalışmalarda sıklıkla ihmal edilen rüzgâr yönü dikkate alınmıştır. Geliştirilen model bir yıllık bir veri setine uygulanmış ve sonuçlar bir FV modülünün gerçek koşul çalışma verileri ile doğrulanmıştır. Termal model,

modül güç üretimini saatlik bazda ortalama 3.08 W/m2‘lik ve modül sıcaklığını ortalama 2.43ºC’lik kök ortalama karesel sapma ile tahmin edebilmiştir.

Anahtar Kelimeler: Güneş Panelleri, Termal Modelleme, Modül Sıcaklığı, Modül Performansı

To the pale blue dot…

ACKNOWLEDGMENTS

First, I would like to express my sincerest thanks and gratitude to my advisor Prof. Dr. Bülent G. Akınoğlu and co-advisor Dr. Robert S. Balog for their invaluable encouragement and patience, immense knowledge and kind guidance.

I also would like to thank Dr. Talat Özden for his support, for enduring my endless questions and answering me always kindly.

I also would like express my thanks to my family, for encouraging me to persevere and having my back no matter what.

Last but not the least, I would like to thank Aslı Gülbike Uluyurt for her support, a friend like family I am blessed to ever meet.

TABLE OF CONTENTS

ABSTRACT v
ÖZ vii
ACKNOWLEDGMENTS x
TABLE OF CONTENTS xi
LIST OF TABLES xiii
LIST OF FIGURES xv
CHAPTERS
1. INTRODUCTION 1
1.1. Solar Energy Utilization Methods 1
1.2. PV Solar Cells 2
1.2.1. Structure and Working Principles 2
1.2.2. Effect of Cell Temperature 4
1.3. Estimating Performance of a PV Solar Cell 5
1.3.1. Previous Studies 6
1.3.1.1. Explicit Methods 6
1.3.1.2. Implicit Methods 7
1.4. Rationale and Outline of the Thesis Study 8
2. THERMAL MODELING OF A PHOTOVOLTAIC MODULE 11
2.1. Heat Transfer Mechanisms 13
2.1.1. Conductive Heat Transfer 14
2.1.2. Convective Heat Transfer 15
2.1.2.1. Natural Convection 18
2.1.2.2. Forced Convection 21
2.1.3. Radiative Heat Transfer 25
2.2. Heat Capacity of the Photovoltaic Module 28
2.3. Electrical Power Yield of Photovoltaic Module 29
3. METHODOLOGY AND IMPLEMENTATION OF THE THERMAL MODEL 35

3.1. Numerical Method 35
3.2. The Data 37
3.2.1. Meteorological Data 39
3.2.2. PV Module Data 45
3.2.3. Mounting Details 45
3.3. The Algorithm 46
3.4. Comparison Method of Estimated and Measured Values 48
4. RESULTS AND DISCUSSION 49
4.1. Results of the Thermal Model in Sample Intervals 49
4.2. Summary of Results of the Thermal Model for 1-Year Data 56
4.3. Possible Reasons for Deviations 59
4.3.1. Roof Surface Temperature 59
4.3.2. Cloud Cover 61
4.3.3. Precipitation 62
4.3.4. Conductive Heat Transfer 62
4.3.5. Module Back Surface Temperature and Cell Temperature 63
4.3.6. Electrical Power Output Correlation 65
4.4. Sensitivity Analysis of the Thermal Model for Heat Capacity of PV Module 66
5. CONCLUSION 69
REFERENCES 71
APPENDICES 79
A. Extended Results 79

LIST OF TABLES

TABLES

Table 1.1: Implicit methods for T_{cell} in literature....8

Table 2.1: Nusselt numbers for natural convection 21

Table 2.2: Nusselt numbers for forced convection 24

Table 2.3: Combination of natural and forced convection....25

Table 2.4: Properties of the PV module layers 28

Table 2.5: Daily averaging of the transmittance-absorbance product of PV module for two typical days in winter and summer 32

Table 3.1: Input data for the thermal module....38

Table 3.2: Wind direction grouping in the thermal model....41

Table 3.3: Sample wind speed and direction data....42

Table 3.4: Wind direction fraction summation at 10 am on April 1st 42

Table 3.5: Wind direction fraction summation at 7 pm on April 1st....42

Table 3.6: Wind direction fraction summation with respect to thermal model wind direction grouping at 7 pm on April 1st....43

Table 3.7:Wind direction fraction summation with respect to thermal model wind direction grouping at 11 am on April 2nd 44

Table 3.8: Wind direction fraction summation with respect to adjusted wind direction grouping at 11 am on April 2nd 44

Table 3.9: Module parameters 45

Table 3.10: Location/Mounting details of the PV module....46

Table 4.1: Selected intervals from 1-year data 49

Table 4.2: MBE and RMSE of module temperature and electrical power output estimations (12 month) 56

LIST OF FIGURES

FIGURES

Figure 1.1:The basic structure of a solar cell 3

Figure 2.1: Schematic representation of the photovoltaic module and heat transfer mechanisms 13

Figure 2.2: Transition to turbulent in the flow over a flat plate 16

Figure 2.3: Characteristics of a fluid flow over an inclined plate in natural convection 19

Figure 2.4: Head on and wake region flow patterns on an inclined plate immersed in a viscous fluid. 22

Figure 2.5: $(\tau\alpha)$ values and regions of the day for calculation of $(\tau\alpha)_{eff}$ for an average day in summer 31

Figure 3.1: PV modules in Outdoor Testing Facility of GÜNAM in Middle East Technical University, Ankara 39

Figure 3.2: Compass rose for wind direction 40

Figure 3.3: Flow chart of the thermal model 47

Figure 4.1: Insolation and electrical output of the PV module on 9-11th and 22-24th of November 50

Figure 4.2: Wind speed and directionon9-11th and 22-24th of November 50

Figure 4.3: Temperatures of the PV module, ambient, dew point and sky on 9-11th and 22-24th of November 51

Figure 4.4: Deviations of module temperature estimations on 9-11th and 22-24th of November 51

Figure 4.5: Electrical output and estimated efficiency of the PV module on 9-11th and 22-24th of November 52

Figure 4.6: Deviations of electrical power output estimations on 9-11th and 22-24th of November 52

Figure 4.7: Insolation and electrical output of the PV module on 18-20th of June and 17-19th of August 53

Figure 4.8: Wind speed and direction on 18-20th of June and 17-19th of August 54

Figure 4.9: Temperatures of the PV module, ambient, dew point and sky on 18-20th of June and 17-19th of August 54

Figure 4.10: Deviations of module temperature estimations on 18-20th of June and 17-19th of August 55

Figure 4.11: Electrical output and estimated efficiency of the PV module on 18-20th of June and 17-19th of August 55

Figure 4.12: Deviations of electrical power output estimations on 18-20th of June and 17-19th of August 56

Figure 4.13: MBE and RMSE of module temperature for 12 months 57

Figure 4.14: MBE and RMSE of module electrical power output for 12 months 58

Figure 4.15: MBE and RMSE of module temperature during daytime hours for 12 months 58

Figure 4.16: MBE and RMSE of module temperature during nighttime hours for 12 months 58

Figure 4.17: Rate of convective and radiative heat transfer from PV module surface on 18-20th of June and 17-19th of August 59

Figure 4.18: Roof, ambient, estimated and measured module temperatures for two clear sky days in June with roof temperature adjustment 60

Figure 4.19: Comparison of module temperature deviations with and without roof temperature adjustment 61

Figure 4.20: Verification of energy balance in the control volume of the PV module 63

Figure 4.21: RMSE and MBE of electrical output deviations calculated using estimated T_{mod} and T_{cell}. 64

Figure 4.22: Electrical power output calculation with measured and estimated module temperature.....65

Figure 4.23: Daytime module temperature calculation with measured and estimated electrical power output.....66

Figure 4.24: Heat capacity sensitivity of the electrical power output and module temperature estimations in April.....67

CHAPTER 1

INTRODUCTION

A secure supply of clean energy is one of the most urgent problems of the world. Fossil fuels are still main source for energy demand; and their impact on the climate is undeniable. Due to greenhouse effect created by increasing amount of CO_2 in the atmosphere, average temperature of the Earth is rising [1]. Increasing sea levels [2], extreme weather conditions [3] and shifting precipitation patterns [4] are only some of outcomes of global warming. Consumption of fossil fuels and the industry are responsible for 90% of human based CO_2 emissions [5] and 81% of the energy demand of the world is supplied by fossil fuels today [6]. For sustainable development and mitigation of climate change, this value should fall to 60% by 2040 [6]. Renewable energy resources are the solution for sustainability and they will have a crucial role in achieving this goal. Solar energy has a special position among the various types of renewable energy. It is freely available around all over the world; and solar energy can be utilized residentially with simple roof-top applications as well as utility scale electricity production in solar photovoltaic (PV) farms with installed capacities reaching gigawatts (GW). At the end of 2018, the total installed capacity of solar energy in the World reached above 485 GW, almost 100 times larger than the total PV installed capacity of Turkey. The installed capacity of solar PV power plants in Turkey is now over 5 GW [7].

1.1. Solar Energy Utilization Methods

There are two distinct ways to convert solar energy into useful energy forms. One of them is thermal conversion of solar energy. It is the older method, simpler and well-studied. The incoming solar energy flux is converted into heat via a thermal absorber

which in a simple form can be coated/painted copper, aluminum or polymer plate with tubes welded to the back surface [8], [9]. Heat is then transferred to a fluid. This method is mainly used for domestic hot water supply, which is very common especially at the south part of Turkey. There are industrial applications as well, though not as common; and there are very few prototypes in Turkey. In these applications thermal energy is converted into mechanical energy which is then it is used to produce electricity by a rotating generator. They can be concentrated systems [10]–[12] or composed of flat plate collectors [13]. A second method of solar energy conversion is photovoltaic conversion, which is the direct conversion of solar energy into electricity without an intermediary mechanical or thermal cycle. PV devices are made up of semiconductor materials that have band-gap energy values corresponding to the photon energies of incoming solar radiation. Silicon is the most commonly used semiconductor material in the photovoltaic cells commercially, above %90 of the market is dominated by wafer based Si solar cells [14]. There are researches on materials that can be alternative to silicon and have larger conversion efficiencies like GaAs [15], or different new materials like perovskite [16], [17], organic [18], [19], dye sensitized [20], [21] and quantum dot [22]–[24] solar cells.

There are also hybrid systems that combine thermal conversion and photovoltaic conversion. These are called thermal/photovoltaic (T/PV) systems [25], [26]. Excess heat is removed from photovoltaic cell by a cooling working fluid, and as a result hot water is produced as well as electricity.

1.2. PV Solar Cells

1.2.1. Structure and Working Principles

A PV solar cell is basically a simple p-n junction diode. An intrinsic semiconductor is doped with impurities to create n-type and p-type extrinsic semiconductor, which are used to create a p-n junction. In an n-type semiconductor, the majority carriers are free electrons (e^-) with localized holes (h^+). In the p-type semiconductor, the majority carriers are h^+s with localized e^-s. When a p-n junction is formed, fixed charges will attract the free carriers and a depletion region will be generated in the junction along

with a built in electric field. For a Si solar cell, phosphorous and boron are used as impurities to produce n-type and p-type Si, respectively.

The principal mechanism of photovoltaic conversion in a solar cell is as follows: Incoming solar irradiation falls upon the solar cell; and the photons absorbed by the bulk of the semiconductor material excites electrons from valance band to conduction band and create free electron-hole pairs. These charge carriers extracted within the semiconductor with the aid of built in electric field of the p-n junction as it is shown in the Figure 1.1.The charge carries are then collected by metal contacts placed on the two sides of the cell and a current drawn from the PV cell to any load.

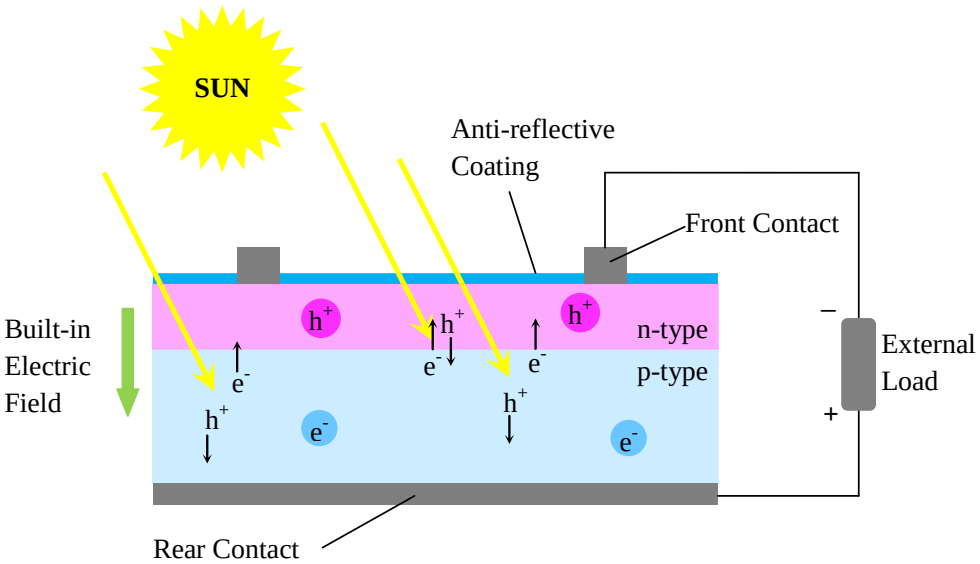

Figure 1.1:The basic structure of a solar cell

Unfortunately, not all of the photons coming from the sun are harvested in PV solar cells. The basic reason is that the band gap of the semiconductor does not allow photons below specific levels of energy to create free carriers. This level corresponds to roughly beginning of the near-infrared (NIR) range for Si cells, Si having band-gap of 1.11 eV at 300°K. The photovoltaic cells are usually designed to absorb visible (VI) and ultraviolet (UV) range of the solar spectrum since the solar spectrum has higher flux in VI leading to creation of more carrier pairs. However, not all of the absorbed photons can be collected as carriers. This is represented by internal quantum efficiency

(IQE) of a solar cell, which is the ratio of collected e^- over absorbed photons. It is a highly wavelength dependent value. While IQE is close to 100% in most of the VI and allowed NIR region for a Si solar cell, UV and violet-blue parts of the VI range has significantly lower IQE [27], meaning carriers created by photons in these ranges less likely to be collected. When a carrier is not collected, its energy is dissipated throughout the solar cell as heat via thermalization. Thermalization of the carriers that have excess energy prior to collection contributes to the heating as well, increasing the temperature of the solar cell.

1.2.2. Effect of Cell Temperature

It is a well-known fact that increasing temperature of the PV cells will cause a decrease in the efficiency, regardless of the type of semiconductor that the cell is made of [28], [29]. In order to understand the reasons, thermal behavior of solar cell parameters like short-circuit current (I_{SC}) and open-circuit voltage (V_{OC}) should be examined. The relationship between I_{SC} and V_{OC} can be expressed as:

$$I_{SC} = I_0 \left(e^{qV_{OC}/kT} - 1 \right) \quad (1)$$

where I_0 is diode saturation current, q is the charge of an electron and k is the Boltzmann coefficient. Saturation current I_0 is defined as following:

$$I_0 = A \cdot T^{\gamma} \cdot e^{-E_{g0}/kT} \quad (2)$$

where E_{g0} band gap of the semiconductor comprising the diode at zero temperature calculated with linear interpolation and γ is the coefficient representing temperature dependence of I_0. Its value is between 1 and 4 in general. A is a parameter depending type of the semiconductor [30] and independent of temperature [31].

Elevated solar cell temperatures will narrow the band-gap of the semiconductor slightly, increasing the number of photons absorbed. Therefore, a small increase in the I_{SC} is observed due to absorption improvement. The temperature dependence of V_{OC} is more complicated. At the first glance it seems that V_{OC} should be increased as well

due to increased photon absorption, hence carrier concentrations. But in fact, V_{OC} is considerably reduced with increasing temperature.

To demonstrate reduction in V_{OC}, equation (2) is plugged into equation (1); and after the negative term is neglected because it is small, the equation is differentiated with respect to temperature, resulting in:

$$\frac{dI_{SC}}{dT} = A \cdot \gamma \cdot T^{\gamma-1} \cdot e^{q(V_{OC}-V_{g0})/kT} + A \cdot T^{\gamma} \cdot \left(\frac{q}{kT}\right) \cdot \left[\frac{dV_{OC}}{dT} - \left(\frac{V_{OC}-V_{g0}}{T}\right)\right] \cdot e^{q(V_{OC}-V_{g0})/kT} \quad (3)$$

where V_{g0} is defined as E_{g0}/q. Change in I_{SC} with temperature increase is negligible compared to other terms. Therefore, left hand side of the equation is assumed to be zero. Simplifying the equation further results in the following equation, which depicts approximately linear drop with rising temperature for V_{OC} [31].

$$\frac{dV_{OC}}{dT} = -\frac{V_{g0} - V_{OC} + \gamma(kT/q)}{T} \quad (4)$$

While the decrease in V_{OC} depends on design of the solar cell for Silicon, it is calculated to be around 0.4% per K [31]. V_{OC} decline dominates over I_{SC} increase; and conversion efficiency of solar cell is affected negatively with elevated cell temperatures.

1.3. Estimating Performance of a PV Solar Cell

Performance of a solar cell is represented with its conversion efficiency. Researchers and manufacturers measure the efficiency under standard testing conditions (STC), which are 1000 W/m^2 of irradiation, 25°C of cell temperature and 1.5 AM (air-mass). However, these conditions are rarely met on the field where stand-alone or utility scale PV systems are installed. Cell temperatures in real circumstances can reach much higher temperatures than 25°C [32]. Since it is established that efficiency of a solar cell strongly depends on the temperature, performance prediction methods must account for cell temperature of PV modules.

1.3.1. Previous Studies

There are large number of equations that correlate electrical power output or efficiency of a solar cell with cell temperature. In [33], [34] Skoplaki and Dubey give an extensive reviews on such correlations for different configurations of PV systems. These equations mainly involve parameters like incoming irradiation, temperature coefficient, cell temperature, reference efficiency under STC (25°C), ambient temperature, transmittance-absorbance product of the module, nominal operation cell temperature (NOCT) (open circuit cell temperature under 800 W/m^2 irradiation, 20°C air temperature, 1 m/s wind speed with open back-side mounting) and other dimensionless correction coefficients. Cell temperature, T_{cell} is one of the most crucial parts in performance predictions for PV modules as its effect on the efficiency is described in Section 1.2.2. Indeed, among aforementioned parameters, T_{cell} is the parameter inserted in many formulations listed in the references.

Reflecting the importance of T_{cell} in performance analyses, there are many equations regarding estimation of PV panel temperature. In a broad way, they can be investigated in two categories: explicit and implicit methods [35].

1.3.1.1. Explicit Methods

Explicit methods involve parameters independent of T_{cell}. They are usually simple and the solution is very straightforward. Explicit methods use empirical means to find coefficients for the variables that the T_{cell} equation contains. In literature, many equations are published with different degrees of complexity.

The simplest way to estimate cell temperature is to link it with ambient temperature, T_{amb} and insolation [36], [37]. NOCT is another parameter used in the T_{cell} correlations. In ref [38] T_{cell} is correlated with T_{amb}, insolation and NOCT of the PV module. Wind is also an important factor; and it is reflected in most explicit equations as average wind speed. Correlations that use wind speed besides T_{amb} and insolation can be found in [39]–[45]. Another study estimates T_{cell} using V_{OC} - I_{SC} values when the cell is in thermal equilibrium for PV modules in an array [46].

There are explicit equations based on the energy balance of the panel, instead of purely empirical models. However, they estimate the terms in the energy balance equation independent of the cell temperature. Most commonly, these estimated terms are electrical output of the cell and heat loss to the environment. Especially, heat loss coefficient, U is hard to predict; and studies involve correlating coefficients for U value for least deviation in cell temperature predictions [47], [48].

Since explicit methods are most commonly based on on-site PV panel experiments, they are location specific equations and do not perform well when the conditions are different from that of the experimental site. Hence, it is also possible to find studies implementing explicit correlations to multiple sites, comparing the results [49]–[51] and modifying the coefficients according to on-site experimental data [52].

1.3.1.2. Implicit Methods

On the other hand, implicit methods contain variables that are functions of T_{cell}. They give more general results than explicit methods, having the flexibility to accommodate parameters of different installing sites without experimental studies. Implicit methods adopt energy conservation law, namely thermal modeling. They process the meteorological data with heat transfer equations that depend on cell/module temperature; and the governing equation is usually complex and require an iterative approach to solve.

Even though the main principle is the same, thermal modeling is applied with various combinations of assumptions in literature. Most distinct one is steady state assumption of PV module under atmospheric conditions. Some of the heat transfer mechanisms can be also neglected in thermal models. Table 1.1 lists the studies found in the literature with their main assumptions used in their methodologies.

It is possible to find comparative studies between implicit and explicit models. [35] presents an extensive review in T_{cell} correlations, both explicit and implicit methods. In [70], [71] and [72], a mixture of explicit and implicit models are implemented and verified.

Table 1.1: Implicit methods for T_{cell} in literature

Reference	ASSUMPTIONS				
	Steady State	Conductive Heat Transfer	Convective Heat Transfer		Radiative Heat Transfer
			Natural	Forced	
[53]–[59]	no	yes	yes	yes	yes
[60]	no	yes	no	yes	yes
[61]–[64]	no	no	yes	yes	yes
[65]	yes	yes	no	yes	yes
[66], [67]	yes	yes	yes	yes	yes
[68], [69]	yes	no	yes	yes	yes

1.4. Rationale and Outline of the Thesis Study

Accurate and precise predictions for PV panel performance are crucial in economical, environmental and physical analyses for effective utilization of solar energy. Unfortunately, electrical power production of PV modules strongly depends on the location of the installation and weather conditions; and efficiency and maximum power production values provided in data sheets are often misleading, as the real life conditions are vastly different than testing conditions in which these values are measured. Therefore, there is a need for accurate methods for performance analyses of PV modules in outdoor conditions. Literature offers such methods as they listed in section 1.3.1, but majority of them are location dependent and do not operate well outside of climate conditions of their testing sites. Thermal modeling offers a solution to this location dependency by applying only basic principle of energy conservation while avoiding expenses of installing a testing site to understand the performance of PV module in a specific location.

In this thesis, a location independent thermal model for performance analysis of PV modules under variable weather conditions is developed based on the model presented in [64]. The model uses meteorological parameters (ambient and dew point temperature, wind, irradiation), module parameters that can be found in data sheet of

PV module and location/mounting parameters as inputs. It provides module temperature and electrical power output of the module as outputs. Wind direction, which is often neglected in similar studies, is taken into consideration as well. The thermal model results are verified with the data from an operational PV module under atmospheric conditions in Ankara.

The thesis is organized as follows. The basic principles used, heat transfer mechanisms and other components of the thermal model are explained in CHAPTER 2. Implementation of the thermal model and methodology to solve resulting equation are described in CHAPTER 3. The data used in the model as input and verification of data is discussed in this chapter as well. CHAPTER 4 gives the results of the thermal model and discusses possible reasons for deviations. A sensitivity analysis of the thermal model is performed. Finally, CHAPTER 5 summarizes the work carried out and outlines possible future work.

CHAPTER 2

THERMAL MODELING OF A PHOTOVOLTAIC MODULE

Thermal modeling is based on the first law of thermodynamics, in other words energy conservation. There are two ways a system can be considered. One is a closed system, which represents a fixed amount of matter in space, and it can be also called control mass. And other is an open system, which refers to a fixed volume through which mass may flow. It is also called a control volume. Whether the system is control mass or control volume, a surface determining the boundary of the system needs to be defined.

A photovoltaic (PV) module has a fixed volume and solar cells do not exchange mass with surroundings during operation. In this case, the system can be considered either as closed system with rigid control surface or an open system which no mass flow is present. It is matter of preference; both considerations are applicable. Note that involvement of a controlled cooling system with a fluid introduces mass flow thus definitely making it an open system (control volume). In this study, the PV module is analyzed as a control mass with a control surface surrounding immediate region of only the module itself. The supporting frame on which module is mounted is not included since contact between the module and the frame is very small.

Interaction of closed systems with surrounding can be realized only via heat transfer and work done by or on the system. Therefore, in the most general form the 1st law of thermodynamics can be written as the following for closed systems:

$$U_{final} - U_{initial} = Q - W \tag{5}$$

where U is the total internal energy of the system, Q is rate of heat transferred through the control surface and W is work done by or on the system. In case of PV system, work will be the electrical power produced by the solar cells, and solar power coming from the Sun. Rate of heat exchange with surroundings will be included in the term Q. Writing internal energy using temperature difference between initial and final states and heat capacity, and expanding the other terms, equation (5) becomes:

$$\frac{dT_{mod}}{dt} \cdot C_{mod} = Q_{solar} - W_{elec.} - Q_{loss} \quad (6)$$

where T_{mod} is equal to T_{cell} in K and C_{mod} is heat capacity of the PV module with units J/m^2K. Q_{solar} and Q_{loss} are the heat fluxes, the rate of incident energy from the sun and rate of heat loss to environment, respectively; all with units W/m^2. The term $W_{elec.}$ is the electrical power output of the PV module in W/m^2.

The thermal modeling can be further investigated in two cases; steady state and transient systems. If left hand side of equation (6) equals to zero, the system does not change over time, meaning that it is steady state. However, if it is non-zero, then the system is in a transient state and internal energy of the system is a function of time. Time dependence of solar irradiation and variable nature of weather necessitates transient analysis, which can also be called dynamic analysis. Therefore, transient analysis is adopted in the present study.

In order to simplify the thermal model, the following assumptions are made:

- Temperature of the PV module is uniform across the PV module surface and throughout the module thickness.
- None of the solar flux that falls on the module is transmitted or reflected. Other than the portion converted into electricity; incoming solar flux transforms into heat within the PV module.
- Edge effects in heat transfer mechanisms are neglected as incident radiation on the module is uniform and the module is very thin compared to its surface area.

- All surfaces of PV module are gray (constant emissivity over the range of used spectrum) and integrated optical properties do not depend on the wavelength of the incident radiation. Additionally, for integrated emissivity of the PV module, the surfaces are assumed diffuse as well, that is, independent of direction of radiation emitted by the module.
- Ambient temperature is uniform around the PV module.
- Soiling effect is neglected. Soiling effect is defined as lowered electrical efficiency of solar cells due to air pollution and accumulation of small particles like dirt, dust, and pollen on the surface of the PV module [73].
- Weather conditions like rain or snow, which introduce mass flow to the control into the surface, are neglected.
- All other electrical components of the system such as inverter are assumed to be working at hundred percent efficiency.

In the following sections, each specific term in equation (6) will be discussed in detail.

2.1. Heat Transfer Mechanisms

Q_{loss} term in equation (6) refers to rate of energy exchange with the surroundings via heat transfer mechanisms. These mechanisms are conduction, convection and radiation.

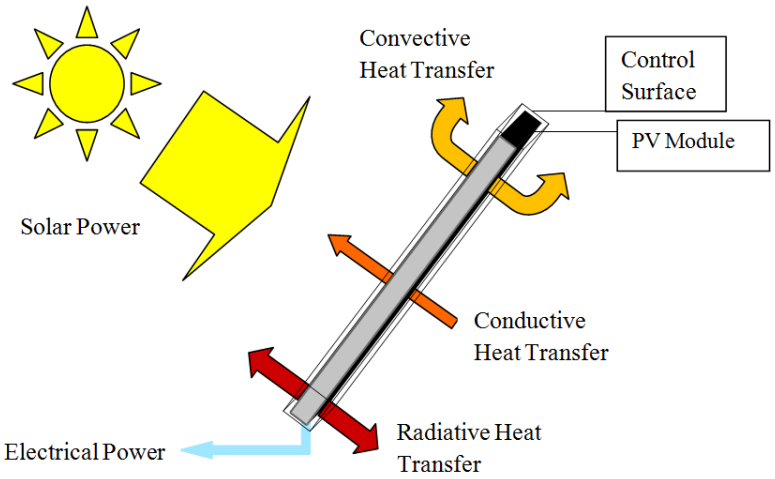

Figure 2.1: Schematic representation of the photovoltaic module and heat transfer mechanisms

Rate of heat loss can then be written as the sum of rate of heat losses of each mechanism:

$$Q_{loss} = Q_{cond.} + Q_{conv.} + Q_{rad.} \quad (7)$$

In Figure 2.1 control surface of the PV module, solar and electrical power, and energy fluxes via heat transfer mechanisms are shown.

2.1.1. Conductive Heat Transfer

Conduction is flow of thermal energy due to temperature gradient in a medium with random motions of the atoms or molecules. This medium can be solid or fluid. Conduction is governed by Fourier's law. For one dimension of the 3D system Fourier's law is written as:

$$q''_x = -k \cdot \frac{dT}{dx} \quad (8)$$

where q''_x is heat flux in the direction of x-axis for unit area perpendicular to direction of transfer, k is thermal conductivity, and dT/dx is the temperature gradient in the x direction.

In the system, conduction occurs from all surfaces of the PV module as well as in the bulk of the material. The module has a rectangular shape with very small depth compared to its other dimensions; with the large surface facing the Sun. Uniform illumination from the sun on the expansive surface of the module and uniformity of outside weather conditions will render conduction parallel to large surface negligible. Moreover, small thickness of the module makes conduction in the direction of depth negligible as well. The supporting frame is in contact with the module and the module also has conductive heat transfer occurring in these regions. But, these are minimal and can be ignored.

Surfaces in contact with air will have conduction also, but conductive effects will be included in convection calculations.

As it was mentioned in the assumptions, temperature of the PV module is assumed to be uniform in accordance with above reasons. When there is no temperature gradient present, conduction will not occur. Therefore, in the thermal model conduction is taken as zero.

$$Q_{cond.} = 0 \tag{9}$$

2.1.2. Convective Heat Transfer

Convection is used to describe the heat transfer between a surface and a fluid flowing over the surface. Convection consists of heat transfer by both the bulk fluid motion (advection) and the random motion of fluid atoms or molecules (conduction via the mobile fluid molecules). Consider a flow over a flat plate; when flow meets the edge of the plate, it slows down significantly and forms a film of fluid which has a different velocity and thermal profile than of free flow as it shown in Figure 2.2. This film which develops over any surface immersed in a fluid flow is called boundary layer. The thermophysical properties of the boundary layer are calculated at film temperature, which is assumed as average temperature of the surface and fluid:

$$T_{film} = \frac{(T_s + T_\infty)}{2} \tag{10}$$

Convective heat transfer strongly depends on properties and behavior of the boundary layer as it will be discussed in the following sections.

Newton's law of cooling gives a general expression of convective heat transfer. For any surface rate of convective heat loss, it can be expressed as:

$$Q_{conv.} = h \cdot (T_s - T_\infty) \tag{11}$$

where h is convective heat transfer coefficient with units W/m^2K, T_s and T_∞ are the temperatures of the surface and the free stream in K, respectively. The objective in convective heat transfer problems is estimating heat transfer coefficient, h for the corresponding surface. Geometry, temperature and texture of the surface, velocity and thermophysical properties of the fluid are the factors affecting h.

In analysis of the boundary layer, several dimensionless parameters emerge. One of them is Reynolds number (Re), and for a semi-infinite plate as in the Figure 2.2, it is defined as:

$$Re_x = \frac{\rho \cdot u_\infty \cdot x}{\mu} \tag{12}$$

where ρ, u_∞, μ are density, free stream velocity and viscosity of the fluid, and x is the characteristic length which is taken as the distance from the leading edge for semi-infinite flat plate. Reynolds number is a ratio of inertial forces to viscous forces within the flow. When inertial forces overcome the viscous ones, a dramatic change occurs in the behavior of the boundary layer. As it can be seen in Figure 2.2, initially when flow meets the edge of the plate, the flow is very orderly because of viscous forces, and fluid particles follow easily identifiable paths along the flow. This flow condition is called laminar flow. When inertial forces begin to dominate, a transition occurs, and orderly behavior of the flow is disrupted by relatively random and highly irregular movement of fluid pockets. This chaotic flow condition is called turbulent. The representation of fluid behavior on these conditions can be seen in the Figure 2.2.

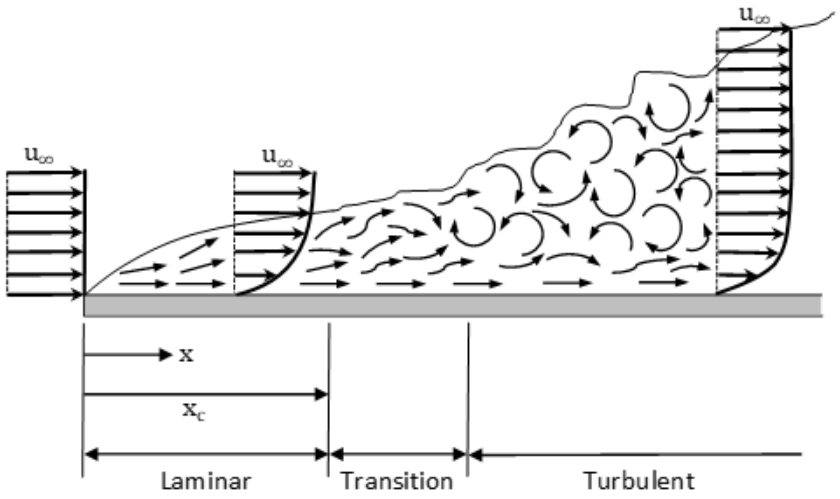

Figure 2.2: Transition to turbulent in the flow over a flat plate

Reynolds number is the dimensionless parameter identifying where this transition occurs. Rate of heat losses from laminar and turbulent flows are vastly different due

to movement characteristics of fluid particles, and when estimating h, it must be considered.

Grashof number is analogous to Reynolds number in which the inertial forces are replaced with buoyancy forces, which become effective when there is no external flow forced upon the surface. It can be said that Grashof number is a ratio of buoyancy forces to viscous forces, and for vertical flat plate, it is defined as:

$$Gr_x \equiv \frac{g \cdot \beta \cdot (T_s - T_\infty) \cdot x^3}{\upsilon^2} \tag{13}$$

where g is the gravitational constant, β (volumetric coefficient of expansion) which can be taken as $1/(T_s + T_\infty)$,and υ is kinematic viscosity of the fluid.

One of the most important parameters in heat transfer is Nusselt number (Nu). It is defined as the following:

$$Nu_x \equiv \frac{h \cdot x}{k} \tag{14}$$

where k is thermal conductivity of the fluid. Nusselt number is a measure of how much convective heat transfer is occurring at the surface with respect to conductive mechanism. That is, it is ratio of convection to conduction heat transfer occurring for a fluid at the same conditions. In the procedure of solving a heat transfer problem, we first calculate Nusselt number, and then find h. From h, rate of heat transferred from the surface can be calculated.

Until now, all definitions are done for a semi-infinite flat plate, defining the characteristic length as the distance from the leading edge of the plate. Characteristic length is a dimension specific to a geometry and flow combination. It is used to determine dimensionless parameters some of which mentioned above in fluid dynamics and heat transfer problems. For instance, the characteristic length of a rectangular plate is the length of the side along which the fluid flows, and for a pipe it is the diameter. In order to find Re, Gr and Nu numbers, x is replaced with the characteristic length determined for the geometry. Photovoltaic modules are often

rectangular shaped as the module used in this study. In this case, characteristic length of the PV module is defined as:

$$L = \frac{\text{area}}{\text{perimeter}} \tag{15}$$

The PV module considered is installed with an inclination angle. Therefore, the thermal modeling accepts the PV module as an inclined rectangular plate immersed in a fluid and proceeds accordingly.

As it was mentioned above two kinds of basic convection modes exist: Natural convection (buoyancy driven) and forced convection (external-flow driven). Due to diversity of the flow climatological conditions, both mechanisms will be considered in the model.

2.1.2.1. Natural Convection

Natural convection is the mode of heat transport occurring when a heated or cooled surface is immersed in a stagnant fluid under gravity. As the surface begins to change the temperature of the fluid in contact with, the density of the fluid will change as well. When buoyancy forces overcome viscous forces, the fluid will begin to move upwards if the surface is hotter or downwards if the surface is colder than the fluid away from surface. This motion causing convective heat transfer between the surface and the fluid is called natural convection. This mode of convection does not require an external flow; it arises naturally in circumstances when there is a temperature difference between a fluid and a surface.

The orientation of the surface is crucial. It determines characteristics of the boundary layer and how fluid behaves around the surface, affecting rate of heat transfer considerably. Therefore, first consideration should be how the surface is positioned with respect to direction of gravity: PV module is an inclined rectangular plate which has an inclination angle β with the floor, corresponding to an angle of $\theta = 90-\beta$ with the vertical. Since the geometry of the PV module, inclined plane of the module is

asymmetric about the direction of gravity, the top and bottom surfaces have different flow characteristics as shown in the Figure 2.3.

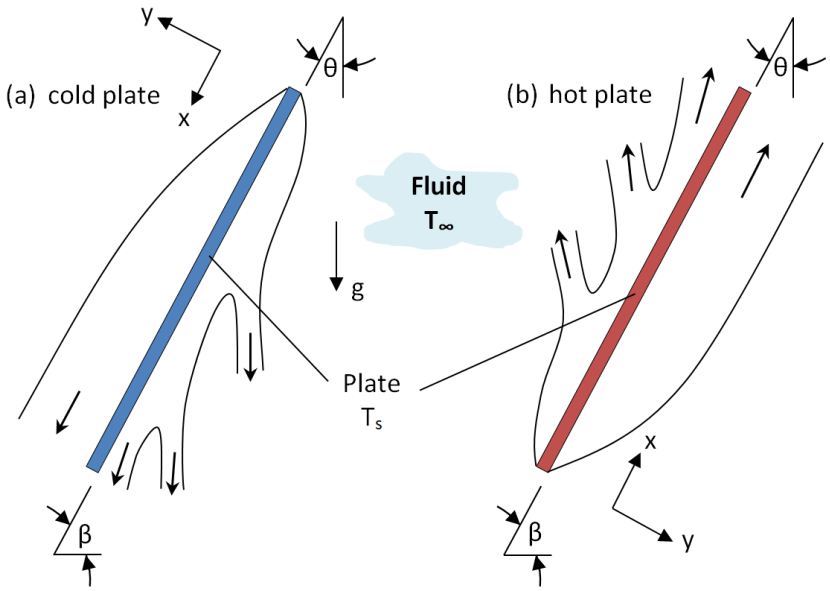

Figure 2.3: Characteristics of a fluid flow over an inclined plate in natural convection

In natural convection, it is possible to make a classification about temperature of the surface with respect to fluid temperature as hot plate and cold plate. Consider the hot plate case, which is usually the case during daytime for a PV module, fluid will begin to rise and move along the surface of the module. Due to viscous forces it will be laminar at first; then buoyancy forces will turn flow to turbulent. Analogous to Reynolds number, natural convection has Rayleigh number, indicating the point the flow becomes turbulent. It is defined as product of Grashof and Prandl number. For inclined plates, gravitational constant is multiplied with cosine of the inclination angle θ that the plate makes with the vertical (90-β), and thus the Rayleigh number can be written as;

$$Ra_x \equiv Gr_x \cdot Pr = \frac{g \cdot \beta \cdot (T_s - T_\infty) \cdot \cos\theta \cdot x^3}{\alpha \cdot \upsilon} \qquad (16)$$

where Pr is Prandl Number and α is thermal diffusivity of the fluid..

Critical Rayleigh number is 10^9 for vertical plates in both surfaces due to symmetry with respect to the direction of gravitational constant. But in the case of inclined plate, symmetry is lost, and flow features of top and bottom surfaces will differ. For a hot plate, bottom part will have a flow similar to vertical plate case while on the top surface the flow will be separated from the plate earlier since gravity will force heated liquid upward. Hence, critical Rayleigh number will be smaller, and this surface will have narrower laminar region compared to bottom surface. For cold plate case reverse is true. Bottom plate will have early flow separation and smaller critical Rayleigh number. This difference in flow will introduce differences in heat transfer mechanisms.

Analytical solution is possible for Nusselt number in laminar regions. If flows remain laminar average Nusselt number for inclined plates can be calculated from:

$$\overline{\mathrm{Nu_x}} = 0.68 + \frac{0.67 \cdot \mathrm{Ra_x^{1/4}}}{\left[1 + \left({}^{0.492}/_{\mathrm{Pr}}\right)^{9/16}\right]^{4/9}} \tag{17}$$

Turbulent regions don't have analytic solutions. However, there are correlations that estimate Nusselt number effectively. For a region that has both laminar and turbulent flows together Nusselt number can be estimated from:

$$\overline{\mathrm{Nu_x}} = \left\{0.85 + \frac{0.387 \cdot \mathrm{Ra_x^{1/6}}}{\left[1 + \left({}^{0.492}/_{\mathrm{Pr}}\right)^{9/16}\right]^{8/27}}\right\}^2 \tag{18}$$

This correlation can be used for vertical plates, bottom surface of hot and top surface of cold plate. As the early flow separation changes flow characteristics, another correlation for Nusselt number is used for top and bottom surface of hot and cold plates as:

$$\overline{\mathrm{Nu_x}} = 0.13 \cdot \left[\left(\frac{\mathrm{Ra_x}}{\cos\theta}\right)^{1/3} - \mathrm{Ra_c^{1/3}}\right] + 0.56 \cdot (\mathrm{Ra_c} \cdot \cos\theta)^{1/4} \tag{19}$$

where, Ra_c is the critical Rayleigh number of the plate making an angle θ with the vertical. The value of the Ra_c depends on the inclination angle and for θ = 60°, critical Rayleigh number is 10^6 [74].

Note that the correlation is used after Rayleigh number exceeds 10^6, where after transition occurs. If the critical Rayleigh number remains below critical value, flow is laminar and equation (17)will be used for Nusselt Number.

These formulae cover all possible flow conditions in natural convection in an inclined plate. Table 2.1 sums the Nusselt numbers for natural convection with validity intervals, references and in which case they are used.

Table 2.1: Nusselt numbers for natural convection

HOT PLATE

Top surface		Bottom Surface		
Equation	Reference	Equation	Reference	Validity Interval
(17)	[75]	(17)	[75]	$\mathrm{Ra_L} < \mathrm{Ra_c}$
(19)	[74]	(17)	[75]	$\mathrm{Ra_c} < Ra_\mathrm{L} < 10^9$
(19)	[74]	(18)	[75]	$\mathrm{Ra_L} < 10^9$

COLD PLATE

Top surface		Bottom Surface		
Equation	Reference	Equation	Reference	Validity Interval
(17)	[75]	(17)	[75]	$\mathrm{Ra_L} < \mathrm{Ra_c}$
(17)	[75]	(19)	[74]	$\mathrm{Ra_c} < Ra_\mathrm{L} < 10^9$
(18)	[75]	(19)	[74]	$\mathrm{Ra_L} < 10^9$

2.1.2.2. Forced Convection

Forced convection occurs when an external driving force modifies the fluid motion. Inertial forces move the fluid against viscous forces; and boundary layer, laminar and

turbulent regions develop over the surface. Analogous to Rayleigh number, where the transition occurs is identified by Reynolds Number. It is a measure of inertial forces to viscous forces and defined as

$$Re_x = \frac{\rho \cdot v_\infty \cdot x}{\mu} \tag{20}$$

Like natural convection, characteristic of the flow is a major factor effecting rate of heat transfer. Three distinct regions are identified regarding the flow on an inclined plate in external flow field; parallel, head-on and wake flow regions. Occurrence of these regions depends on the orientation of the inclined plate with respect to external flow field direction.

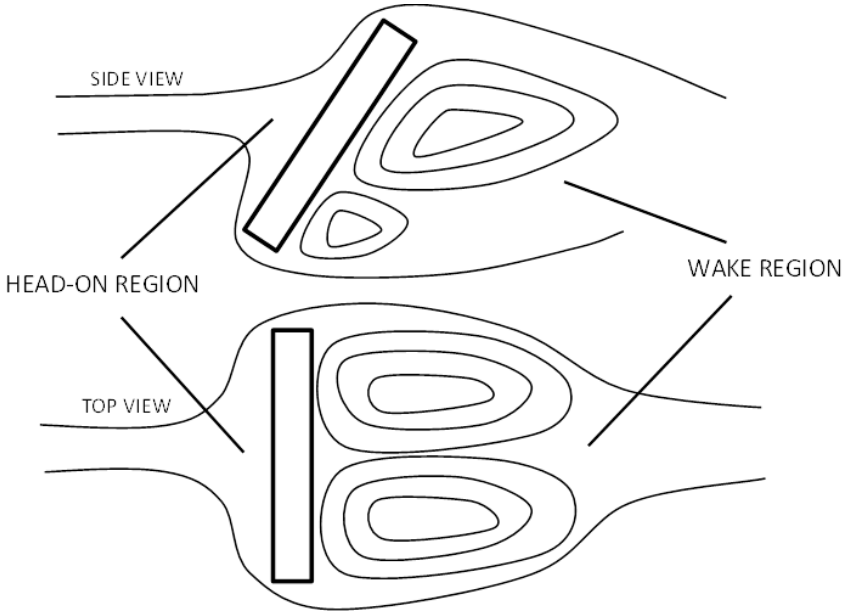

Figure 2.4: Head on and wake region flow patterns on an inclined plate immersed in a viscous fluid.

Wake and head on regions ensue when the positioning of the plate is as seen in the Figure 2.4; the plate acts like a blunt object. Front surface of the plate will have head on region and back will have wake region. Typical characterization of laminar and turbulent flow will not be applicable in wake region since flow separation will occur, and the flow will be turbulent inherently. For head on region, flow characteristics highly depend on the inclination angle. For both of these regions, Nusselt numbers are

estimated. For a south-facing module, if wind blows from southern direction, regardless of the yaw angle, Nusselt number for head on region which corresponds to top surface is estimated as

$$\overline{\mathrm{Nu_x}} = 0.931 \cdot \frac{(\mathrm{v_\infty}.\upsilon \cdot \mathrm{x})^{1/2} \cdot \rho \cdot \mathrm{c_p}}{\mathrm{k} \cdot \mathrm{Pr}^{2/3}} \tag{21}$$

where v_∞ is the speed ρ is the density, υ is kinematic viscosity and of the external flow, and for wake region which corresponds to bottom surface, Nusselt number is estimated as

$$\overline{\mathrm{Nu_x}} = 0.191 \cdot \mathrm{Re_x^{2/3}} \cdot \mathrm{Pr}^{1/3} \tag{22}$$

If the wind blows from northern direction, reverse will be true.

Parallel flow region is observed when the wind direction is edgewise to the plate, in case of a south facing module direction being east or west. Flow characteristics will be very similar to that of the natural convection. Transition to turbulent from laminar is identified by Reynolds Number. The critical value is 5×10^5. In case of laminar flow, analytical solution is possible and Nusselt number is calculated as:

$$\overline{\mathrm{Nu_x}} = 0.664 \cdot \mathrm{Re_x^{1/2}} \cdot \mathrm{Pr}^{1/3} \tag{23}$$

If the flow turns turbulent, Nusselt number is estimated as:

$$\overline{\mathrm{Nu_x}} = \left(0.037 \cdot \mathrm{Re_x^{4/5}} - 871\right) \cdot \mathrm{Pr}^{1/3} \tag{24}$$

For both surfaces, heat transfer characteristics will be the same due to symmetry.

Table 2.2shows all possible cases regarding the wind direction and speed for a south facing PV module and summarizes Nusselt numbers with validity intervals and references.

Usually, when both natural and forced convection is present in a heat transfer problem, one of the mechanisms dominates, and the other is neglected. But in the problem of

Table 2.2: Nusselt numbers for forced convection

	Equation	Reference	Validity Interval
SOUTHERN WIND DIRECTION			
Top surface	(21)	[76]	$2 \cdot 10^4 < Re_L < 1 \cdot 10^5$
Bottom Surface	(22)		$7 \cdot 10^3 < Re_L < 8 \cdot 10^4$
EAST-WEST WIND DIRECTION			
Top surface	(23)	[75]	$Re_L < 5 \cdot 10^5$
	(24)	[75]	$Re_L > 5 \cdot 10^5$
Bottom Surface	(23)	[75]	$Re_L < 5 \cdot 10^5$
	(24)	[75]	$Re_L > 5 \cdot 10^5$
NORTHERN WIND DIRECTION			
Top surface	(22)	[75]	$7 \cdot 10^3 < Re_L < 8 \cdot 10^4$
Bottom Surface	(21)	[76]	$2 \cdot 10^4 < Re_L < 1 \cdot 10^5$

PV panel exposed to the real-time weather conditions, both modes of convection have to be recognized due to erratic nature of the weather. Combination of natural and forced convection is not a simple summation of Nusselt numbers. Depending on the flow directions of both mechanisms, they assist or resist each other. An effective Nusselt number is calculated for both surfaces using:

$$\overline{Nu}_{x_{eff,top/bot}}^{3} = \overline{Nu}_{x_{natural,top/bot}}^{3} \mp \overline{Nu}_{x_{forced,top/bot}}^{3} \quad (25)$$

where the sign depends on whether the flows are assisting or resisting [75]. Table 2.3 shows how the Nusselt numbers are combined for a south facing PV plane, (+) representing assisting flow and (–) representing resisting flow.

After calculation of effective Nusselt numbers for both surfaces, they are summed up to find overall effective Nusselt number for the whole PV module convection heat transfer. Combining equations (11) and (14) with x replaced on the formulae with

characteristic length L defined at equation (15), rate of convective heat transfer from whole system can be written as:

$$Q_{conv.} = \left(\overline{Nu}_{L,eff,top} + \overline{Nu}_{L,eff,bot}\right) \cdot \frac{k}{L}(T_s - T_\infty) \quad (26)$$

Table 2.3: Combination of natural and forced convection

	TOP SURFACE	BOTTOM SURFACE
HOT PLATE		
Southern Wind	+	+
East-West Wind	+	+
Northern Wind	+	−
COLD PLATE		
Southern Wind	−	+
East-West Wind	+	+
Northern Wind	+	+

2.1.3. Radiative Heat Transfer

Radiative heat transfer does not require a media to transfer energy. Heat is dissipated or absorbed as electromagnetic wave. The rate of transferred energy highly depends on the temperature and emissivity of the surface radiating electromagnetic wave. Rate of energy radiated from a blackbody (an ideal object to define the emitting power of heated objects) with temperature T can be calculated by the Stefan-Boltzmann law of blackbody radiation:

$$Q_{rad} = \sigma \cdot T^4 \quad (27)$$

where σ is Stefan-Boltzmann constant. Total radiative energy exchange q_i on a surface i with emissivity of ε_i can be written as

$$q_i = \frac{E_{bi} - J_i}{(1-\varepsilon_i)/\varepsilon_i \cdot A_i} = \sum_{j=1}^{N} A_i \cdot F_{ij} \cdot (J_i - J_j) \quad (28)$$

where J is radiocity, F is the view factor, ε is the emissivity, E_{bi} is blackbody radiation of a surface at T_i and N is the number of the surfaces present. Radiocity J_i is rate of all radiation leaving surface i per unit area including emitted radiation, reflected and transmitted incident radiation. We can write N number of equations for N number of surfaces. Solving for J_i, radiative heat transfer for all surfaces can be found, assuming emissivity, temperature and area of the all surfaces are known.

In the case of PV panel, we have three surfaces: panel top/bottom surface, sky and earth/roof surface. Top surface is assumed to see the sky and earth; and bottom surface is assumed to see sky and roof/floor only. In the radiative heat transfer problems, if the area of one surface is relatively large compared to other surfaces, it can be treated as blackbody. Reasoning is that only an infinitesimal portion of radiation emitted from the small surface will be reflected back to it, which means the large surface will absorb almost all radiation emitted by the small surface, like a blackbody does. We can safely assume areas of sky and earth are infinite, hence they can be assumed as blackbodies. Here, area of the roof is assumed to be large compared to the PV panel, so the roof is assumed as a blackbody as well. Writing equation (28) for the PV panel top surface, we have:

$$\frac{\sigma \cdot T_{mod}^4 - J_{mod}}{(1-\varepsilon_{mod})/(\varepsilon_{mod} \cdot A_{mod})} = \frac{J_{mod} - \sigma \cdot T_{sky}^4}{(A_{mod} \cdot F_{t,sky})^{-1}} + \frac{J_{mod} - \sigma \cdot T_{earth}^4}{(A_{mod} \cdot F_{t,earth})^{-1}} \quad (29)$$

Only unknown in equation(29)is J_{mod}. Solving for J_{mod} and rearranging the equation(28), total rate of radiative heat transfer of the top surface can be found as:

$$Q_{rad} = \sigma \cdot F_{t,sky} \cdot \varepsilon_{mod} \cdot (T_{mod}^4 - T_{sky}^4) + \sigma \cdot F_{t,earth} \cdot \varepsilon_{mod} \cdot (T_{mod}^4 - T_{earth}^4) \quad (30)$$

where view factors are taken as:

$$F_{t,sky} = (1 + \sin\theta)/2 \tag{31}$$

$$F_{t,earth} = (1 - \sin\theta)/2 \tag{32}$$

And for the bottom surface rate of radiative heat transfer becomes

$$Q_{rad} = \sigma \cdot F_{b,sky} \cdot \varepsilon_{mod} \cdot \left(T_{mod}^4 - T_{sky}^4\right) + \sigma \cdot F_{b,roof} \cdot \varepsilon_{mod} \cdot \left(T_{mod}^4 - T_{roof}^4\right) \tag{33}$$

where view factors are taken as:

$$F_{b,sky} = (1 - \sin\theta)/2 \tag{34}$$

$$F_{b,roof} = (1 + \sin\theta)/2 \tag{35}$$

As it can be recognized emissivity values other than the panel become irrelevant since surface of sky, earth and roof are large compared to panel surface and behave like blackbodies. Total rate of radiative heat transferred from the PV panel to the environment can then be written as:

$$Q_{rad} = \sigma \cdot F_{t,sky} \cdot \varepsilon_{mod} \cdot \left(T_{mod}^4 - T_{sky}^4\right) + \sigma \cdot F_{t,earth} \cdot \varepsilon_{mod} \cdot \left(T_{mod}^4 - T_{earth}^4\right) + \sigma \cdot F_{b,sky} \cdot \varepsilon_{mod} \cdot \left(T_{mod}^4 - T_{sky}^4\right) + \sigma \cdot F_{b,roof} \cdot \varepsilon_{mod} \cdot \left(T_{mod}^4 - T_{roof}^4\right) \tag{36}$$

Temperatures of the sky, earth and roof need to be determined for calculation of the radiative heat transfer. Sky temperature is not a measurable value; it is correlated from heat transfer experiments. Sky assumed to be a blackbody at the temperature of T_{sky}. Using ambient temperature, dew point temperature and time, a correlation is derived from the experiments:

$$T_{sky} = T_{amb} \cdot \left[0.711 + 0.0056 \cdot T_{dp} + 0.000073 \cdot T_{dp}^2 + 0.013 \cdot \cos t\right]^{1/4} \tag{37}$$

where T_{amb} is ambient, T_{dp} is dew point temperature and t is the hour of the day [77]. T_{sky} and T_{amb} are in Kelvin T_{dp} is in degrees Celsius.

Temperature of earth depends on amount of the vegetation and land characteristics on the surrounding area [78]. Environment of outdoor testing facility of GÜNAM is populated by trees and green areas with a few buildings. For green urban areas, earth temperature can be estimated as ambient temperature [53], [59], [79]–[81]. Roof temperature is a lot harder to determine. It depends on the time, insolation and material of the roof. Here, it will be assumed as ambient temperature like earth temperature [54].

2.2. Heat Capacity of the Photovoltaic Module

Dynamic analysis of the control volume requires heat capacity of the system to determine the response of the control volume to changes in the environmental factors. The most accurate way of determining heat capacity would be to measuring it. However, since there are no studies on this with PV solar panels, heat capacity is estimated using the following formula for n layers of different materials stacked on top of each other [82].

$$C_{mod} = \sum_{n} d_n \cdot c_{p_n} \cdot \rho_n \tag{38}$$

where d is thickness, c_p is the specific heat capacity and ρ is the density of the n^{th} layer.

Table 2.4: Properties of the PV module layers

Layers of the PV Module	Thickness d [m]	Specific Heat Capacity c_p [J/kg-K]	Density ρ [kg/m^3]
Glazing (glass)	0.003	500	3000
PV cells (poly-c Si)	0.0003	677	2330
Back sheet (Polyester / Tedlar Trilaminate)	0.0005	1250	1200
Total			5723

A typical PV module is composed of glazing, solar cells and a back sheet. Thin EVA (Ethylene vinyl acetate) films are used between these layers to bond them to each other. In the calculation of heat capacity of the module EVA film layers are neglected and three main layers are considered for C_{mod}. Their properties are given in the Table 2.4 [83].

2.3. Electrical Power Yield of Photovoltaic Module

Electrical power output of PV module is one of the most important part of the thermal model. Power output determines how much energy left in the system to generate heat. Actual electrical power extracted from a PV module is multiplication of voltage and current. However, it is not possible to reach this information without the actual PV module mounted in the specific location. Using this information for calculation will preclude any feasibility analysis without installing a field site. So, it is important to have an estimation of the electrical power output with respect to some other parameters. In literature there are many correlations for power of PV module; most commonly used ones can be found in reference [34]. Using suitable correlation for the module and installation conditions and also verifying it are crucial for the power yield estimations. In this thermal model following correlation is chosen to estimate electrical power output:

$$W_{elec.} = Q_{solar} \cdot (\tau\alpha)_{eff} \cdot \eta_{ref} \cdot [1 - \beta_{ref} \cdot (T_{ref} - T_{mod})] \qquad (39)$$

where $(\tau\alpha)$ is transmittance-absorbance product, β_{ref} is temperature coefficient of the PV module, η_{ref} is electrical conversion efficiency of the PV module under standard testing conditions (STC), whose reference values are 25°C temperature, 1000 W/m^2 irradiation and 1 m/s wind speed. η_{ref} and β_{ref} are provided by the manufacturing company of the module in the data sheet. T_{mod} is the module temperature.

Temperature coefficient, β_{ref} is a measure of efficiency loss of the PV panel under increasing cell temperatures; and this parameter is very important when calculating the electrical power produced by the module.

Effective transmittance-absorbance product, $(\tau\alpha)_{eff}$ of the PV module is a parameter which determines how much solar irradiance is transmitted through the glazing and is absorbed by the PV cells. Usually it is taken as constant with values between 0.9 and 0.80 [47], [84]–[86] in thermal modeling of PV modules. However, $(\tau\alpha)$ in fact strongly depends on the direction of the incident solar radiation. It can be calculated using the following formula [82]:

$$(\tau\alpha) = e^{\left(\frac{-K\cdot L}{\cos\theta_r}\right)} \cdot \left[1 - \frac{1}{2}\cdot\left(\frac{\sin^2(\theta_r - \theta)}{\sin^2(\theta_r + \theta)} + \frac{\tan^2(\theta_r - \theta)}{\tan^2(\theta_r + \theta)}\right)\right] \quad (40)$$

where K and L are extinction coefficient and thickness of the glazing, and θ and θ_r are angles of incidence and refraction, respectively. For a sloped surface the incident angle of Sun beams is calculated using:

$$\begin{aligned}\theta = \cos^{-1}(&\sin\delta\cdot\sin\phi\cdot\cos\beta - \sin\delta\cdot\cos\phi\cdot\sin\beta\cdot\cos\gamma + \cos\delta \\ &\cdot\cos\phi\cdot\cos\beta\cdot\cos\omega + \cos\delta\cdot\sin\phi\cdot\sin\beta\cdot\cos\gamma \\ &\cdot\cos\omega + \cos\delta\cdot\sin\beta\cdot\sin\gamma\cdot\sin\omega)\end{aligned} \quad (41)$$

where δ is declination angle, ϕ is the latitude angle of the location, β is tilt and γ is azimuth angle of the surface. For a south facing surface azimuth angle is zero. ω is the hour angle. Refraction angle is found from Snell's law using incident angle and refraction indexes of the glazing and the air. In the thermal model, refraction index of regular glass is used which has the value of 1.526.

Since incident angle depends on the day of the year and hour of the day, $(\tau\alpha)$ is a highly variable parameter with respect to time. The values of $(\tau\alpha)$ change between 0 and 0.95 for Ankara, with highest $(\tau\alpha)$ values being at noon hours where incident angle of solar radiation is at its smallest. Unfortunately, plugging in equation (40) in equation (39) introduces errors in electrical power output estimations at evening and morning hours.

Figure 2.5 depicts the solar flux and $(\tau\alpha)$ values for an average summer day. There is are deviations in $(\tau\alpha)$ values when it is calculated using equation (40) because it only accounts for the beam radiation.

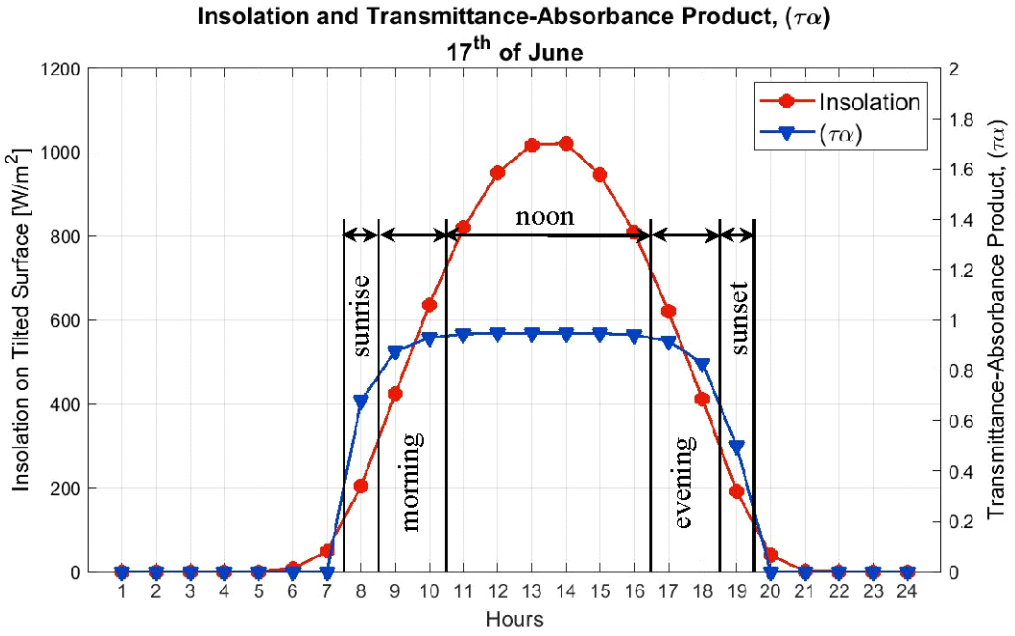

Figure 2.5: (τα) values and regions of the day for calculation of $(\tau\alpha)_{eff}$ for an average day in summer

Moreover, diffuse radiation which is more effective in morning and evening when the incident angle of the sun beams on the surface are large, are not considered in the calculation of (τα). Especially in summer, a south facing surface of the module is in shadow in early morning and late evening even though the Sun is in the sky. In this scenario, (τα) and consequently electrical output of the PV module are estimated as zero, which is not the case. Therefore, instead of using (τα) calculation in the thermal model directly, a sort of averaging is needed. A weighted daily averaging method for (τα) is developed for the thermal modeling of PV modules in Ankara.

The day is divided into five regions as it can be seen in Figure 2.5 sunrise hour, morning (two hours after sunrise hour), noon, evening (two hours before sunset hour) and sunset hour. Grouping was done using values of (τα). Notice that around noon, (τα) is almost constant. These values are considered as noon hours. Then it steadily falls towards morning and evening, which are divided into two regions: one hour for sunrise and sunset (the smallest (τα)s) and two hours in intermediary morning an evening regions. Each region has a different predetermined assigned weight, w. Largest weight is assigned to noon hours since insolation is highest, and majority of

electrical power is generated during this interval. Calculated (τα)s for each hour is multiplied with their respective weights and averaged over the whole day to find an effective transmittance-absorbance product, $(\tau\alpha)_{eff}$. Calculation of $(\tau\alpha)_{eff}$ for a winter and summer day for Ankara is shown in Table 2.5.

Table 2.5: Daily averaging of the transmittance-absorbance product of PV module for two typical days in winter and summer

January, 25th					**June, 17th**			
Hour (Solar Time)		(τα)	w	(τα)·w		(τα)	w	(τα)·w
07:00	Sunrise	0.5912	2	1.1824	Sunrise	0.6796	2	1.3592
08:00	Morning	0.8524	3	2.5572	Morning	0.8765	3	2.6295
09:00		0.9219	3	2.7656		0.9300	3	2.7900
10:00	Noon	0.9412	4	3.7649	Noon	0.9445	4	3.7780
11:00		0.9465	4	3.7860		0.9481	4	3.7924
12:00		0.9476	4	3.7905		0.9488	4	3.7951
13:00		0.9470	4	3.7879		0.9487	4	3.7946
14:00		0.9432	4	3.7727		0.9473	4	3.7892
15:00	Evening	0.9289	3	2.7868		0.9410	4	3.7641
16:00		0.8778	3	2.6335	Evening	0.9169	3	2.7507
17:00	Sunset	0.6891	2	1.3783		0.8288	3	2.4864
18:00					Sunset	0.4978	2	0.9957
Total			36	32.21			40	35.72
$(\tau\alpha)_{eff}$			32/32.21 ≅0.895				35.72/40 ≅0.893	

The argument for increased weights towards midday is the consideration of immense variation of solar irradiance with respect to hour, irradiance at noon being the highest of the day. Contribution of (τα) to electrical power output is greater at noon compared to morning and evenings.

After all modes of rate of energy transfer is defined for the system, 1st law of thermodynamics can be written as:

$$\frac{dT_{mod}}{dt} \cdot C_{mod} = Q_{solar} - Q_{solar} \cdot (\tau\alpha)_{eff} \cdot \eta_{ref} \cdot [1 - \beta_{ref} \cdot (T_{ref} - T_{mod})] - \left(\overline{Nu}_{L,eff,top} + \overline{Nu}_{L,eff,bot}\right) \cdot \frac{k}{L}(T_{mod} - T_{\infty}) - \sigma \cdot F_{t,sky} \cdot \varepsilon_s \cdot \left(T_{mod}^4 - T_{sky}^4\right) - \sigma \cdot F_{t,earth} \cdot \varepsilon_s \cdot (T_{mod}^4 - T_{earth}^4) - \sigma \cdot F_{b,sky} \cdot \varepsilon_s \cdot \left(T_{mod}^4 - T_{sky}^4\right) - \sigma \cdot F_{b,roof} \cdot \varepsilon_s \cdot \left(T_{mod}^4 - T_{roof}^4\right) \quad (42)$$

Solving this ordinary differential equation (ODE), temperature of the module to be used in equation (39) can be obtained.

CHAPTER 3

METHODOLOGY AND IMPLEMENTATION OF THE THERMAL MODEL

After the principles and the formalism of the model are explained, next is the solution of resulting ODE with input data. For the implementation of the thermal model, algorithms realizing the formalism are developed using MATLAB. In this chapter, numerical method for the ODE solution, input data and overall MATLAB algorithm will be explained.

3.1. Numerical Method

The resulting ODE, equation (42), of the thermal model is a complex equation and analytical solution is not possible. In this case, the solution is approximated with numerical methods. There are several methods for solving ODEs like Euler's, Heun's, midpoint and other higher order Runge-Kutta methods. Each method can be used to solve ODEs with different converging speeds and degree of accuracies. In this work, Euler's method is considered because of its simplicity compared to other higher order methods. Higher order methods give more accurate results but they require second order derivatives, which is hard to obtain when the ODE is complicated. Considering an ordinary differential equation in the form of

$$\frac{dT}{dt} = f(t, T) \tag{43}$$

where f(t,T), which is a function of time t and module temperature T, is known and T(t) needs to be determined as a function of time t. An initial guess for the T value T_i, and a step interval Δt are needed. And then using T_i, Δt and known value of f at the point (t_i,T_i), which is the slope at the point t_i, $T_{i+1}$is estimated using:

$$T_{i+1} = T_i + f(t_i, T_i) \cdot \Delta t \quad (44)$$

From this step T_{i+2} can be found using $t_i+\Delta t$, T_{i+1}, $f(t_i+\Delta t, T_{i+1})$, and T(t) can be estimated for the values of t_i, $t_i+\Delta t$, $t_i+2\Delta t$ … repeating the procedure. Smaller the step size is taken, more accurate the results will be; but it will lengthen the computation time significantly.

This method is called Euler's method. But Euler's method can be numerically unstable with large step sizes. The numerical solution oscillates largely above some step size limit in some equations. In order to avoid this problem in the estimations, implicit (backwards) Euler's method is employed in the solution of the ODE.

Implicit Euler method uses the slope at the point t_{i+1} instead of at t_i and the T_{i+1}can be estimated from:

$$T_{i+1} = T_i + f(t_i + \Delta t, T_{i+1}) \cdot \Delta t \quad (45)$$

In this case unknown value $T_{i+}1$ is in the both sides of the equation. Arranging (45) as

$$0 = T_i + f(t_i + \Delta t, T_{i+1}) \cdot \Delta t - T_{i+1} \quad (46)$$

results a complicated equation whose root will give us the solution, that is the module temperature at the time of $t_i+\Delta t$.

The thermal model uses the module temperature in order to determine thermophysical properties of the fluid before the estimation of the module temperature via solving the ODE. Therefore, an initial guess of the module temperature for determination of these properties is necessary. This guess would not be correct; and in order to estimate the module temperature accurately, an iterative method should be adopted. After the initial guess, calculated T_{mod} is used for determination of thermophysical properties and a new T_{mod} is found. Iteration goes on until the solution converges and difference between two consecutive iterations falls below a chosen tolerance limit, which is taken as 0.001°C. Limits of 0.01 and 0.0001 also tried but, former gave results not accurate

enough; and the latter did not improve it significantly compared to long computational time it took.

Solving for the root of equation (46) to find T_{mod} is another challenge, there are no analytical solutions. Several bracketed and open methods are available for finding roots numerically. Instead of choosing one numerical method in order to find the root, a MATLAB function "fzero" is implemented for the solution. fzero uses several open and bracketed methods together to determine the closest root to given initial value or the first root within the given interval [87]. Since fzero gives only one root, it is critical that initial value is chosen smartly in case the equation (46) has other roots, which do not have physical meaning. In the implementation of the thermal model, the very first initial guess of the module temperature is taken as 0°C. After the first estimation of the module temperature converges, for the next time increment initial guess is taken as module temperature estimation in the previous time increment.

3.2. The Data

The data used in thermal model are very important for the accuracy of the results. The testing and data gathering in order to apply the model in real life conditions and the verification of the model results are done in the Outdoor Testing Facility of GÜNAM in Middle East Technical University, Ankara (Figure 3.1). The data from testing site can be grouped into three categories: meteorological data, the PV module data and mounting data, see Table 3.1. Most of the measured data is used as input in the thermal model; however, temperature and electrical power output of the PV module are used to verify the model as these parameters are the outputs of the model.

In the testing facility, the data are taken using two instrumentations. One is to follow the performance of the PV modules and one is for measurement of meteorological data. The measurements on PV module has been done by multi-tracer PV analyzer which measures current and voltage produced by the module at pre-determined intervals. Connected to the multi-tracer PV analyzer, there are two high precision Kipp&Zonen CMP 11 pyranometers for insolation measurements on the horizontal and tilted surface. Hence, in the thermal model instead of estimated inclined surface

solar insolation, direct measurements on the tilted surface are used. A T-type thermocouple sensor to measure module temperature has been adhered to the center of the back side of the PV module, which is also connected to multi-tracer.

A meteorological weather station, which has been installed in the facility, is used to measure ambient air temperature, dew temperature, wind speed and direction. The meteorological data has been gathered in a separate logger.

PV module measurements are recorded in every hour while for meteorological station time interval is 10 minutes. The recorded values are averages of many measurements taken within pre-determined time intervals.

The testing duration for data gathering is one year, April 2016 to March 2017.

Table 3.1: Input data for the thermal module

	Meteorological Parameters	**PV Module Parameters**	**Mounting Parameters**
Input parameters	1. Ambient temperature 2. Dew point temperature 3. Wind speed 4. Wind direction 5. Irradiance	1. Heat capacity 2. Dimensions 3. Conversion efficiency 4. Temperature coefficient 5. Emissivity	1. Latitude 2. Tilt angle 3. Azimuth angle 4. View factors 5. Rear surface condition
Verification parameters		1. Module temperature 2. Electrical power output	

Figure 3.1: PV modules in Outdoor Testing Facility of GÜNAM in Middle East Technical University, Ankara

The thermal model has been run for hourly data, meaning the step size in the numerical method is one hour. Actually, due to the changeability of the weather conditions, shorter time intervals will give more accurate results. Despite that, hourly analysis has been chosen. Because unlike hourly meteorological data that can be found freely in government meteorological reports, data in intervals like seconds or minutes are not widely or freely available, if not recorded specifically. Therefore, it is imperative that the model have sufficient accuracy with hourly analysis; and can give conclusive results for different locations and modules with data easily accessible. In this way the thermal model will give a definite idea how much power can be produced in a location if a specific PV module were to be installed, without actual experiments to be conducted in sites and without extra expenses.

3.2.1. Meteorological Data

As it is listed in the Table 3.1, meteorological data consists of ambient temperature, dew point temperature, irradiance, wind direction and speed.

In the testing facility, irradiance on the tilted surface and ambient temperature are measured hourly along with PV module parameters. Others are recorded in 10 minute intervals. Since we are using hourly analysis, 10 minute data needs to be converted into hourly data. The process is very straightforward with the dew temperature and wind speed; for 6 data points in every hour, an arithmetic mean is taken to form hourly data. But averaging wind direction is rather complicated.

The wind direction is generally represented in 8-point compass, which consists of cardinal points (North, East, South, and West) and inter-cardinal points (Northeast, Southeast, Southwest and Northwest) of the compass. For more precise measuring, 8 intermediate compass points like North-Northeast (NNE), East-Northeast (ENE) and East-Southeast (ESE) are sometimes used as well. Then, 16 different directions are defined for the wind measurements as it can be seen in wind direction compass rose in Figure 3.2. In the testing facility, the measured wind direction data are recorded in all 16 directions.

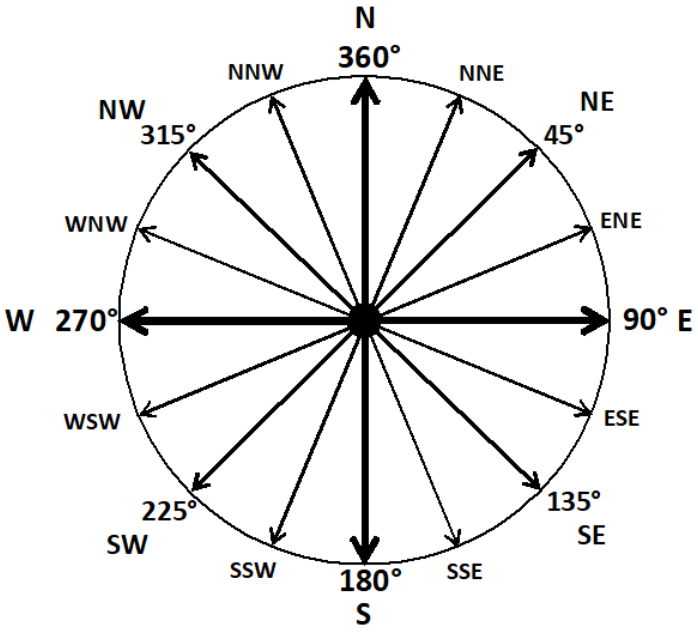

Figure 3.2: Compass rose for wind direction

As it is mentioned in section 2.1.2.2, the thermal model considers the direction of the wind in three categories regarding the correlations of the Nusselt number: East-West,

Northern and Southern. Due to insensitivity of the yaw angle in head-on region rate of convective heat transfer [76], and azimuth angle of the module being zero (south-facing module), all wind directions coming from the north or south can be lumped in one category. Wind coming directly from East or West will form parallel flow over the module. All wind directions, that is the16 of them are separated into 3 groups considering the flow characteristics they create on the module surface as given in Table 3.2.

Table 3.2: Wind direction grouping in the thermal model

Southern Direction	ESE, SE, SSE, S, SSW, SW, WSW
Northern Direction	WNW, NW, NNW, N, NNE, NE, ENE
East-West Direction	W,E

The direction of the wind can be very inconsistent though; and it can change drastically within minutes. This behavior is observed in the data gathered in the testing facility; both Southern and Northern direction can be observed within the same hour. The trouble is determining a direction among many observed values which should be good representation of an average value for an hourly analysis. In order to derive hourly wind speed and direction from 10 minute data, an averaging method is developed.

The method determines hourly wind direction considering the speed. In one hour data set there are 6 values. A fraction is assigned to all 6 data points which is determined in accord with their respective speed over sum of all measured speed values within the hour as:

$$f_j = \frac{v_j}{\sum_{j=1}^{j=6} v_j} \tag{47}$$

where v_j is the wind speed and f_j is fraction of the data point. In Table 3.3, sample wind direction measurements are listed for four different hours, and their calculated fractions are given.

Table 3.3: Sample wind speed and direction data

April 1st 2016				**April 2nd 2016**			
Time	Speed v_j	Direction	Fraction f_j	Time	Speed v_j	Direction	Fraction f_j
10:00	0	ENE	0	19:00	0,4	NW	0.200
10:10	0,4	ENE	0.0930	19:10	0,4	WSW	0.200
10:20	0	ESE	0	19:20	0,4	SW	0.200
10:30	0,4	NNE	0.0930	19:30	0,4	WNW	0.200
10:40	1,3	S	0,3023	19:40	0,4	W	0.200
10:50	2,2	S	0,5116	19:50	0	W	0
April 2nd 2016				**October 8th 2016**			
Time	Speed v_j	Direction	Fraction f_j	Time	Speed v_j	Direction	Fraction f_j
11:00	0,4	WNW	0.0833	03:00	0	SW	0
11:10	0,9	W	0.1875	03:10	0,4	SW	0.500
11:20	0,9	WSW	0.1875	03:20	0	SW	0
11:30	0,4	W	0.0833	03:30	0	SW	0
11:40	1,3	SW	0.2708	03:40	0	W	0
11:50	0,9	NW	0.1875	03:50	0,4	NE	0.500

In order to determine average wind direction, fractions of each hour is summed with respect to their directions. Table 3.4 shows fraction values after summation for 1st of April at 10 am. The direction corresponding the largest fraction is chosen as the average direction. For April 1st 10 am, it is S, see bold value in Table 3.4.

Table 3.4: Wind direction fraction summation at 10 am on April 1st

ESE	SE	SSE	S	SSW	SW	WSW	WNW	NW	NNW	N	NNE	NE	ENE	W	E
0	0	0	**0,8139**	0	0	0	0	0	0	0	0.0930	0	0.0930	0	0

However, sometimes two or more directions share the largest value after the summation. The Table 3.5 shows fractions of wind directions after the summation at 7 pm on April 2nd. SW and E direction have equal to fraction value of 0.2708.

Table 3.5: Wind direction fraction summation at 7 pm on April 1st

ESE	SE	SSE	S	SSW	SW	WSW	WNW	NW	NNW	N	NNE	NE	ENE	W	E
0	0	0	0	0	**0.2708**	0.1875	0.0833	0.1875	0	0	0	0	0.0930	**0.2708**	0

In this case, to decide an hourly averaged direction the three groups of Table 3.2 are used. That is, the 16 fraction values are separately summed up which are

corresponding to three wind direction groups in Table 3.2. In terms of the effect on the convective heat transfer of PV module, the directions within their respective groups can be considered the same [76]. Therefore, a representative direction is chosen for each group: southern (S), northern (N) and East-West (E). After the fractions are summed up, the direction having the largest fraction value between groups is chosen as the average direction. Table 3.6 shows fraction summation with respect to thermal model wind direction grouping at 7 pm on April 1st for an example. Southern direction has largest fraction value with 0.4583; and S is chosen as average wind direction.

Table 3.6: Wind direction fraction summation with respect to thermal model wind direction grouping at 7 pm on April 1st

Group	Directions	Fraction	Selected Direction
Southern Direction	**ESE, SE, SSE, S, SSW, SW, WSW**	**0.4583**	**S**
Northern Direction	WNW, NW, NNW, N, NNE, NE, ENE	0.2708	N
East-West Direction	W, E	0.2708	E

This procedure of grouping and calculation scheme in some hours still gives the same fraction values, making the average direction indeterminate for the hour. So, in order to choose a direction, the approach is adjusted as below. When two of the fraction values are equal, there are three possibilities:

1. $f_E = f_S$ (southern and east-west fractions are equal to each other)
2. $f_E = f_N$ (northern and east-west fractions are equal to each other)
3. $f_S = f_N$ (northern and southern fractions are equal to each other)

If first is the case, the average direction is taken as SE; second is the case, average direction is taken as NE. But if the third above is the case, then a different action is needed since they are opposite directions. Table 3.7shows such a situation that the fraction summation of wind direction grouping at 11 am on April 2nd. Fraction values of southern and northern directions are both equal to 0.4.

Table 3.7:Wind direction fraction summation with respect to thermal model wind direction grouping at 11 am on April 2nd

Group	Directions	Fraction	Selected Direction
Southern Direction	ESE, SE, SSE, S, SSW, SW, WSW	0.4	S
Northern Direction	WNW, NW, NNW, N, NNE, NE, ENE	0.4	N
East-West Direction	W, E	0.2	E-W

Then the grouping is adjusted if this is the case as explained below. The directions WNW, ENE, WSW and ESE are included in E-W of Table 3.2. As an example, after the adjustment, the fraction of 11 am on April 2nd are summed according to the new grouping in the Table 3.8. East-West direction has largest value with 0.6; and E is chosen as average wind direction.

Table 3.8: Wind direction fraction summation with respect to adjusted wind direction grouping at 11 am on April 2nd

Group	Directions	Fraction	Selected Direction
Southern Direction	SE, SSE, S, SSW, SW,	0.2	S
Northern Direction	NW, NNW, N, NNE, NE	0.2	N
East-West Direction	**W, E, WSW, ESE, WNW, ENE**	**0.6**	**E**

Implementation of the averaging of the 10 min data into hourly data is carried out with a simple MATLAB code. With this code, final input hourly data file (an excel file) is created.

There are another group of input we need in the thermal model which is not in meteorological data but it must be considered for the thermal model: thermophysical properties of the ambient air. These properties include Prandl number, thermal conductivity, specific heat capacity, density and kinematic viscosity. They are not constants and most of them have strong temperature dependency. In the model, these properties are taken at the film temperature, which involves module temperature as well as ambient. Therefore, they must be determined within the iteration. There are tables available containing the values of these properties of air for different temperatures and pressures. In the model, the tables given in [88] are used. For the

temperatures between the reference temperature of the tables, linear interpolation is used and the values are determined within the code.

3.2.2. PV Module Data

The module selected for the verification is from Solara S-Series and the model number is S520P36Ultra. Table 3.9 gives the data for this module to be used in the model. It is a poly-c-Si solar cell and has the conversion efficiency of 12.7% under STC.

Table 3.9: Module parameters

Heat capacity: 5723 (Calculated in Table 2.4)
Dimensions: 0.68 X 1.50 m
Conversion efficiency: 12.7%
Temperature coefficient: – 0.45 % / K
Emissivity: 0.9

Dimensions, conversion efficiency and temperature coefficient are taken from the data sheet of the module directly.

Another important parameter of the module is emissivity; a direct factor affecting the radiative heat transfer rate from the module. Unlike temperature coefficient, detailed material properties, including emissivity are not provided in the data sheet of the module. Since radiative heat transfer occurs from outer surfaces of the panel, which is the glazing, reference emissivity value of 0.9 for regular glass [89] for both top and bottom surfaces is used in the thermal model

Heat capacity of the module, like emissivity, had not been included in the data sheet, so it is calculated using the method explained in Section 2.2.

3.2.3. Mounting Details

These parameters are static; once the module is mounted they do not change as the system is not a tracking system. They consist of latitude of the location, tilt, azimuth angle and view factors of the PV module and rear surface condition, whether it is open

to the ambient or not. Their respective values used in the thermal model can be found in the Table 3.10.

Table 3.10: Location/Mounting details of the PV module

Latitude of Ankara:	39.89 ºN
Tilt angle of PV Module:	32º
Azimuth angle of PV Module:	0º (South-facing)
View factors of PV Module:	Calculated (section 3.1.3.)
Rear surface condition of PV Module (open/closed):	open

Location and orientation of the PV module determines how much insolation PV module is receiving from the Sun, hence is a major factor affecting the model. For most direct exposure to the sun, tilt angle is taken 32º and azimuth is taken as zero. View factors are calculated using the tilt angle, as given in Section 2.1.3.

Rear surface condition is another parameter that needs to be considered since it affects rate of heat transfer from the module surfaces. When the bottom surface is closed to the ambient air, only conduction through the roof can occur, which will slow the heat removal. In the experimental set-up, the back of the module is exposed to the ambient air, so both surfaces are considered as described in Section 2.1.2.

3.3. The Algorithm

MATLAB code follows the steps laid out in to estimate module temperature and respective electrical power output with the methods explained in this chapter. A flow chart is provided in Figure 3.3.

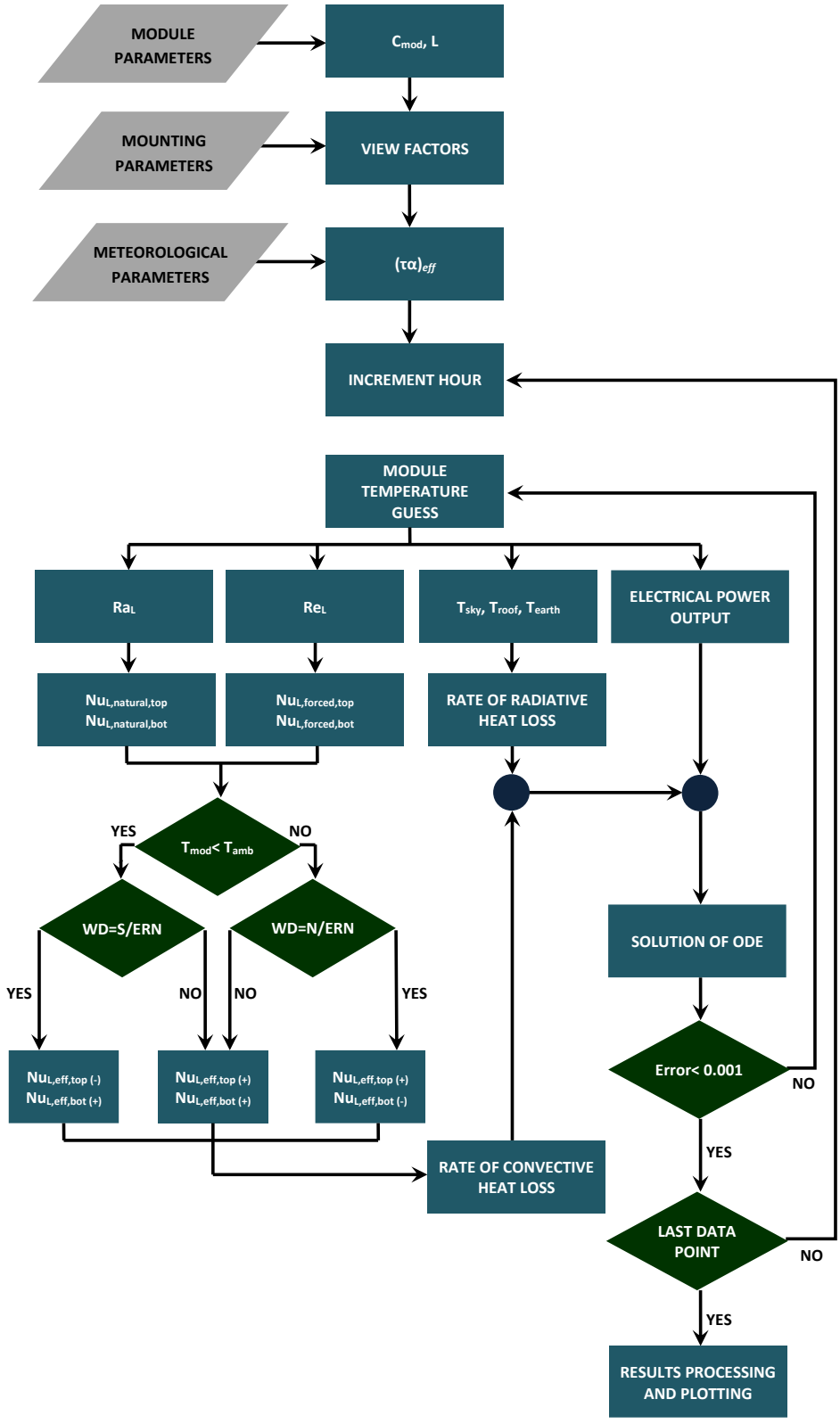

Figure 3.3: Flow chart of the thermal model

3.4. Comparison Method of Estimated and Measured Values

The estimated quantities calculated by the thermal model are compared with the one-year measured values. The comparisons are carried out using the following statistical error expressions; root mean square error (RMSE), and mean biased error (MBE) as follows:

$$\mathrm{RMSE} = \left(\frac{1}{\mathrm{N}} \sum_{\mathrm{i}=1}^{\mathrm{i}=\mathrm{N}} (\mathrm{y}_{\mathrm{est,i}} - \mathrm{y}_{\mathrm{mes,i}})^2 \right)^{1/2} \tag{48}$$

$$\mathrm{MBE} = \frac{1}{\mathrm{N}} \sum_{\mathrm{i}=1}^{\mathrm{i}=\mathrm{N}} (\mathrm{y}_{\mathrm{est,i}} - \mathrm{y}_{\mathrm{mes,i}}) \tag{49}$$

where N is number of estimations, y_{est} is estimated value and y_{mes} is measured value.

In addition to above expressions, directly the deviations and relative deviations are also used whenever needed. These values are plotted as a time series within a day.

CHAPTER 4

RESULTS AND DISCUSSION

Since one year hourly values of daily data is used in the analysis, only some sample days representing different weather conditions and insolation values are discussed here. In addition, the discussions are carried out for whole year are provided on a monthly base. The full-year graphs of the results are also given in Appendix-A. For the verification of the model, the overall accuracy and precision of the results are discussed using mean absolute error (MBE) and root mean square error (RMSE). Possible reasons for the deviations are discussed. Finally, results of sensitivity analysis for heat capacity of PV module is presented and discussed.

4.1. Results of the Thermal Model in Sample Intervals

The performance of the thermal model is evaluated with respect to resulting module temperature deviations and electrical output deviations since the end goal of the thermal model is accurate performance predictions under variable conditions. Four sample 3-day intervals with high and low wind velocities from hot and cold seasons are selected; details can be seen in the Table 4.1.

Table 4.1: Selected intervals from 1-year data

#	Date	Wind Speed (Beaufort Scale)	Cloudiness
1st	November 9-11	Light – Gentle Breeze	Cloudy
2nd	November 22-24	Calm – Light Air	Clear
3rd	June 18-20	Light Air- Gentle Breeze	Clear
4th	August 17-19	Light Air- Light Breeze	Clear

For cold season, two intervals which have different weather conditions are chosen from November. Solar irradiance, measured electrical power output values, wind speed and direction for these days are presented in Figure 4.1 and Figure 4.2, respectively. First interval in Figure 4.1 is the days between 9th and 11th of November. As it can be observed these days are rather cloudy (and the days are rainy), The wind speeds are relatively high with an average of 2.20 m/s as depicted in Figure 4.2. Average ambient, dew point and sky temperature for this interval are 14.93°C, 4.80°C and -5.95°C respectively. The second intervals in the figures, the days between 22nd and 24th of November, the sky is clear as can be seen in Figure 4.1. The wind speeds are small and always below 1 m/s with an average of 0.13 m/s, so these days are mostly calm. Average ambient, dew point and sky temperatures are 7.47°C, -7.02°C and -18.70°C respectively.

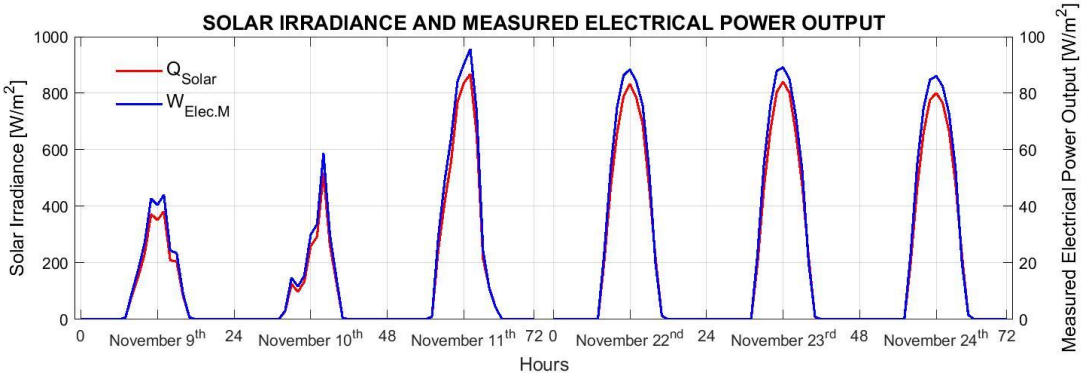

Figure 4.1: Insolation and electrical output of the PV module on 9-11th and 22-24th of November

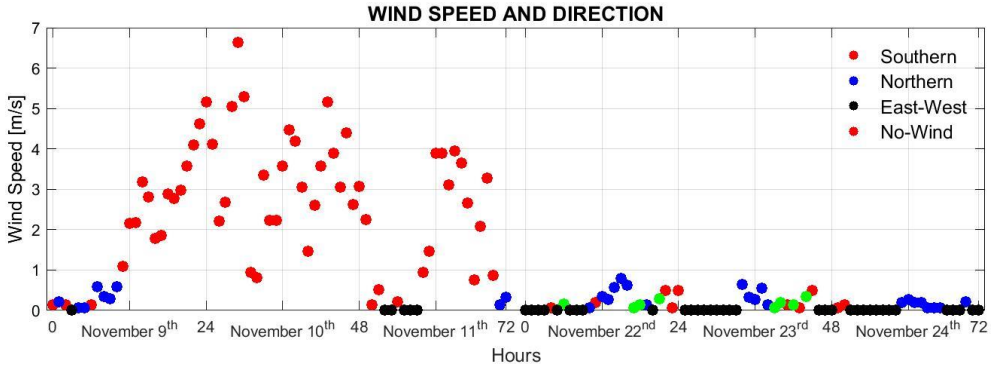

Figure 4.2: Wind speed and directionon9-11th and 22-24th of November

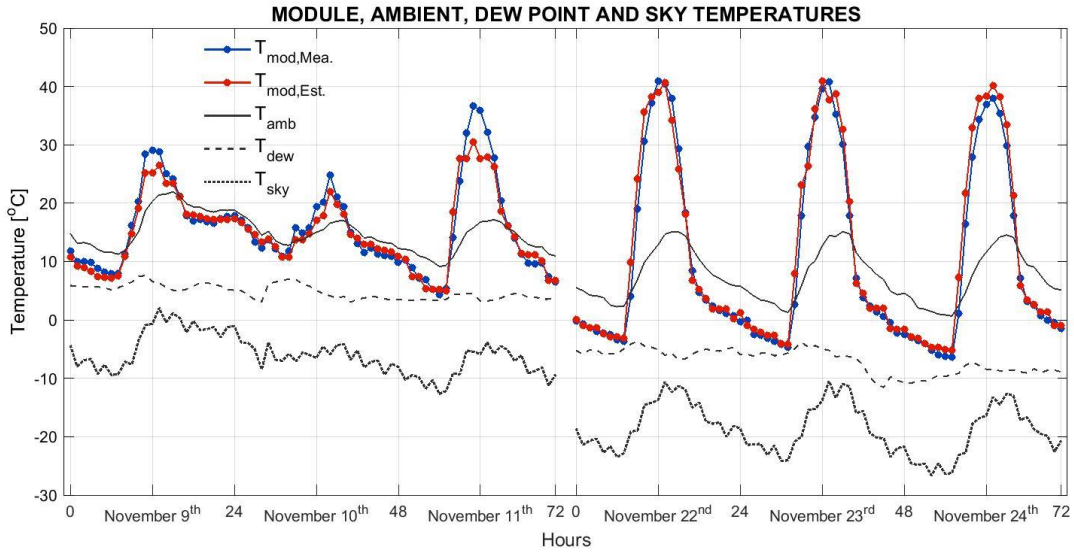

Figure 4.3: Temperatures of the PV module, ambient, dew point and sky on 9-11th and 22-24th of November

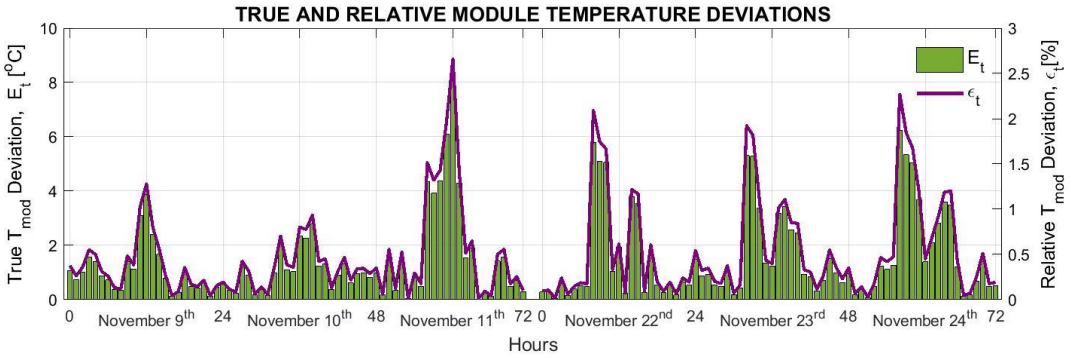

Figure 4.4: Deviations of module temperature estimations on 9-11th and 22-24th of November

Measured and estimated module temperature together with three weather temperatures for the mentioned intervals are depicted in curves in Figure 4.3. The module temperature true deviations and relative deviations are given in Figure 4.4. The thermal model underestimates the module temperature for the first interval with MBE of -1.49°C; but for the second interval it is mostly overestimated with MBE value of 1.66°C during daytime hours. On both intervals largest deviations are observed around solar noon where the insolation is at its highest values. RMSE of temperature estimations are 2.75°C and 3.37°C during daytime hours for the first and second intervals, respectively. During the nighttime, temperature estimations are much better with an RMSE of 0.89°C and 0.72 °C for the first and second intervals respectively.

In both intervals, module temperature slightly overestimated during nighttime hours with MBE values of 0.12°C and 0.36°C for the first and second intervals, respectively. Relative module temperature deviation closely follows the true deviation trend, with highest values corresponding to largest true deviations.

Figure 4.5 and Figure 4.6 gives measured and estimated power outputs, efficiency and absolute and relative deviations, respectively. The model partly underestimates the electrical power output for the first interval of cloudy days with a MBE of -0.98 W/m^2 and it underestimates the electrical power output for the second interval with a MBE of -2.49 W/m^2. RMSE values for electrical power output estimations are equal to 1.66 W/m^2 and 4.02 W/m^2 for first and second intervals, respectively.

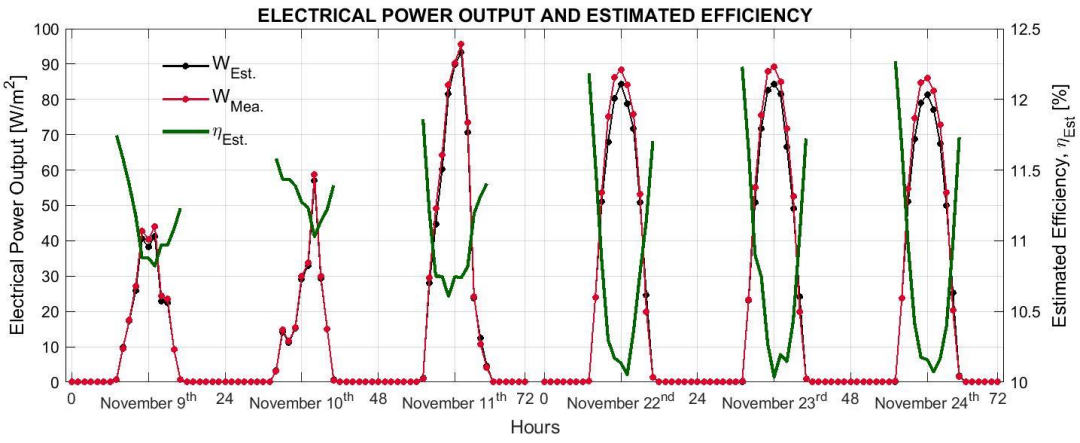

Figure 4.5: Electrical output and estimated efficiency of the PV module on 9-11th and 22-24th of November

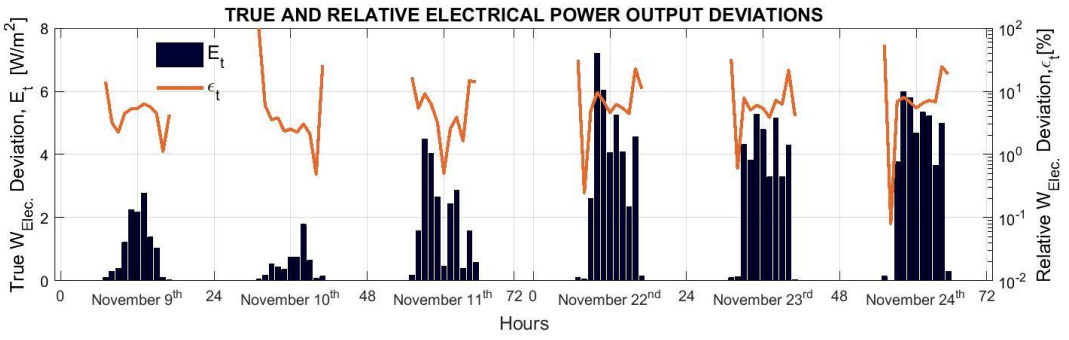

Figure 4.6: Deviations of electrical power output estimations on 9-11th and 22-24th of November

Relative deviations depicted in the curve in Figure 4.6 are significantly high at morning and evening hours. It might be caused by the assumption of constant (τα) value, which is very small during these hours due to large incident angle of the sun beams. Nevertheless, large relative deviations for these hours are physically insignificant as the true deviations are very small for these hours.

Estimated efficiency values that can be seen in Figure 4.5, is at their lowest around noon as expected. It falls to almost 10%. They are high during morning and evening hours since the irradiation values are significantly lower for those hours, their contribution to overall PV performance is not quite effective.

For hot season, two intervals from July and August are chosen. Solar irradiance, measured electrical power output values, wind speed and direction for these days are presented in Figure 4.7, and Figure 4.8. First interval for the hot season is the days between 18th and 20th of June with clear and windy days. Average ambient, dew point and sky temperatures are 25.51^{o}C, 10.73^{o}C and 7.51^{o}C; and average wind speed of 1.63m/s. Second interval from hot season is the days between 17th and 19th of August. They are mostly sunny with smaller wind speeds of 0.6m/s. Average ambient, dew point and sky temperatures are 25.56^{o}C, 11.02^{o}C and 7.75^{o}C for this interval.

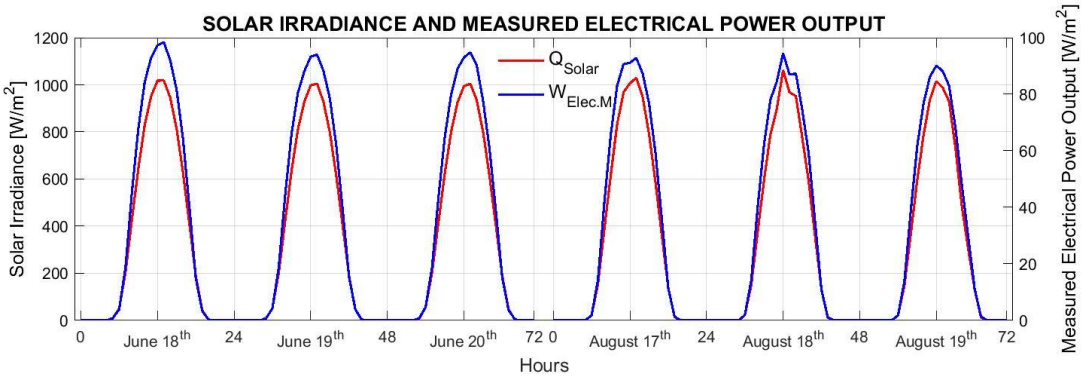

Figure 4.7: Insolation and electrical output of the PV module on 18-20th of June and 17-19th of August

Figure 4.9 depicts the measured and estimated module temperatures for the selected days in June and August. The thermal model underestimates module temperature by a

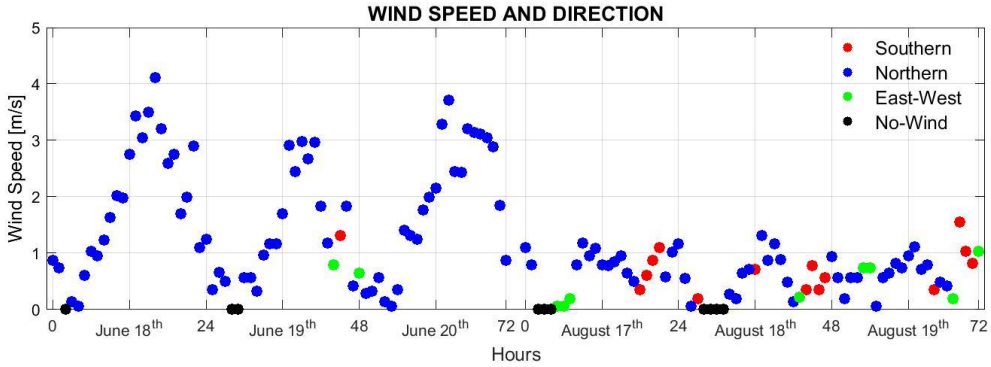

Figure 4.8: Wind speed and direction on 18-20th of June and 17-19th of August

significant margin during daytime for both intervals with MBE values of -2.72°C and -1.58°C. In Figure 4.10, true deviation values are presented. Largest deviations always occur around noon hours. RMSE during daytime hours is 4.34°C for June; and 3.32°C for August respectively. During the nighttime, thermal model performs very well with MBA of 1.15°C and RMSE of 1.23°C for June; and MBA of 0.74°C and RMSE of 0.90°C for August.

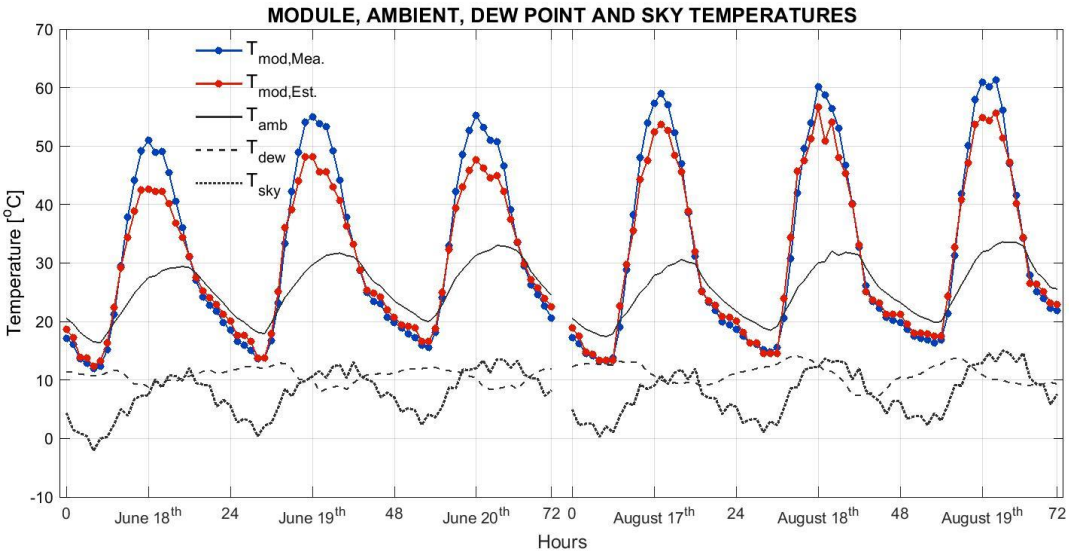

Figure 4.9: Temperatures of the PV module, ambient, dew point and sky on 18-20th of June and 17-19th of August

Measured and estimated electrical power output of the module is plotted in Figure 4.11. Corresponding to large module temperature deviations, electrical power output estimations also have large deviations compared to cold season with RMSE of 4.73 W/m^2 and 3.21 W/m^2 for June and August respectively. The thermal model

overestimates electrical power output with MBE values for June and August equal to 3.93 W/m^2 and 3.20 W/m^2, respectively.

Figure 4.12 presents true and relative deviations for electrical power output estimations. True deviations can reach above 9W/m^2 with 10% relative deviations around solar noon. Around morning and evening hours, relative deviations have very large values, but as it explained before due to low solar irradiation, these deviations are not physically significant. In Figure 4.11, estimated efficiency is depicted; it falls to as far as 9.6%.

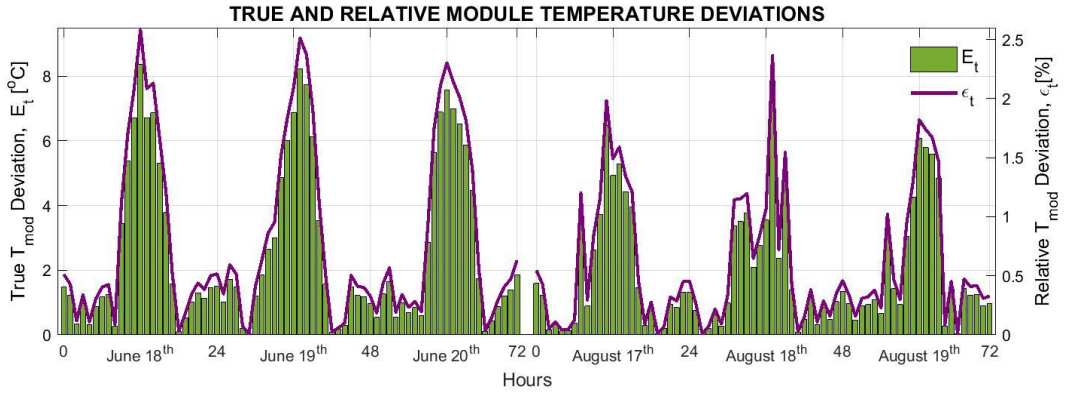

Figure 4.10: Deviations of module temperature estimations on 18-20th of June and 17-19th of August

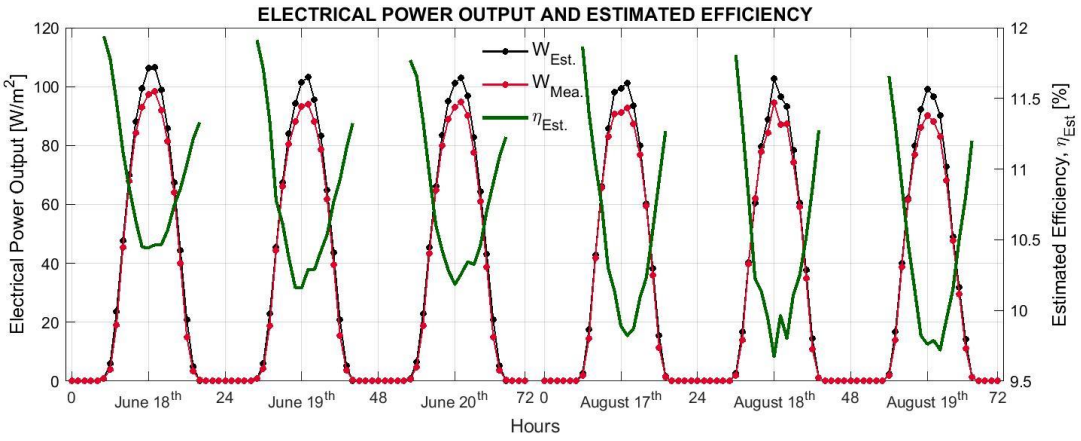

Figure 4.11: Electrical output and estimated efficiency of the PV module on 18-20th of June and 17-19th of August

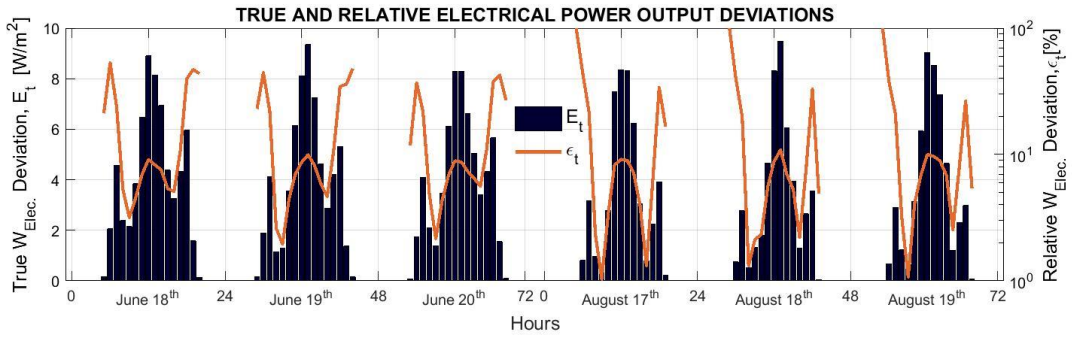

Figure 4.12: Deviations of electrical power output estimations on 18-20th of June and 17-19th of August

4.2. Summary of Results of the Thermal Model for 1-Year Data

Table 4.2 lists MBE and RMSE values for module temperature and electrical output estimations for all 12 months.

Table 4.2: MBE and RMSE of module temperature and electrical power output estimations (12 month)

Month #	$W_{Elec.}$ MBE	$W_{Elec.}$ RSME	T_{mod} MBE	T_{mod} RSME	T_{mod} MBE daytime	T_{mod} RSME daytime	T_{mod} MBE nighttime	T_{mod} RSME nighttime
1	0,5967	2,7031	-0,9953	2,4356	-0,4746	2,7556	-1,4611	2,1087
2	1,3991	3,9930	-1,0271	2,6207	-0,8636	3,1385	-1,1958	1,9469
3	-0,2057	1,4408	-1,1728	1,7749	-1,1663	1,8767	-1,1801	1,6544
4	1,1696	2,4316	-0,3225	2,2063	-0,5744	2,7367	0,0489	1,0011
5	1,2126	2,5057	-0,5589	2,1140	-0,6834	2,4858	-0,3272	1,1339
6	2,4555	3,5591	-0,5747	2,6401	-1,1505	3,1509	0,5841	1,0085
7	3,9903	5,0404	-1,0535	3,0858	-2,0102	3,6993	0,8771	1,0593
8	2,7313	3,9135	-0,9241	2,7014	-1,8307	3,3932	0,4653	0,9142
9	2,2823	3,4937	-0,8478	2,6246	-1,6362	3,3731	0,2343	0,8527
10	-0,4034	1,6101	-0,5580	2,0986	-0,7870	2,6447	-0,3069	1,2508
11	-1,5370	2,9012	-0,3729	2,2554	-0,3797	3,0719	-0,3672	1,1944
12	-1,2773	3,4188	-0,5932	2,6214	0,0691	3,2581	-1,1822	1,8823
mean	1,0345	3,0843	-0,7501	2,4316	-0,9573	2,9654	-0,3176	1,3339

Overall evaluation of the thermal model over one year period gives average MBE and average RMSE of 1.03 W/m^2 and 3.08 W/m^2 for electrical power output estimations;

and MBE of -0.75ºC and RMSE of 2.43ºC for module temperature estimations. All estimated values of module temperature and electrical power output are depicted in the curves in graphs in Appendix-A for 1-year analysis.

RMSE and MBE values for the whole year with a monthly basis are presented in Figure 4.13 (module temperature), Figure 4.14 (module electrical power output), Figure 4.15 (daytime module temperature) and Figure 4.16 (nighttime module temperature).

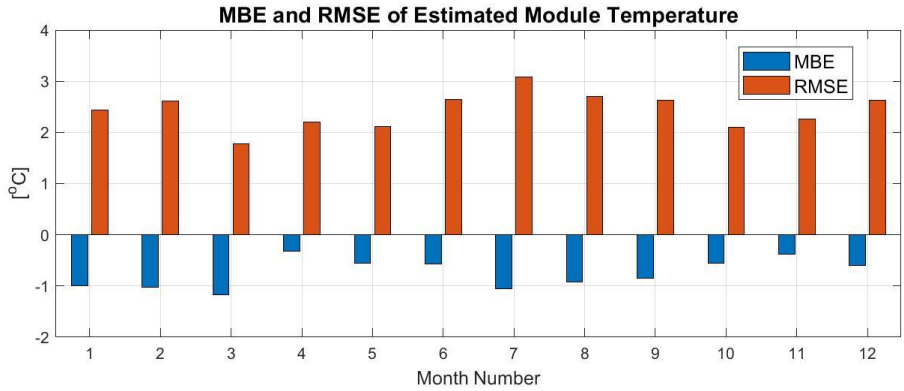

Figure 4.13: MBE and RMSE of module temperature for 12 months

From the RMSE values depicted in Figure 4.13, Figure 4.14 and Figure 4.15, it is clear that, accuracy of thermal model in prediction of module performance is reduced during summer months, July having the highest RMSE for both module temperature (overall and daytime) and electrical power output. In general, the model performs better in module temperature predictions during nighttime, see Figure 4.16.

Thermal model underestimates module temperature during daytime throughout 12 months, indicated by negative MBE values in Figure 4.15. Signs of MBE values nighttime module temperature estimations vary with respect to season, see Figure 4.16. Although the values are small, a clear underestimation in winter months and over estimation in summer months in nighttime module temperature are displayed in Figure 4.16. In the figure, according to RMSE values, unlike daytime module temperature, the model predicts nighttime module temperatures better in summer.

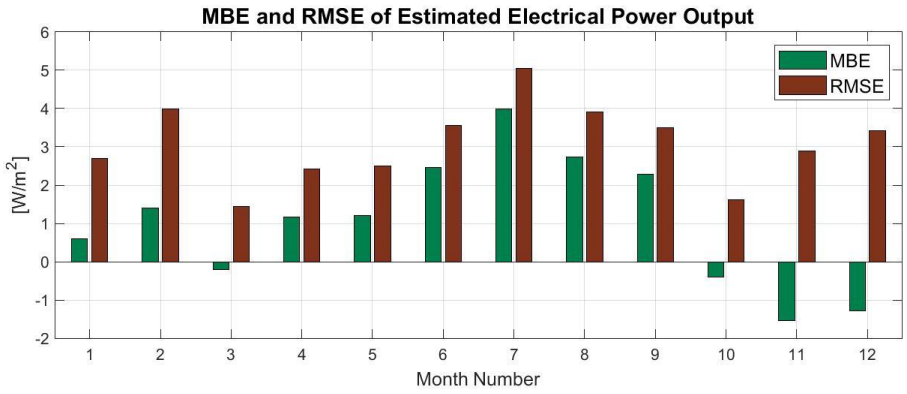

Figure 4.14: MBE and RMSE of module electrical power output for 12 months

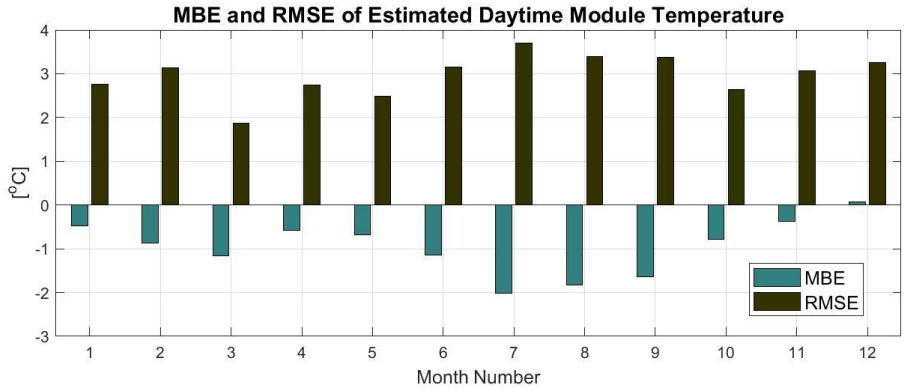

Figure 4.15: MBE and RMSE of module temperature during daytime hours for 12 months

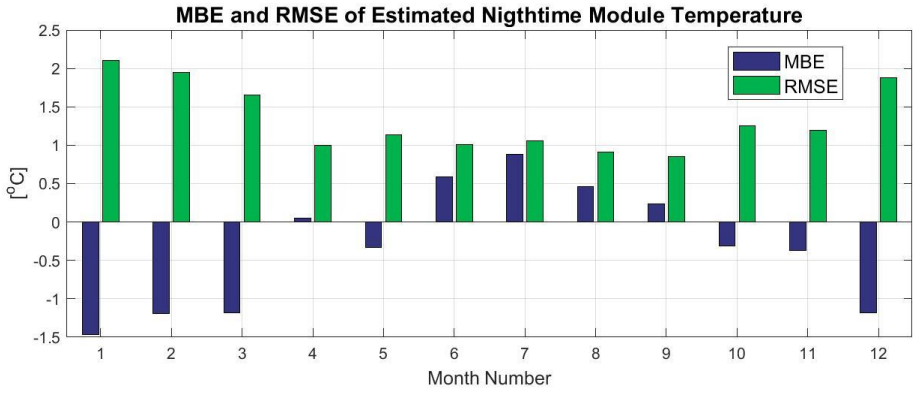

Figure 4.16: MBE and RMSE of module temperature during nighttime hours for 12 months

4.3. Possible Reasons for Deviations

Small deviations of module temperature predictions of thermal model in the nights show that heat transfer estimations methodology are working well. This indicates that the reason behind the large deviations may not be the methodology of the thermal model itself. There are several possible causes that may lead to the large errors during the day. Following sections explain these causes and investigate effects of some of them on the performance of the thermal model.

4.3.1. Roof Surface Temperature

In the model the roof temperature is assumed to be equal to ambient temperature. However, in reality roof temperatures can be much higher than the ambient, especially during clear sky noon hours. It strongly depends on the material of the roof, insolation and the wind speed [90]. The temperature difference between roof surface and ambient air can be as high as 40°C in summer months [91]. Therefore, the assumption that T_{roof} is equal to T_{amb} leads to deviations in radiative heat transfer estimations. Figure 4.17 depicts rate of heat transfer from the PV module.

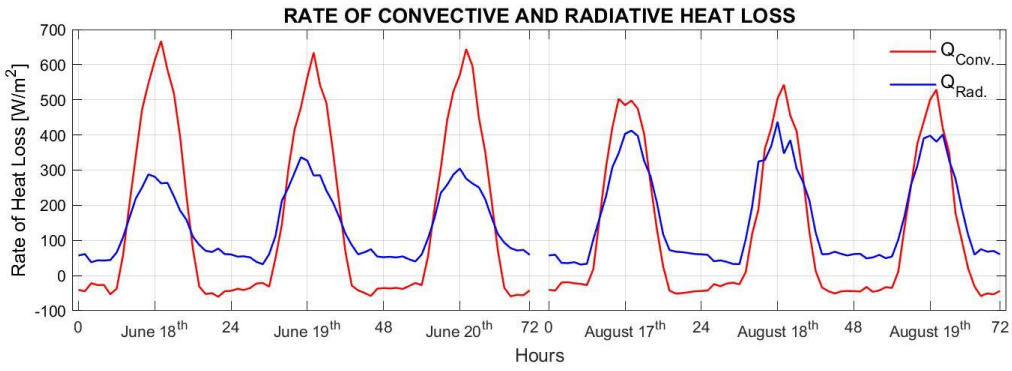

Figure 4.17: Rate of convective and radiative heat transfer from PV module surface on 18-20th of June and 17-19th of August

It is clear that rate of radiative heat transfer is comparable with rate of convective heat transfer and far superior to electrical power production. Lower roof temperature assumption leads to higher radiative rate of heat loss; and thermal model underestimates module temperature and consequently overestimates electrical power

output. Especially in summer season, the deviations created by the assumption become more apparent. In order to quantify the effect of roof temperature on the module temperature predictions, following linear correlation is employed [61].

$$T_{roof} = T_{amb} + a_r \cdot Q_{solar} \quad (50)$$

where a_r is absorptivity coefficient of the roof. It depends on the material of the roof; and determining proper value requires measurements of roof temperature, which is not available for the experimental set-up of this thesis. In order to demonstrate effect of roof temperature, a_r is assumed 0.026 in order to get temperature difference between T_{amb} and T_{roof} of around 25ºC at solar noon, which is a reasonable difference for dark roofs during summer [92]–[94]. Figure 4.18 depicts estimated and measured module temperatures, roof temperature, and ambient temperature with application of equation (50) for two clear sky sample days in summer. Roof temperatures reach up to55 ºC in this case, but the thermal model still underestimates the module temperature.

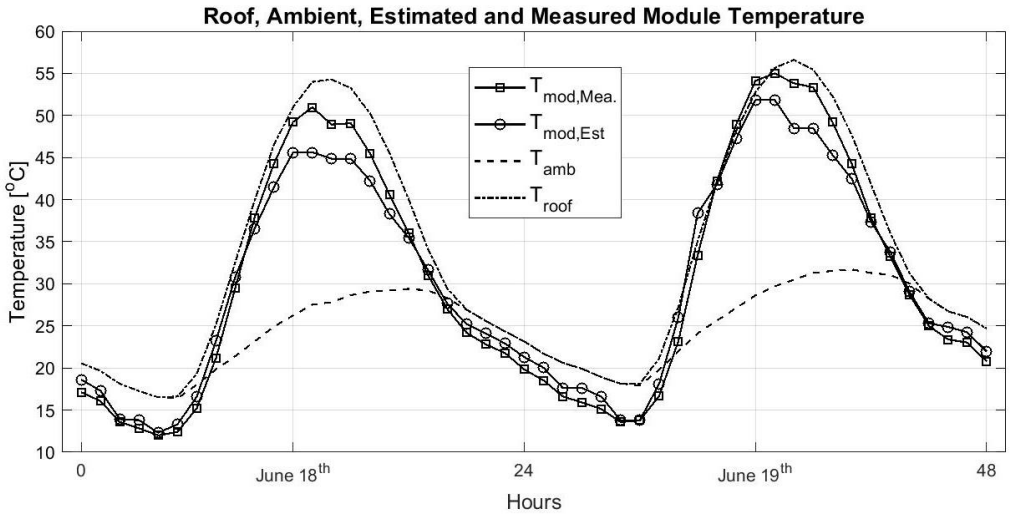

Figure 4.18: Roof, ambient, estimated and measured module temperatures for two clear sky days in June with roof temperature adjustment

Figure 4.19 compares module temperature deviations obtained assuming roof temperature is equal to ambient temperature and deviations obtained assuming an adjustment to roof temperature. There is a clear improvement in accuracy of the estimations. While without the adjustment RMSE and MBE of module temperature

estimations are 3.62 and –1.40 ºC for these two sample days; with the roof temperature adjustment RMSE and MBE decreases to 2.33 and –0.31 ºC, respectfully. These correspond to 35.7% reduction in RMSE and 77.9% reduction in MBE.

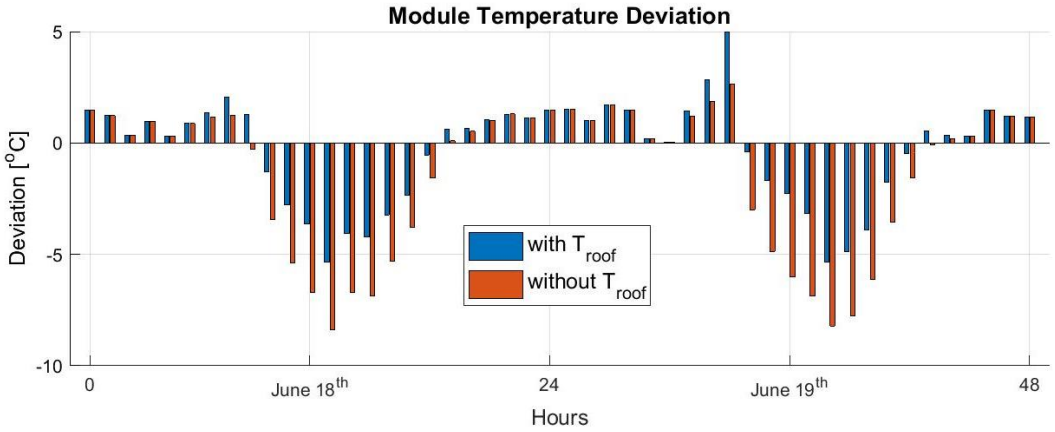

Figure 4.19: Comparison of module temperature deviations with and without roof temperature adjustment

From these values it can be safely concluded that effect of roof temperature on the thermal model is very significant. An accurate roof temperature adjustment depending on the experimental data would improve the performance of the thermal model.

4.3.2. Cloud Cover

Along with roof surface temperature, sky temperature is another parameter affecting the estimations. Sky temperature is calculated from empirical equations, which are the results of the radiative heat transfer experiments. The equation used in the thermal model, which can be found in (37), assumes sky behaves like a blackbody and correlates T_{sky} under the assumption of clear skies. However, when a cloud cover is present in the sky, radiative properties of it change and so does T_{sky}. A cloud cover may increase T_{sky} between 11ºC to 18ºC [95], which is a significant difference considering radiative heat transfer is proportional to 4^{th} power of temperature. Some of the deviations in overcast days may be caused as a cloud cover can skew the results of radiative heat loss estimations like it is demonstrated in section 4.3.1 for roof surface temperature.

4.3.3. Precipitation

One other meteorological phenomenon the thermal model does not recognize is the precipitation. When there is rain or snow, in addition to convective and radiative heat transfer mechanism, evaporative cooling is involved. Since it is hard to estimate the amount of rain and its temperature, this case is not considered. Also, snow will block sunlight when it is accumulated on the PV module surface, a case that can be deduced from the insolation vs measured electrical power output curves. Such days are present within the data considered for the thermal model i.e. the first five days of the January, see Appendix-1, but they are not included in RMSE and MBE of the overall results.

4.3.4. Conductive Heat Transfer

Rate of conductive heat transfer is neglected in the thermal model, which may be a contributing factor in module temperature deviations. As a validation process for the assumption of zero conduction, after the thermal model had run, overall energy balance of the module is checked by replacing the terms in the governing equation, equation (6). Rewriting the equation (6) as;

$$E = Q_{solar} - W_{elec.} - Q_{loss} - \frac{dT_{mod}}{dt} \cdot C_{mod} \qquad (51)$$

where E is the error in the energy balance, calculated values of each term are put into place.

Figure 4.20 shows values of each individual term and resulting E value for a sample summer day. Magnitude of term E is small compared to most of the other terms in the governing equation. It has an average value of 12.41 W/m^2 for the sample day. A consistent overestimation of rate of heat loss during nighttime can be observed. Daytime has more varying values of E with mostly underestimation of either rate of heat transfer or electrical output. These can be caused by a multitude of reasons one of which is the omission of conductive heat transfer. At noon, which is taken as hours between to 1 pm and 3pm with an average insolation 976.9 W/m^2, average ratio distributions of the electrical output, convective and radiative heat transfer with

respect to solar irradiance are 10.25%, 59.33% and 30.62%, respectively. Internal energy change ratio is 0.28%, and it is negligible. Energy balance term has ratio of 1.28% with respect to incoming energy from the Sun, which is very small. From these values, it can be concluded that although thermal model is fairly close to the energy balance with low E values compared to other terms, conductive heat transfer may be considered in the future studies in order to determine its effect on the model performance and potential improvement of the thermal model.

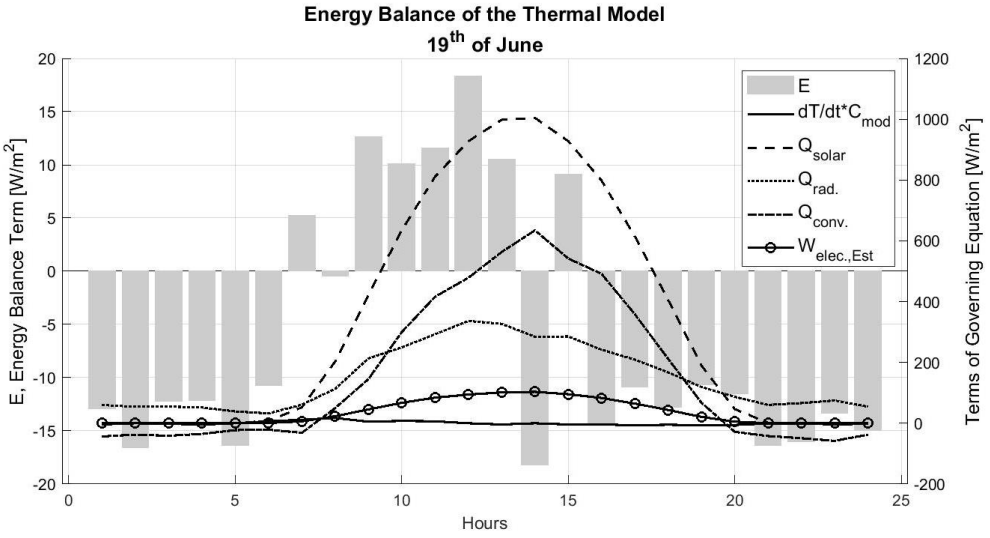

Figure 4.20: Verification of energy balance in the control volume of the PV module

4.3.5. Module Back Surface Temperature and Cell Temperature

Electrical power output correlation in equation (39) uses cell temperature in order to predict efficiency loss due to temperature increase. In the scope of this thesis, module temperature is assumed to be equal to cell temperature since temperature gradient within the laminated structure of the module is neglected. But in reality, cell temperature is higher than the temperature of module back surface. Thermal model mostly overestimates the electrical power output of the module. Therefore, introducing a simple offset in predicted module temperature values to calculate cell temperature will improve the electrical power output predictions. A simple correlation for cell temperature is presented in [45].

$$T_{cell} = T_{mod} + \frac{Q_{solar}}{Q_{solar,ref}} \cdot \Delta T \quad (52)$$

where T_{cell} and T_{mod} are cell and module back surface temperatures respectively, Q_{solar} is incoming solar irradiance and $Q_{solar,ref}$ is the reference solar irradiance, which is equal to 1000W/m^2. ΔT is predetermined difference between module back surface and cell temperature at reference solar irradiance. For open back modules laminated with glass and polymer back sheet, ΔT can be taken as 3ºC [45].

Figure 4.21 depicts monthly RMSE and MBE for electrical power output deviations for the whole year with and without offset in the module temperature. From the figure a clear improvement in electrical power output estimations can be seen.

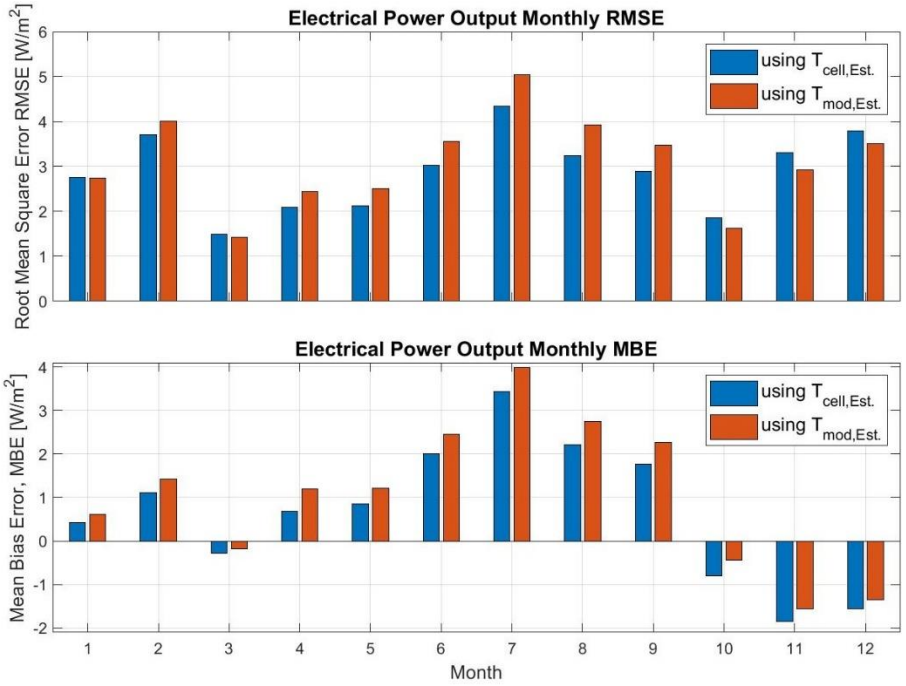

Figure 4.21: RMSE and MBE of electrical output deviations calculated using estimated T_{mod} and T_{cell}.

Using cell temperature RMSE and MBE of electrical power deviations are equal to 2.87 W/m^2 and –0.67 W/m^2, respectively for one year. When there is no offset in module temperature RMSE and MBE are equal to 3.10 W/m^2 and –1.03 W/m^2, respectively. Using calculated cell temperature reduces RMSE by 6.87% and MBE by 35.3%. From these values, it is seen that a significant reduction in electrical power

output deviations are possible with a simple adjustment of module temperature estimations.

4.3.6. Electrical Power Output Correlation

In the thermal model, electrical power output calculation are performed using a correlation shown in the equation (39). This equation is relatively simple. For more accurate power estimations, electrical components of the module and supporting equipment should be considered as well [96]. There are some deviations introduced by simplifying this process with a single correlation.

Figure 4.22 depicts daily RSME of calculated electrical power output deviations using estimated and measured module temperature values the first two weeks of July. Using measured module temperature does not significantly improve the power estimations. The difference between RSME values is small with an average of 1.21 W/m^2, corresponding to 25.3% improvement. However, it was expected that if measured module temperature was used, reduction in deviations would be close to 100%, which is not the case. Therefore, it can be said that, using equation (39) is contributing deviations in electrical power output estimation of the thermal model.

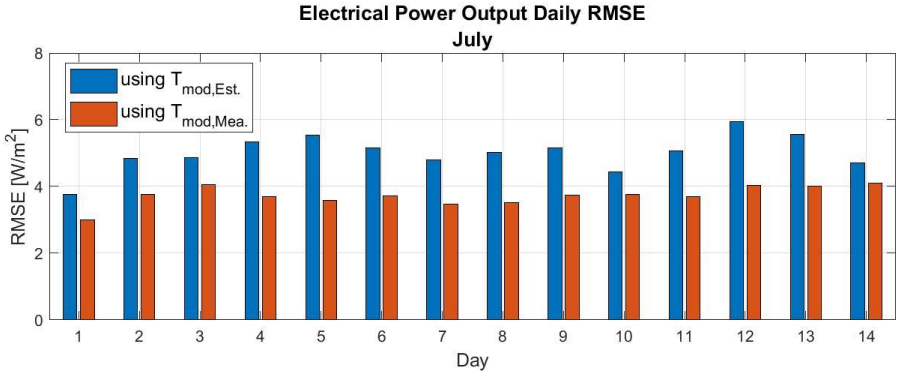

Figure 4.22: Electrical power output calculation with measured and estimated module temperature

In order to evaluate the effect of deviations caused by equation (39), the thermal model was run using measured electrical power output instead of estimated values. Figure 4.23 depicts daily RMSE of daytime module temperatures of the first two weeks of

July calculated by using estimated $W_{elec.}$ and measured $W_{elec.}$ values. The difference between them is very small with an average of 0.092 ºC, corresponding to 2.58% reduction of deviations on average. Therefore, large deviations of module temperature estimations are not sourced from choice of method for electrical power calculation.

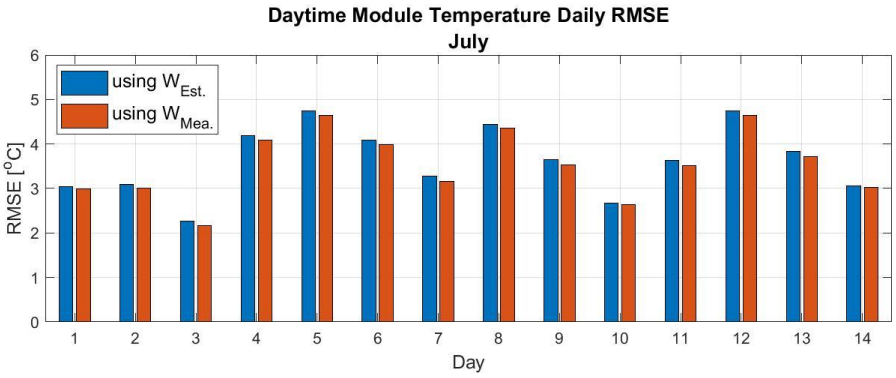

Figure 4.23: Daytime module temperature calculation with measured and estimated electrical power output

4.4. Sensitivity Analysis of the Thermal Model for Heat Capacity of PV Module

Heat capacity of the PV module, C_{mod} is an essential parameter in a dynamic thermal model. But, determining heat capacity of a PV module conclusively can be a difficult task. PV module is a laminated structure that can be composed of very different materials. Properties of these materials like specific heat capacity, density and thickness of the corresponding layers are rarely shared with the public by the manufacturers due to commercial reasons. Most of the time, calculation of heat capacity of the PV module is a guesswork. Hence, it is imperative to know how much choice of heat capacity is affecting the performance of the thermal model. A sensitivity analysis for C_{mod} is carried out to see influence of different C_{mod} values on deviations in module temperature and electrical power output.

Figure 4.24 depicts averaged deviations of temperature and electrical output of the PV module over a range of heat capacity values. A very slight decrease in RMSE of module temperature deviations is observed with increasing C_{mod} values. RMSE of electrical power deviations displays a small increase with rising C_{mod} values. Considering these variations are well under 4% of average RMSEs, the thermal model

is rather insensitive to value of module heat capacity. The reason may be the fact that temperature change of the module is gradual. The system approaches to steady state conditions very quickly with lack of abrupt and large shifts in module temperature. From Figure 4.20 in section 4.3.4, it can be seen that internal energy change has the smallest share in the energy balance with an average of 4.50 W/m^2. Although the heat capacity is calculated to be high, 5723 J/K-m^2, its contribution to energy balance is minimal since time interval of the analysis is one hour. If a smaller interval was considered, the effect of heat capacity is expected to be more visible.

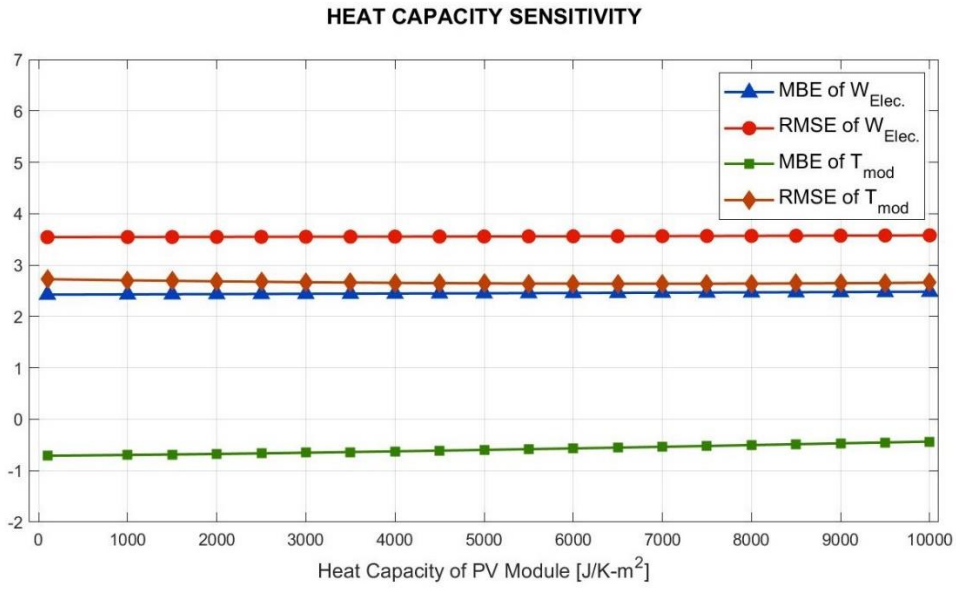

Figure 4.24: Heat capacity sensitivity of the electrical power output and module temperature estimations in April

CHAPTER 5

CONCLUSION

Performance of the PV systems in outdoor conditions is one of the most critical aspects of the feasibility analyses for the effective utilization of the solar energy. Accurate and precise models for performance predictions of PV systems are needed for successful and efficient applications of photovoltaics. Literature provides a variety of models for such task, but majority of them depend on the location or PV solar cell parameters. They do not function well outside of these parameters. Thermal modeling provides a method free of such restrictions by employing energy conservation principles and heat transfer mechanisms to find module temperature and consequently electrical output of a PV module.

In this thesis a transient thermal model for outdoor performance predictions of PV modules has been realized. The model uses meteorological data, module parameters and location/mounting information as inputs. Input data are easily accessible and do not require a pilot testing of the PV module in a specific location, making the developed model very flexible. The model can be implemented for any location and can give reasonably good results.

Wind direction is often disregarded in thermal modeling of PV modules in atmospheric conditions. The study considers wind direction as well as the wind speed in its methodology of heat transfer mechanisms. Characteristics of the flow occurring over the PV module in different wind directions are categorized and correlations for heat transfer are chosen accordingly. The thermal model considers both natural and forced convective and radiative heat loss from the PV module.

The relation between module temperature and electrical power output of the module is modified in this study. A new averaging method for time-dependent transmittance-absorbance product has been developed and implemented in the electrical power output calculation of the PV module.

The thermal model is applied for 1-year hourly data gathered in Outdoor Testing Facility of GÜNAM in Middle East Technical University, Ankara. MATLAB is used for its implementation. It is seen that the model performs well in prediction of the module temperature during the nighttime with and RMSE of 1.33°C. During the day, RMSE for module temperature is elevated to 2.96°C, accompanied with RMSE of 3.08W/m^2 in electrical power output of the PV module. The RMSEs for electrical power output and module temperature are higher in summer compared to winter months. These results are fairly good considering hourly analysis employed for increased utility of the model.

Finally, in order to determine effect of heat capacity of the module on the performance of the thermal model, a sensitivity analysis has been realized. It has been found that value of heat capacity has little to no influence on the performance predictions.

There are multiple possible sources for high deviations like high roof temperature in summer and cloud cover as it was discussed in the section 4.3. These considerations can be included in the thermal model to increase accuracy. And the model can be scaled up to consider large PV arrays or building integrated PVs. But, these systems will bring other challenges like elevated ambient temperature due to PV arrays, wind blocking etc. The thermal model can be modified to address these issues in the future studies such as predicting the performance of large arrays and/or building integrated PV systems.

REFERENCES

[1] K. B. Tokarska and N. P. Gillett, "Cumulative carbon emissions budgets consistent with 1.5 °c global warming," *Nat. Clim. Chang.*, vol. 8, no. 4, pp. 296–299, 2018.

[2] R. S. Nerem, B. D. Beckley, J. T. Fasullo, B. D. Hamlington, D. Masters, and G. T. Mitchum, "Climate-change–driven accelerated sea-level rise detected in the altimeter era," *Proc. Natl. Acad. Sci. U. S. A.*, vol. 115, no. 9, pp. 2022–2025, 2018.

[3] S. C. Herring, M. P. Hoerling, T. C. Peterson, and P. A. Stott, "Explaining extreme events of 2016 from a climate perspective," *Bulletin of the American Meteorological Society*, vol. 95, no. 9. pp. S1–S96, 2014.

[4] A. Dai, T. Zhao, and J. Chen, "Climate Change and Drought: a Precipitation and Evaporation Perspective," *Curr. Clim. Chang. Reports*, vol. 4, no. 3, pp. 301–312, 2018.

[5] R. B. Jackson *et al.*, "Global energy growth is outpacing decarbonization," *Environ. Res. Lett.*, vol. 13, no. 12, 2018.

[6] International Energy Agency (IEA), "World Energy Outlook 2018: The Future is Electrifying," *Oecd/Iea*, 2018.

[7] "Renewable capacity statistics 2018," 2018.

[8] C. Cristofari, G. Notton, P. Poggi, and A. Louche, "Modelling and performance of a copolymer solar water heating collector," *Sol. Energy*, vol. 72, no. 2, pp. 99–112, 2002.

[9] M. A. Alghoul, M. Y. Sulaiman, B. Z. Azmi, and M. abd Wahab, "Review of materials for solar thermal collectors," *Anti-Corrosion Methods Mater.*, vol. 52, no. 4, pp. 199–206, 2005.

[10] E. Z. Moya, "Parabolic-trough concentrating solar power (CSP) systems," *Conc. Sol. Power Technol.*, pp. 197–239, Jan. 2012.

[11] D. R. Mills and G. L. Morrison, "Compact linear fresnel reflector solar thermal powerplants," *Sol. Energy*, vol. 68, no. 3, pp. 263–283, 2000.

[12] O. Behar, A. Khellaf, and K. Mohammedi, "A review of studies on central receiver solar thermal power plants," *Renew. Sustain. Energy Rev.*, vol. 23, pp. 12–39, 2013.

[13] D. Pietruschka, R. Fedrizzi, F. Orioli, R. Söll, and R. Stauss, “Demonstration of three large scale solar process heat applications with different solar thermal collector technologies,” *Energy Procedia*, vol. 30, pp. 755–764, 2012.

[14] L. C. Andreani, A. Bozzola, P. Kowalczewski, M. Liscidini, and L. Redorici, “Silicon solar cells: Toward the efficiency limits,” *Adv. Phys. X*, vol. 4, no. 1, 2019.

[15] E. D. Kosten, J. H. Atwater, J. Parsons, A. Polman, and H. A. Atwater, “Highly efficient GaAs solar cells by limiting light emission angle,” *Light Sci. Appl.*, vol. 2, no. JANUARY, 2013.

[16] M. K. Assadi, S. Bakhoda, R. Saidur, and H. Hanaei, “Recent progress in perovskite solar cells,” *Renew. Sustain. Energy Rev.*, vol. 81, no. October 2016, pp. 2812–2822, 2018.

[17] P. Tonui, S. O. Oseni, G. Sharma, Q. Yan, and G. Tessema Mola, “Perovskites photovoltaic solar cells: An overview of current status,” *Renew. Sustain. Energy Rev.*, vol. 91, no. April, pp. 1025–1044, 2018.

[18] S. M. Menke, N. A. Ran, G. C. Bazan, and R. H. Friend, “Understanding Energy Loss in Organic Solar Cells: Toward a New Efficiency Regime,” *Joule*, vol. 2, no. 1, pp. 25–35, 2018.

[19] I. Etxebarria, J. Ajuria, and R. Pacios, “Solution-processable polymeric solar cells: A review on materials, strategies and cell architectures to overcome 10%,” *Org. Electron. physics, Mater. Appl.*, vol. 19, pp. 34–60, 2015.

[20] V. Sugathan, E. John, and K. Sudhakar, “Recent improvements in dye sensitized solar cells: A review,” *Renew. Sustain. Energy Rev.*, vol. 52, pp. 54–64, 2015.

[21] O. Mohiuddin, M. Obaidullah, and C. Sabah, “Improvement in dye sensitized solar cells from past to present,” *Opt. Quantum Electron.*, vol. 50, no. 10, pp. 1–28, 2018.

[22] G. Bedi and R. Singh, “Quantum dot solar cells,” in *2017 IEEE 17th International Conference on Nanotechnology (IEEE-NANO)*, 2017.

[23] J. Duan, H. Zhang, Q. Tang, B. He, and L. Yu, “Recent advances in critical materials for quantum dot-sensitized solar cells: A review,” *J. Mater. Chem. A*, vol. 3, no. 34, pp. 17497–17510, 2015.

[24] Z. Pan, H. Rao, I. Mora-Seró, J. Bisquert, and X. Zhong, “Quantum dot-sensitized solar cells,” *Chem. Soc. Rev.*, vol. 47, no. 20, pp. 7659–7702, 2018.

[25] N. Aste, C. del Pero, and F. Leonforte, “Water flat plate PV-thermal collectors: A review,” *Sol. Energy*, vol. 102, pp. 98–115, 2014.

[26] A. Chauhan, V. V. Tyagi, and S. Anand, “Futuristic approach for thermal

management in solar PV/thermal systems with possible applications," *Energy Convers. Manag.*, vol. 163, pp. 314–354, 2018.

[27] M. Nicolai, M. Zanuccoli, F. Feldmann, M. Hermle, and C. Fiegna, "Analysis of silicon solar cells with poly-Si/SiOx carrier-selective base and emitter contacts," *IEEE J. Photovoltaics*, vol. 8, no. 1, pp. 103–109, 2018.

[28] G. Friesen, D. Pavanello, and a. Virtuani, "Overview of Temperature Coefficients of Different Thin Film Photovoltaic Technologies," *25th Eur. Photovolt. Sol. Energy Conf. Exhib. / 5th World Conf. Photovolt. Energy Conversion, 6-10 Sept. 2010, Val. Spain*, no. JANUARY, pp. 4248–4252, 2010.

[29] P. Singh and N. M. Ravindra, "Temperature dependence of solar cell performance—an analysis," *Sol. Energy Mater. Sol. Cells*, vol. 101, pp. 36–45, Jun. 2012.

[30] N. M. Ravindra and B. Prasad, "Saturation Current in Solar Cells - an Analysis.," *Sol. Cells Their Sci. Technol. Appl. Econ.*, vol. 2, no. 2, pp. 109–113, 1980.

[31] M. A. Green, *Solar cells: operating principles, technology, and system applications*. Englewood Cliffs, N.J.: Prentice-Hall, Inc., 1982.

[32] T. Özden, D. Tolgay, and B. G. Akinoglu, "Daily and monthly module temperature variation for 9 different modules," *PVCon 2018 - Int. Conf. Photovolt. Sci. Technol.*, 2018.

[33] S. Dubey, J. N. Sarvaiya, and B. Seshadri, "Temperature dependent photovoltaic (PV) efficiency and its effect on PV production in the world - A review," *Energy Procedia*, vol. 33, pp. 311–321, 2013.

[34] E. Skoplaki and J. A. Palyvos, "On the temperature dependence of photovoltaic module electrical performance: A review of efficiency/power correlations," *Sol. Energy*, vol. 83, no. 5, pp. 614–624, 2009.

[35] E. Skoplaki and J. A. Palyvos, "Operating temperature of photovoltaic modules: A survey of pertinent correlations," *Renew. Energy*, vol. 34, no. 1, pp. 23–29, 2009.

[36] R. G. Ross, "Interface design consideration for terrestrial solar cell modules," in *Proceedings of the 12th IEEE Photovoltaic Specialists Conference*, 1976, pp. 801–806.

[37] J. D. Mondol, Y. G. Yohanis, and B. Norton, "Comparison of measured and predicted long term performance of grid a connected photovoltaic system," *Energy Convers. Manag.*, vol. 48, no. 4, pp. 1065–1080, 2007.

[38] A. Luque and S. Hegedus, *Handbook of Photovoltaic Science and Engineering*. 2011.

[39] A. G. Gaglia, S. Lykoudis, A. A. Argiriou, C. A. Balaras, and E. Dialynas, “Energy efficiency of PV panels under real outdoor conditions–An experimental assessment in Athens, Greece,” *Renew. Energy*, vol. 101, pp. 236–243, 2017.

[40] E. Skoplaki, A. G. Boudouvis, and J. A. Palyvos, “A simple correlation for the operating temperature of photovoltaic modules of arbitrary mounting,” *Sol. Energy Mater. Sol. Cells*, vol. 92, no. 11, pp. 1393–1402, 2008.

[41] G. Tamizhmani, L. Ji, Y. Tang, L. Petacci, and C. Osterwald, “Photovoltaic Module Thermal / Wind Performance : Long -Term Monitoring and Model Development For Energy Rating,” *NCPV Sol. Progr. Rev. Meet.*, pp. 936–939, 2003.

[42] D. Faiman, “Assessing the outdoor operating temperature of photovoltaic modules,” *Prog. Photovoltaics Res. Appl.*, vol. 16, no. 4, pp. 307–315, 2008.

[43] E. Barykina and A. Hammer, “Modeling of photovoltaic module temperature using Faiman model : Sensitivity analysis for different climates,” *Sol. Energy*, vol. 146, pp. 401–416, 2017.

[44] F. Bizzarri, M. Bongiorno, A. Brambilla, G. Gruosso, and G. S. Gajani, “Model of photovoltaic power plants for performance analysis and production forecast,” *IEEE Trans. Sustain. Energy*, vol. 4, no. 2, pp. 278–285, 2013.

[45] D. L. King, J. a Kratochvil, and W. E. Boyson, “Photovoltaic array performance model,” *Online*, vol. 8, no. December, pp. 1–19, 2004.

[46] D. L. King, “Photovoltaic module and array performance characterization methods for all system operating conditions,” pp. 347–368, 2008.

[47] M. Mattei, G. Notton, C. Cristofari, M. Muselli, and P. Poggi, “Calculation of the polycrystalline PV module temperature using a simple method of energy balance,” *Renew. Energy*, vol. 31, no. 4, pp. 553–567, 2006.

[48] J. K. Kaldellis, M. Kapsali, and K. A. Kavadias, “Temperature and wind speed impact on the efficiency of PV installations. Experience obtained from outdoor measurements in Greece,” *Renew. Energy*, vol. 66, pp. 612–624, 2014.

[49] N. Gökmen, W. Hu, P. Hou, Z. Chen, D. Sera, and S. Spataru, “Investigation of wind speed cooling effect on PV panels in windy locations,” *Renew. Energy*, vol. 90, pp. 283–290, 2016.

[50] M. Koehl, M. Heck, S. Wiesmeier, and J. Wirth, “Modeling of the nominal operating cell temperature based on outdoor weathering,” *Sol. Energy Mater. Sol. Cells*, vol. 95, no. 7, pp. 1638–1646, 2011.

[51] C. Correa-Betanzo, H. Calleja, and S. De León-Aldaco, “Module temperature models assessment of photovoltaic seasonal energy yield,” *Sustain. Energy Technol. Assessments*, vol. 27, no. January, pp. 9–16, 2018.

[52] C. Coskun, U. Toygar, O. Sarpdag, and Z. Oktay, “Sensitivity analysis of implicit correlations for photovoltaic module temperature: A review,” *J. Clean. Prod.*, vol. 164, pp. 1474–1485, 2017.

[53] S. Armstrong and W. G. Hurley, “A thermal model for photovoltaic panels under varying atmospheric conditions,” *Appl. Therm. Eng.*, vol. 30, no. 11–12, pp. 1488–1495, 2010.

[54] L. Migliorini, L. Molinaroli, R. Simonetti, and G. Manzolini, “Development and experimental validation of a comprehensive thermoelectric dynamic model of photovoltaic modules,” *Sol. Energy*, vol. 144, pp. 489–501, 2017.

[55] Y. Lee, C. J. Kuo, W. Weng, C. Huang, and C. Peng, “Dynamic modeling and entity validation of a photovoltaic system,” *Appl. Energy*, vol. 200, pp. 370–382, 2017.

[56] M. Sahli, J. P. M. Correia, S. Ahzi, and S. Touchal, “Multi-physics modeling and simulation of heat and electrical yield generation in photovoltaics,” *Sol. Energy Mater. Sol. Cells*, vol. 180, no. April 2017, pp. 358–372, 2018.

[57] M. U. Siddiqui and A. F. M. Arif, “Electrical, thermal and structural performance of a cooled PV module: Transient analysis using a multiphysics model,” *Appl. Energy*, vol. 112, pp. 300–312, 2013.

[58] Y. Du, W. Tao, Y. Liu, J. Jiang, and H. Huang, “Heat transfer modeling and temperature experiments of crystalline silicon photovoltaic modules,” *Sol. Energy*, vol. 146, pp. 257–263, 2017.

[59] M. Usama Siddiqui, A. F. M. Arif, L. Kelley, and S. Dubowsky, “Three-dimensional thermal modeling of a photovoltaic module under varying conditions,” *Sol. Energy*, vol. 86, no. 9, pp. 2620–2631, 2012.

[60] G. Notton, C. Cristofari, M. Mattei, and P. Poggi, “Modelling of a double-glass photovoltaic module using finite differences,” *Appl. Therm. Eng.*, vol. 25, no. 17–18, pp. 2854–2877, Dec. 2005.

[61] D. Torres Lobera and S. Valkealahti, “Dynamic thermal model of solar PV systems under varying climatic conditions,” *Sol. Energy*, vol. 93, pp. 183–194, 2013.

[62] D. Torres-Lobera and S. Valkealahti, “Inclusive dynamic thermal and electric simulation model of solar PV systems under varying atmospheric conditions,” *Sol. Energy*, vol. 105, pp. 632–647, 2014.

[63] M. Malinek *et al.*, “Modelling of Photovoltaic Module Convective Heat Transfer Coefficient,” pp. 877–882, 2016.

[64] R. S. Balog, Y. Kuai, and G. Uhrhan, “A photovoltaic module thermal model using observed insolation and meteorological data to support a long life, highly reliable module-integrated inverter design by predicting expected operating

temperature," in *2009 IEEE Energy Conversion Congress and Exposition, ECCE 2009*, 2009, pp. 3343–3349.

[65] V. Poulek, T. Matuška, M. Libra, E. Kachalouski, and J. Sedláček, "Influence of increased temperature on energy production of roof integrated PV panels," *Energy Build.*, vol. 166, pp. 418–425, 2018.

[66] J. A. Del Cueto, "Model for the thermal characteristics of flat-plate photovoltaic modules deployed at fixed tilt," *Conf. Rec. IEEE Photovolt. Spec. Conf.*, vol. 2000-Janua, pp. 1441–1445, 2000.

[67] J. cheng Zhou, Z. Zhang, H. jian Liu, and Q. Yi, "Temperature distribution and back sheet role of polycrystalline silicon photovoltaic modules," *Appl. Therm. Eng.*, vol. 111, pp. 1296–1303, 2017.

[68] E. Kaplani and S. Kaplanis, "Thermal modelling and experimental assessment of the dependence of PV module temperature on wind velocity and direction, module orientation and inclination," *Sol. Energy*, vol. 107, pp. 443–460, 2014.

[69] I. R. Caluianu and F. Bălătreţu, "Thermal modelling of a photovoltaic module under variable free convection conditions," *Appl. Therm. Eng.*, vol. 33–34, no. 1, pp. 86–91, 2012.

[70] C. Schwingshackl *et al.*, "Wind effect on PV module temperature: Analysis of different techniques for an accurate estimation," *Energy Procedia*, vol. 40, pp. 77–86, 2013.

[71] M. Akhsassi *et al.*, "Experimental investigation and modeling of the thermal behavior of a solar PV module," *Sol. Energy Mater. Sol. Cells*, vol. 180, no. June 2017, pp. 271–279, 2018.

[72] I. Santiago, D. Trillo-Montero, I. M. Moreno-Garcia, V. Pallarés-López, and J. J. Luna-Rodríguez, "Modeling of photovoltaic cell temperature losses: A review and a practice case in South Spain," *Renew. Sustain. Energy Rev.*, vol. 90, no. March, pp. 70–89, 2018.

[73] M. R. Maghami, H. Hizam, C. Gomes, M. A. Radzi, M. I. Rezadad, and S. Hajighorbani, "Power loss due to soiling on solar panel: A review," *Renew. Sustain. Energy Rev.*, vol. 59, pp. 1307–1316, 2016.

[74] T. Fujii and H. Imura, "Natural-convection heat transfer from a plate with arbitrary inclination," *Int. J. Heat Mass Transf.*, vol. 15, no. 4, pp. 755–767, Apr. 1972.

[75] T. L. Bergman, A. S. Lavine, F. P. Incropera, and D. P. Dewitt, *Fundamentals of Heat and Mass Transfer*, 7th ed. 2011.

[76] E. M. Sparrow and K. K. Tien, "Forced Convection Heat Transfer at an Inclined and Yawed Square Plate—Application to Solar Collectors," *J. Heat Transfer*, vol. 99, no. 4, p. 507, 1997.

[77] P. Berdahl and M. Martin, “Emissivity of clear skies,” *Sol. Energy*, vol. 32, no. 5, pp. 663–664, 1984.

[78] D. Kumar and S. Shekhar, “Statistical analysis of land surface temperature–vegetation indexes relationship through thermal remote sensing,” *Ecotoxicol. Environ. Saf.*, vol. 121, pp. 39–44, Nov. 2015.

[79] M. Abdolzadeh and T. Zarei, “Optical and thermal modeling of a photovoltaic module and experimental evaluation of the modeling performance,” *Environ. Prog. Sustain. Energy*, vol. 36, no. 1, pp. 277–293, 2017.

[80] M. Hammami, S. Torretti, F. Grimaccia, and G. Grandi, “Thermal and Performance Analysis of a Photovoltaic Module with an Integrated Energy Storage System,” *Appl. Sci.*, vol. 7, no. 11, p. 1107, 2017.

[81] M. Bardhi, G. Grandi, and G. M. Tina, “Comparison of PV Cell Temperature Estimation by Different Thermal Power Exchange Calculation Methods,” *Renew. Energy Power Qual. J.*, vol. 1, no. 10, pp. 653–658, 2017.

[82] B. W. A. Duffie John A., *Solar Engineering of Thermal Processes.pdf*, 4th ed. 2013.

[83] A. D. Jones and C. P. Underwood, “A thermal model for photovoltaic systems,” *Sol. Energy*, vol. 70, no. 4, pp. 349–359, Jan. 2001.

[84] M. Brogren, P. Nostell, and B. Karlsson, “Optical efficiency of a PV-thermal hybrid CPC module for high latitudes,” *Sol. Energy*, vol. 69, pp. 173–185, 2000.

[85] J. H. Eckstein, “Detailed Modelling of Phtovoltaic System Components,” 1990.

[86] A. A. Hegazy, “Comparative study of the performances of four photovoltaic/thermal solar air collectors,” *Energy Convers. Manag.*, vol. 41, no. 8, pp. 861–881, 2000.

[87] “MATLAB Function Reference: fzero.” [Online]. Available: http://www.ece.northwestern.edu/local-apps/matlabhelp/techdoc/ref/fzero.html#999916.

[88] Y. Cengel, “Appendix 1 - Property tables and charts (SI units),” in *Heat Transfer A pratical Approach*, 2003, p. 992.

[89] Mikron Instrument Company, “Table of Emissivity of Various Surfaces,” pp. 1–13, 2014.

[90] R. T. A. Prado and F. L. Ferreira, “Measurement of albedo and analysis of its influence the surface temperature of building roof materials,” *Energy Build.*, vol. 37, no. 4, pp. 295–300, 2005.

[91] R. D. Clear, L. Gartland, and F. C. Winkelmann, “An empirical correlation for

the outside convective air-film coefficient for horizontal roofs," *Energy Build.*, vol. 35, no. 8, pp. 797–811, 2003.

[92] V. Garg *et al.*, "Assessment of the impact of cool roofs in rural buildings in India," *Energy Build.*, vol. 114, pp. 156–163, 2016.

[93] K. K. Roman, T. O'Brien, J. B. Alvey, and O. J. Woo, "Simulating the effects of cool roof and PCM (phase change materials) based roof to mitigate UHI (urban heat island) in prominent US cities," *Energy*, vol. 96, pp. 103–117, 2016.

[94] L. L. H. Peng *et al.*, "Thermal and energy performance of two distinct green roofs: Temporal pattern and underlying factors in a subtropical climate," *Energy Build.*, vol. 185, pp. 247–258, 2019.

[95] A. H. Maghrabi, "Modification of the IR sky temperature under different atmospheric conditions in an arid region in central Saudi Arabia: Experimental and theoretical justification," *J. Geophys. Res. Atmos.*, vol. 117, no. 19, 2012.

[96] J. S. Stein and B. Farnung, "PV Performance Modeling Methods and Practices Results from the 4th PV Performance Modelling Collaborative Workshop," 2017.

APPENDICES

A. Extended Results

Detailed results of thermal model for 1-year interval are provided in this section. for each month three graphs are plotted. First graph shows weather conditions with insolation, wind speed and direction, also presents calculated values of Rayleigh and Reynolds numbers. Second graph contains module temperature estimations and deviations along with ambient temperature for reference. Third graph shows estimated and measured electrical power output of the PV module and estimated efficiency. It also includes rate of convective and radiative heat transfer from the PV module.

Note that there are some problems with the data and measurements that create large deviations that are not caused by the model. Due to equipment maintenance problems, some of the electrical power output measurements were incorrect, especially around noon in March. These results are excluded in overall assessment of the thermal model. Also, winter days during snow storms were not considered in the MBE and RMSE values due to accumulation of snow on PV module surface.

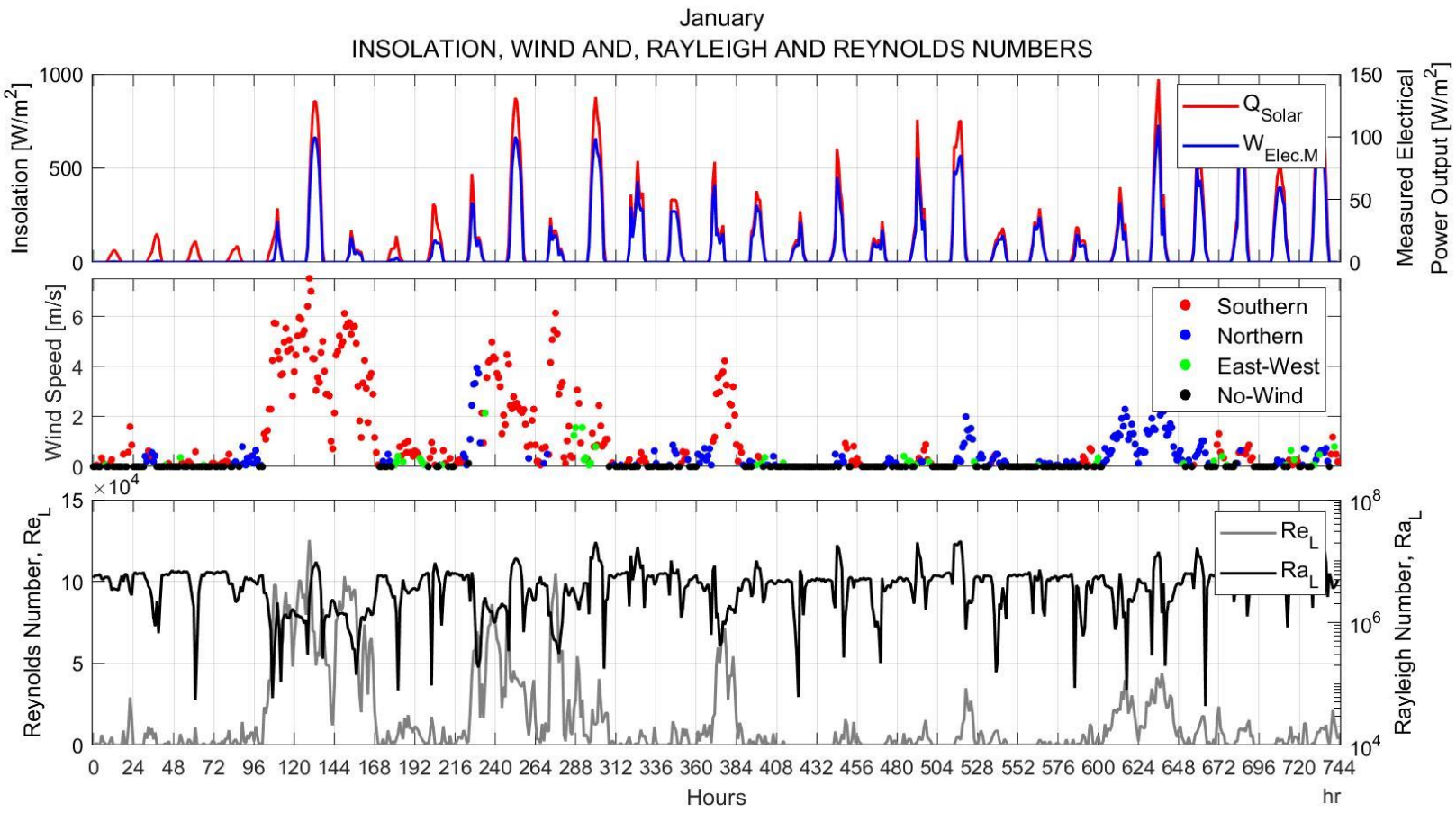

Figure A. 1: Solar irradiation and measured module electrical power output (Graph 1), wind speed and direction (Graph 2), Rayleigh and Reynolds numbers (Graph 3) for January

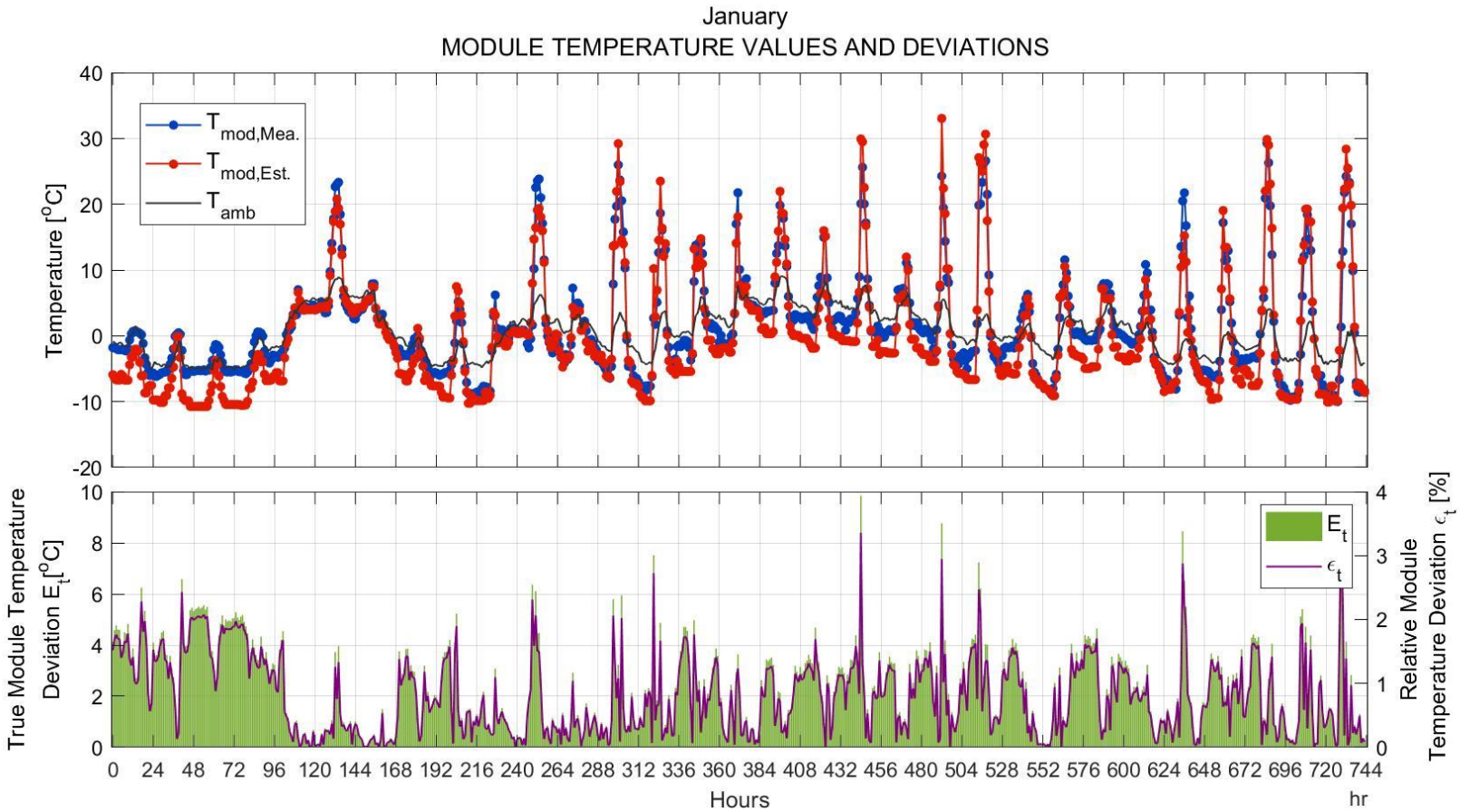

Figure A. 2: Estimated and measured module temperature, ambient, dew point and sky temperatures (Graph 1), deviations of estimated module temperature (Graph 2) for January

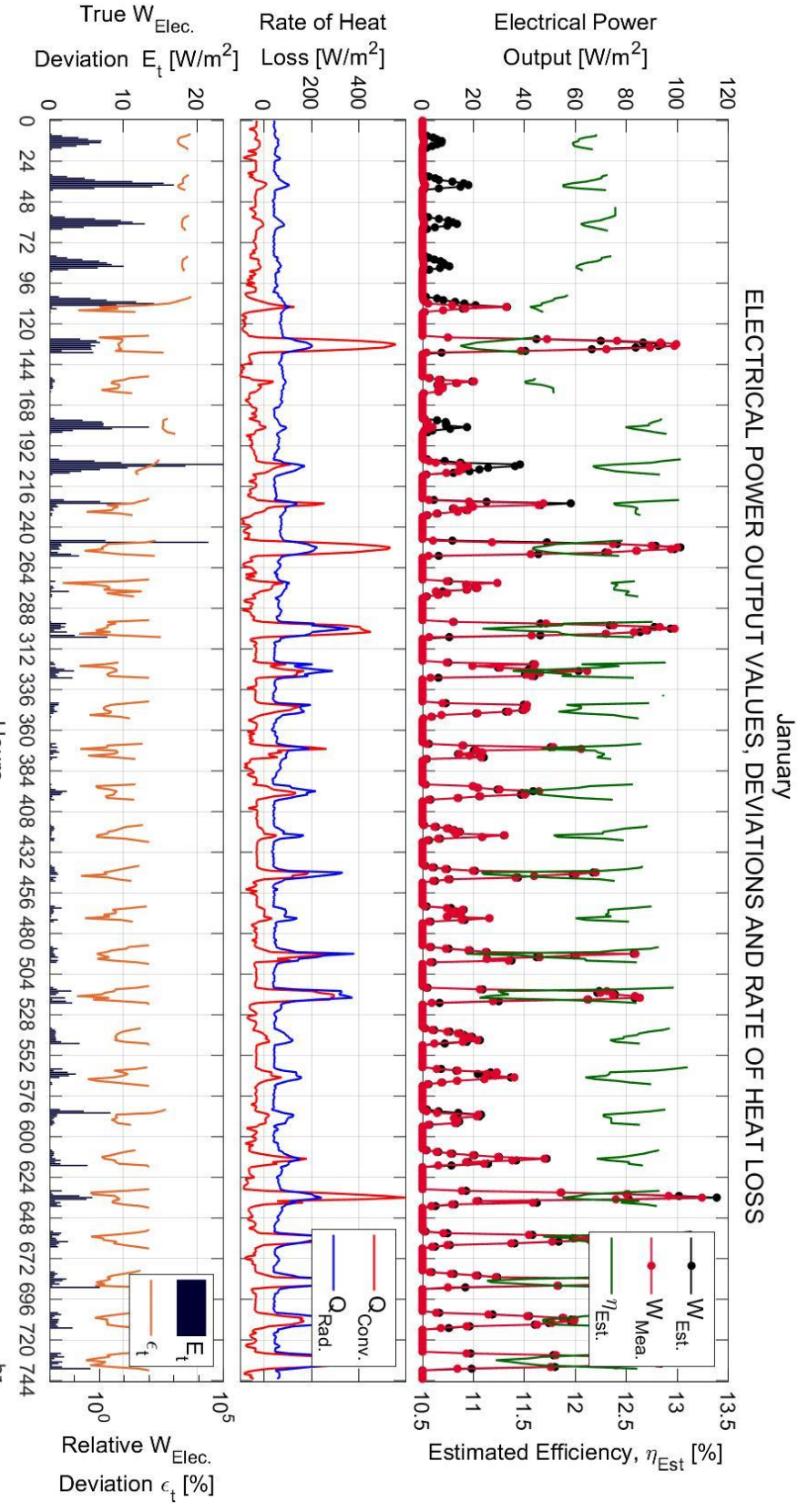

Figure A. 3: Estimated and measured module electrical power output and estimated efficiency (Graph 1), rate of convective and radiative heat transfer (Graph 2), deviations of estimated module electrical power output (Graph 3) for January

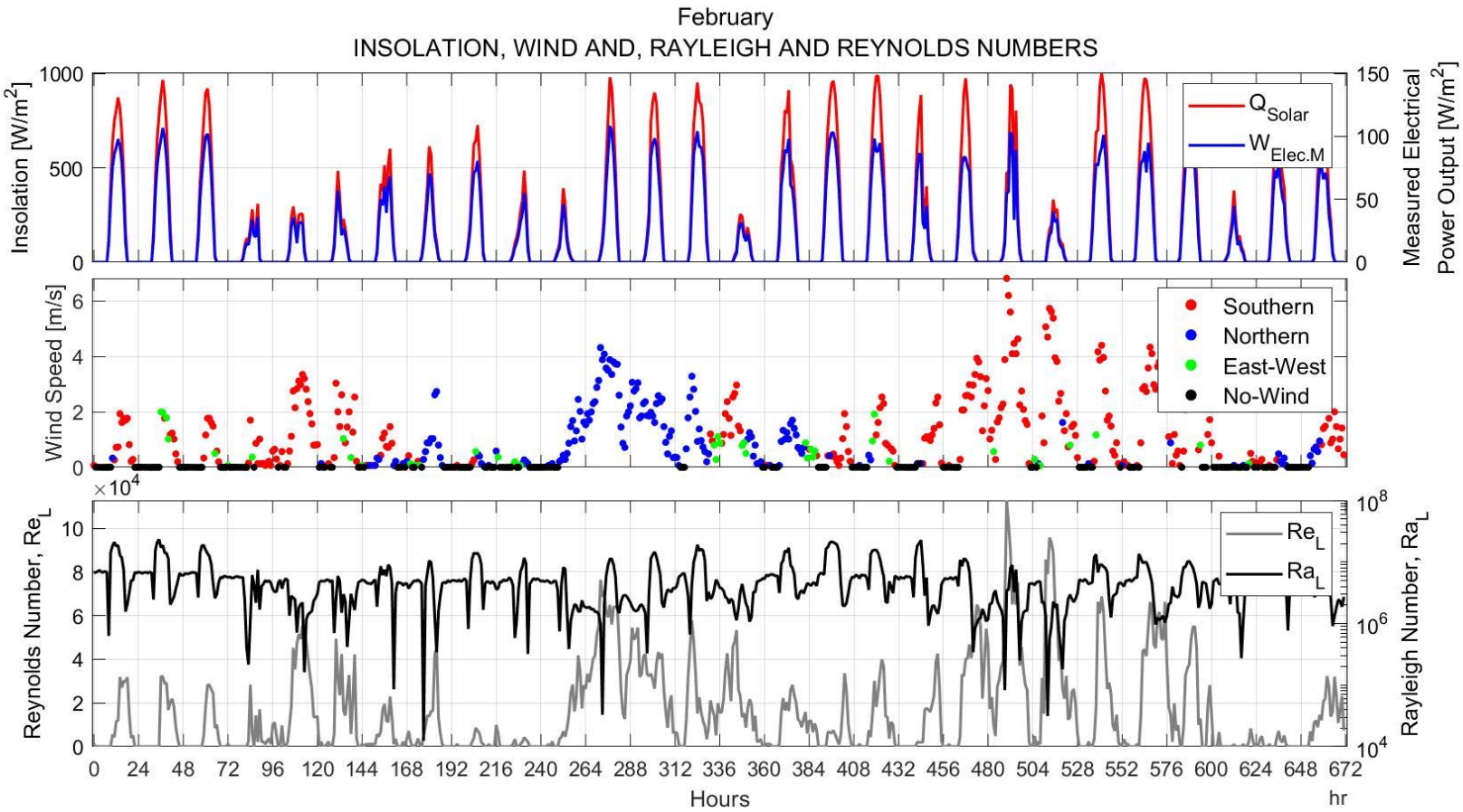

Figure A. 4: Solar irradiation and measured module electrical power output (Graph 1), wind speed and direction (Graph 2), Rayleigh and Reynolds numbers (Graph 3) for February

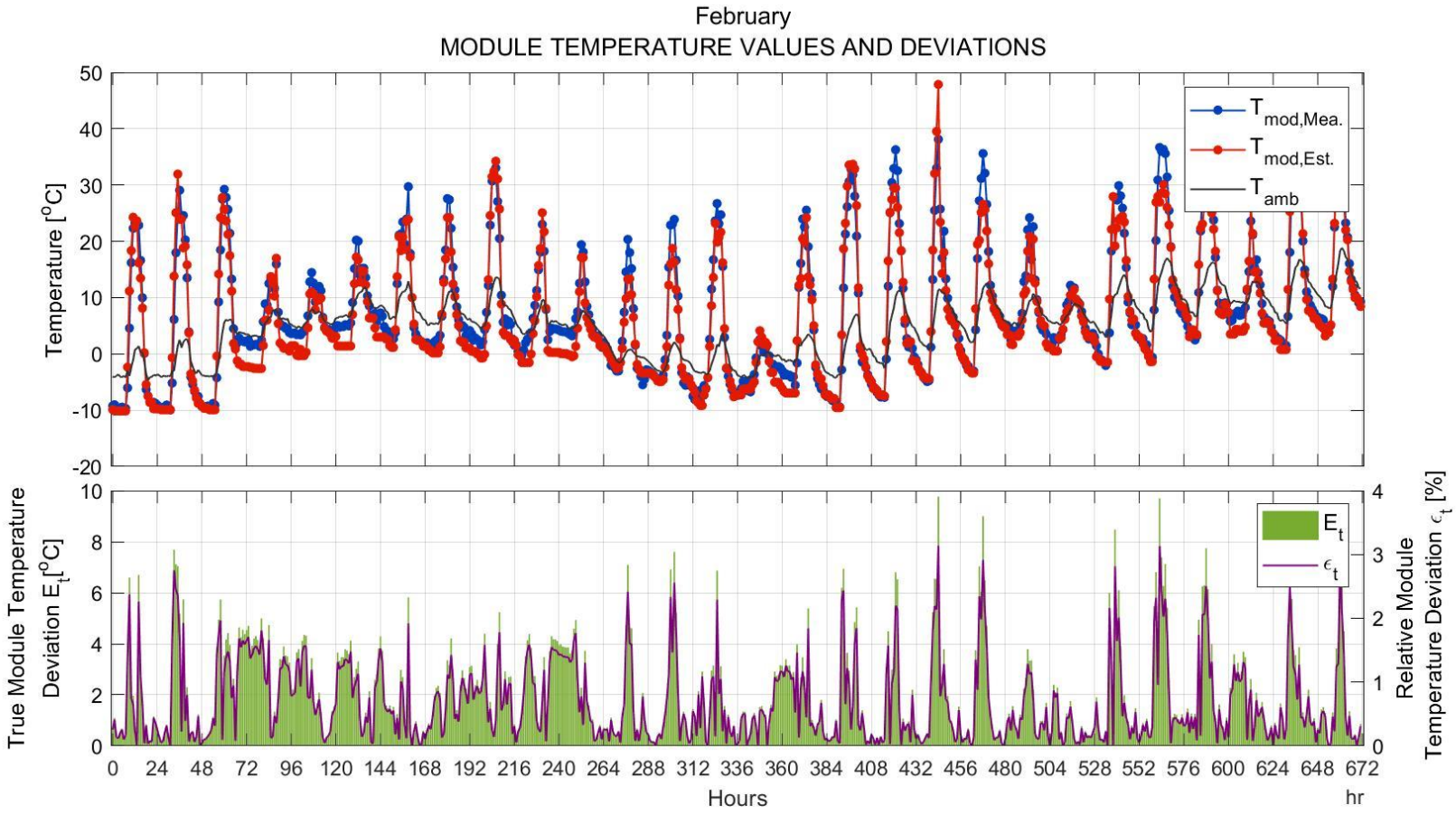

Figure A. 5: Estimated and measured module temperature, ambient, dew point and sky temperatures (Graph 1), deviations of estimated module temperature (Graph 2) for February

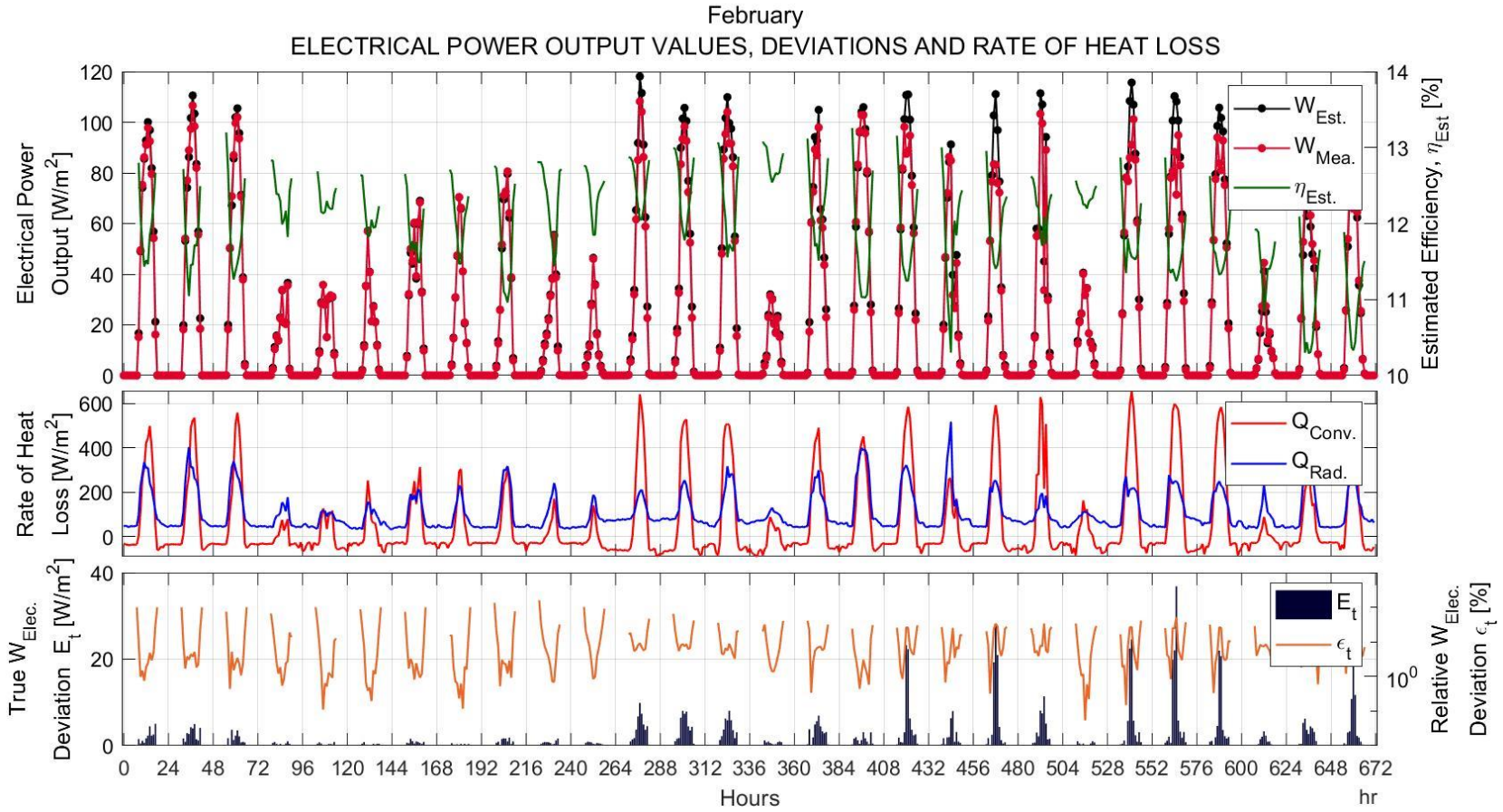

Figure A. 6: Estimated and measured module electrical power output and estimated efficiency (Graph 1), rate of convective and radiative heat transfer (Graph 2), deviations of estimated module electrical power output (Graph 3) for February

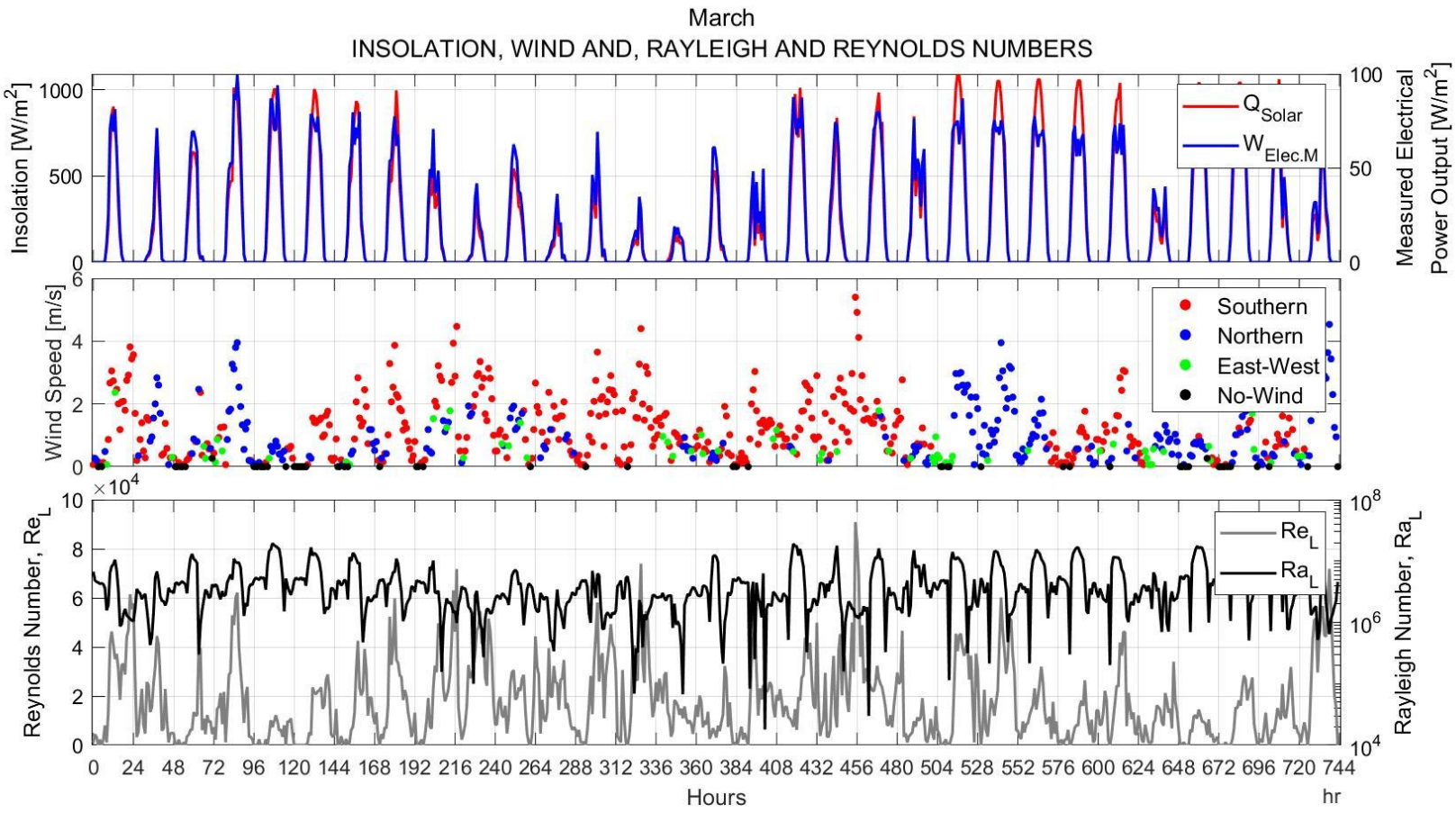

Figure A. 7: Solar irradiation and measured module electrical power output (Graph 1), wind speed and direction (Graph 2), Rayleigh and Reynolds numbers (Graph 3) for March

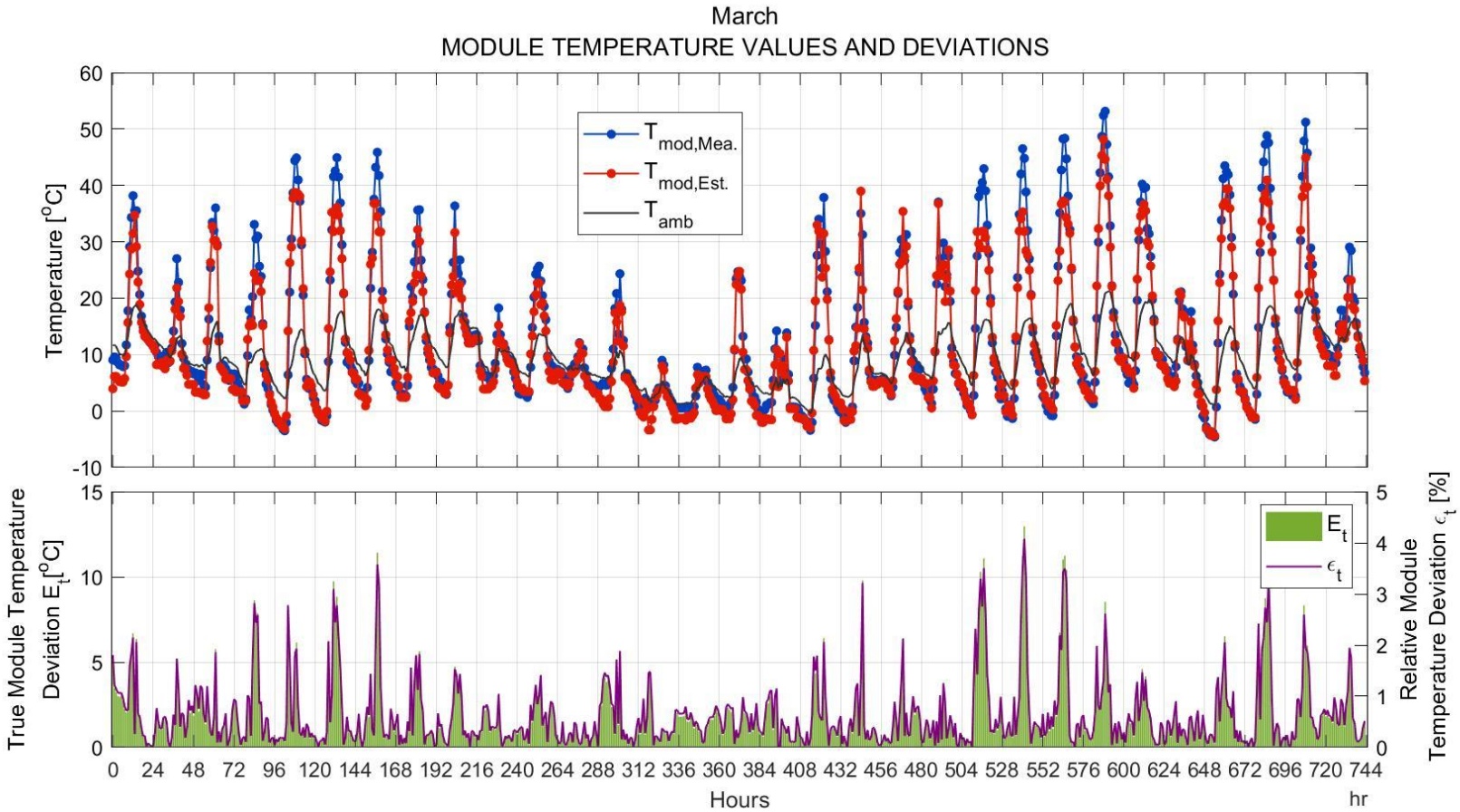

Figure A. 8: Estimated and measured module temperature, ambient, dew point and sky temperatures (Graph 1), deviations of estimated module temperature (Graph 2) for March

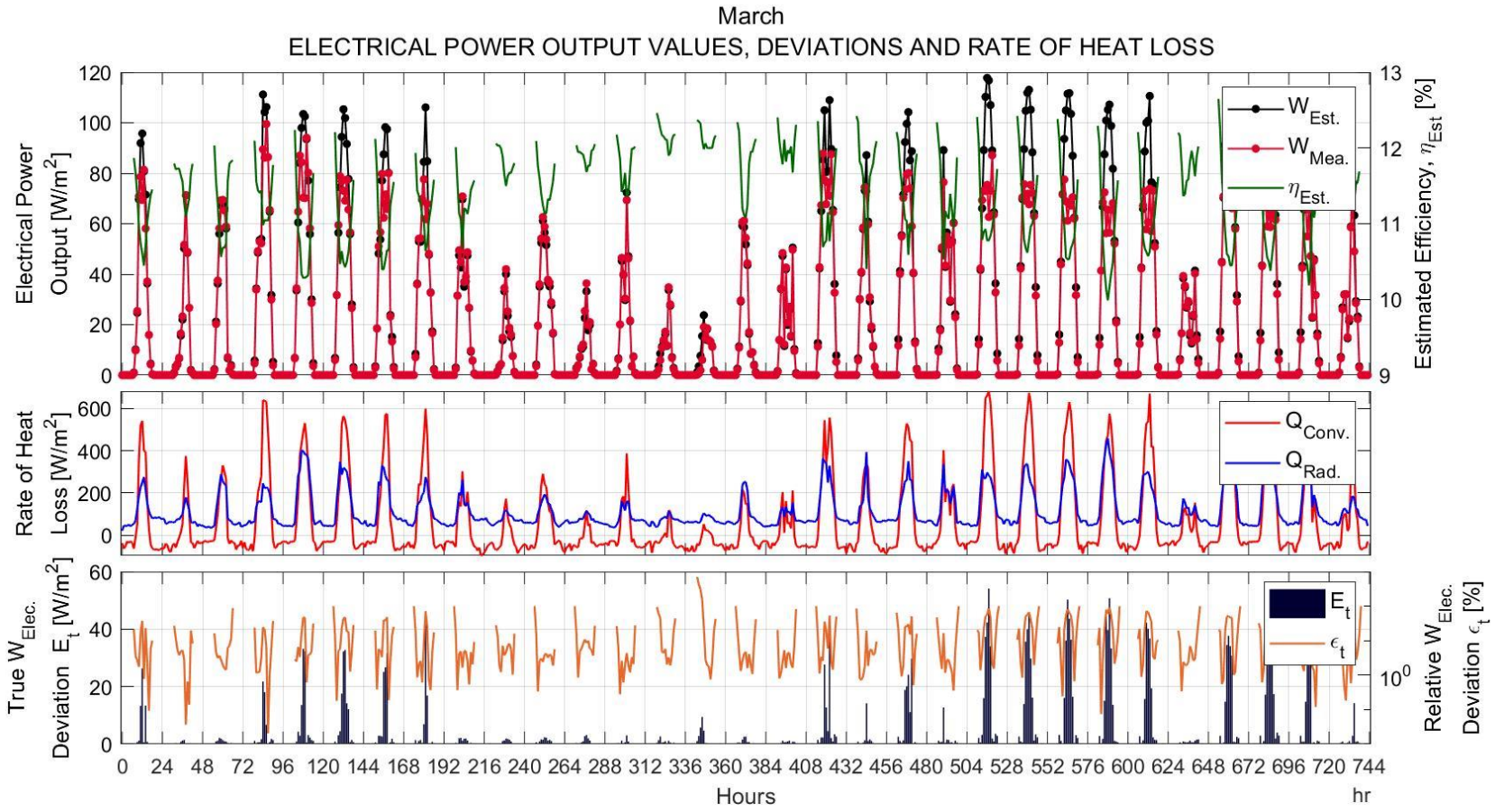

Figure A. 9: Estimated and measured module electrical power output and estimated efficiency (Graph 1), rate of convective and radiative heat transfer (Graph 2), deviations of estimated module electrical power output (Graph 3) for March

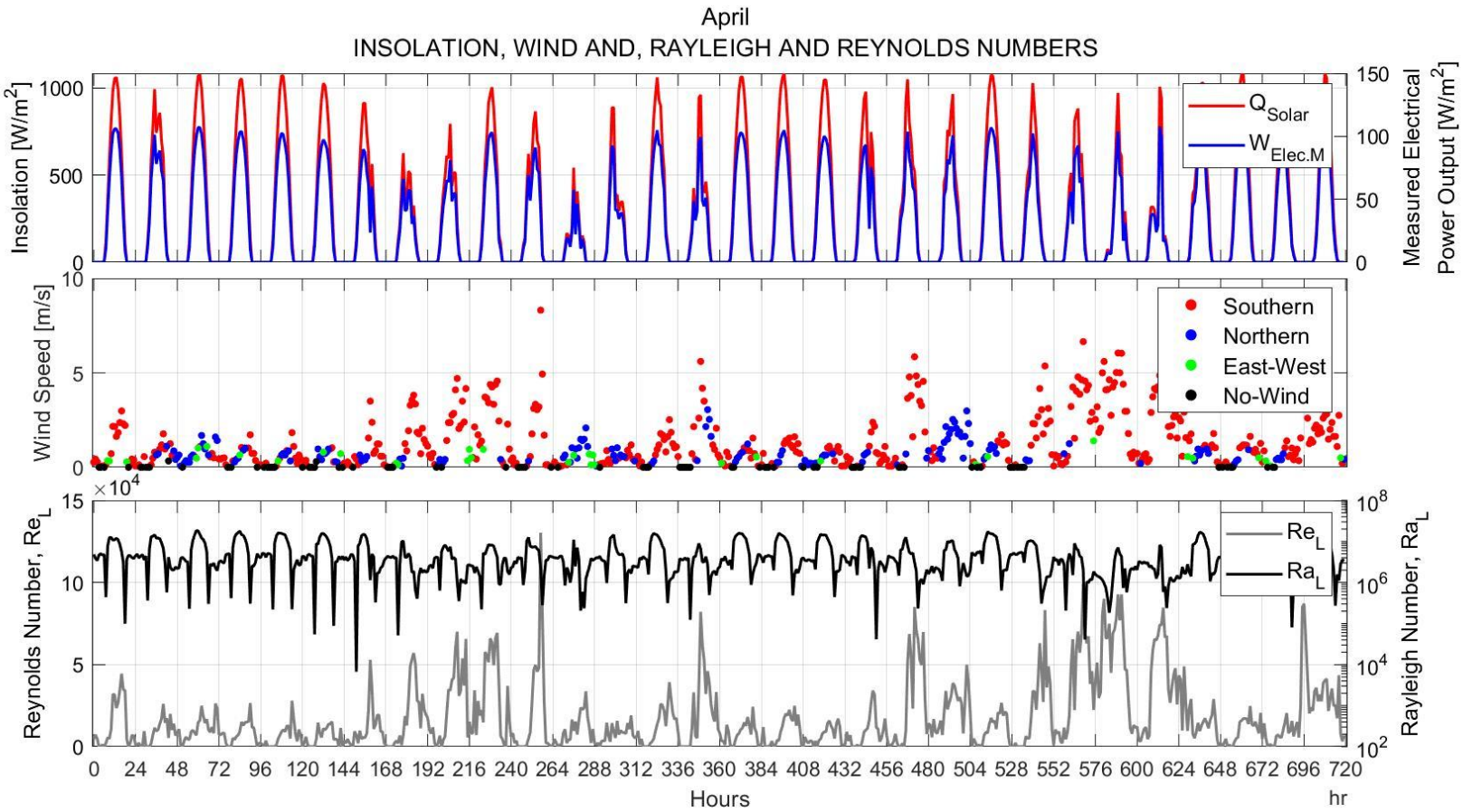

Figure A. 10: Solar irradiation and measured module electrical power output (Graph 1), wind speed and direction (Graph 2), Rayleigh and Reynolds numbers (Graph 3) for April

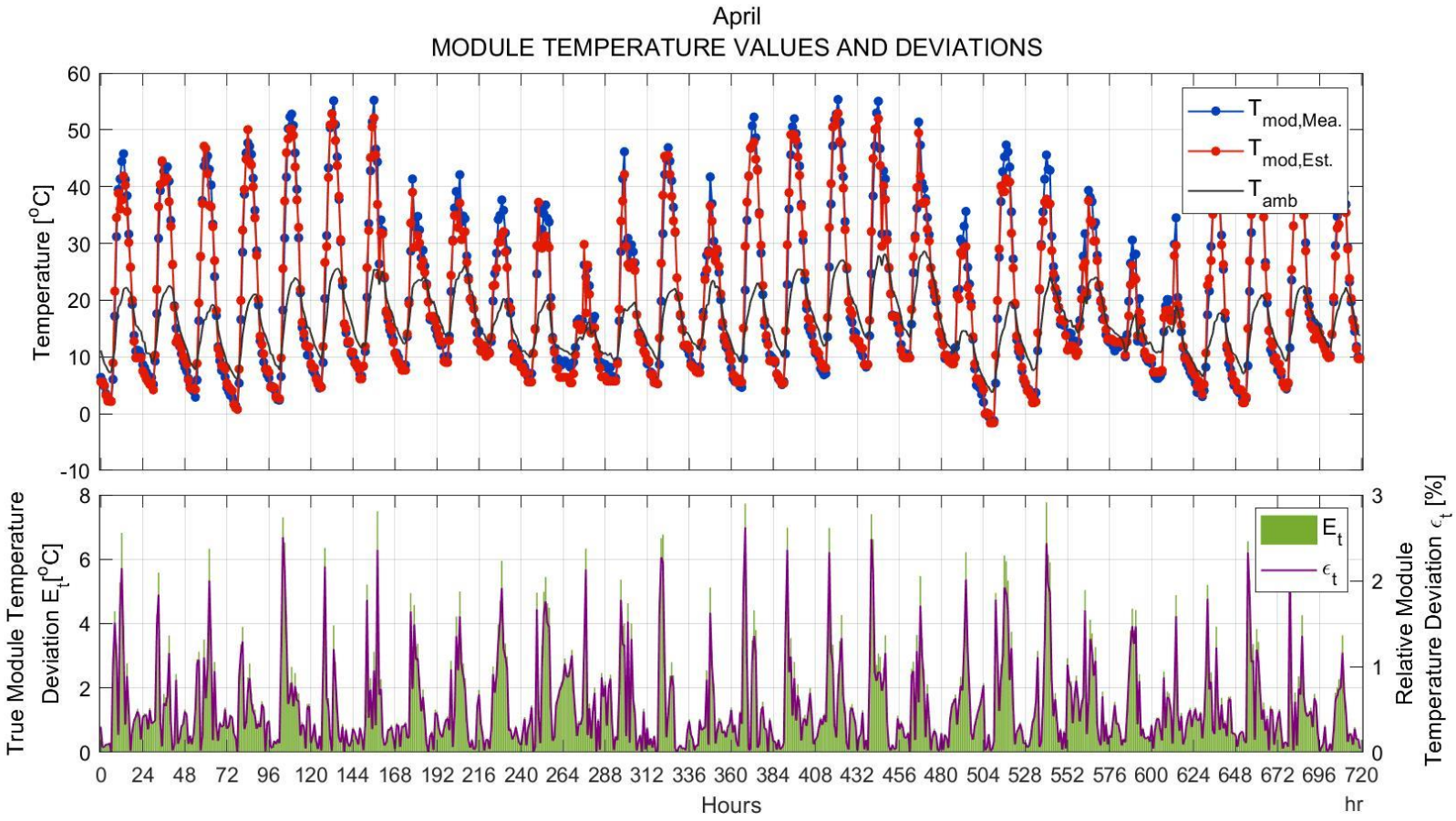

Figure A. 11: Estimated and measured module temperature, ambient, dew point and sky temperatures (Graph 1), deviations of estimated module temperature (Graph 2) for March

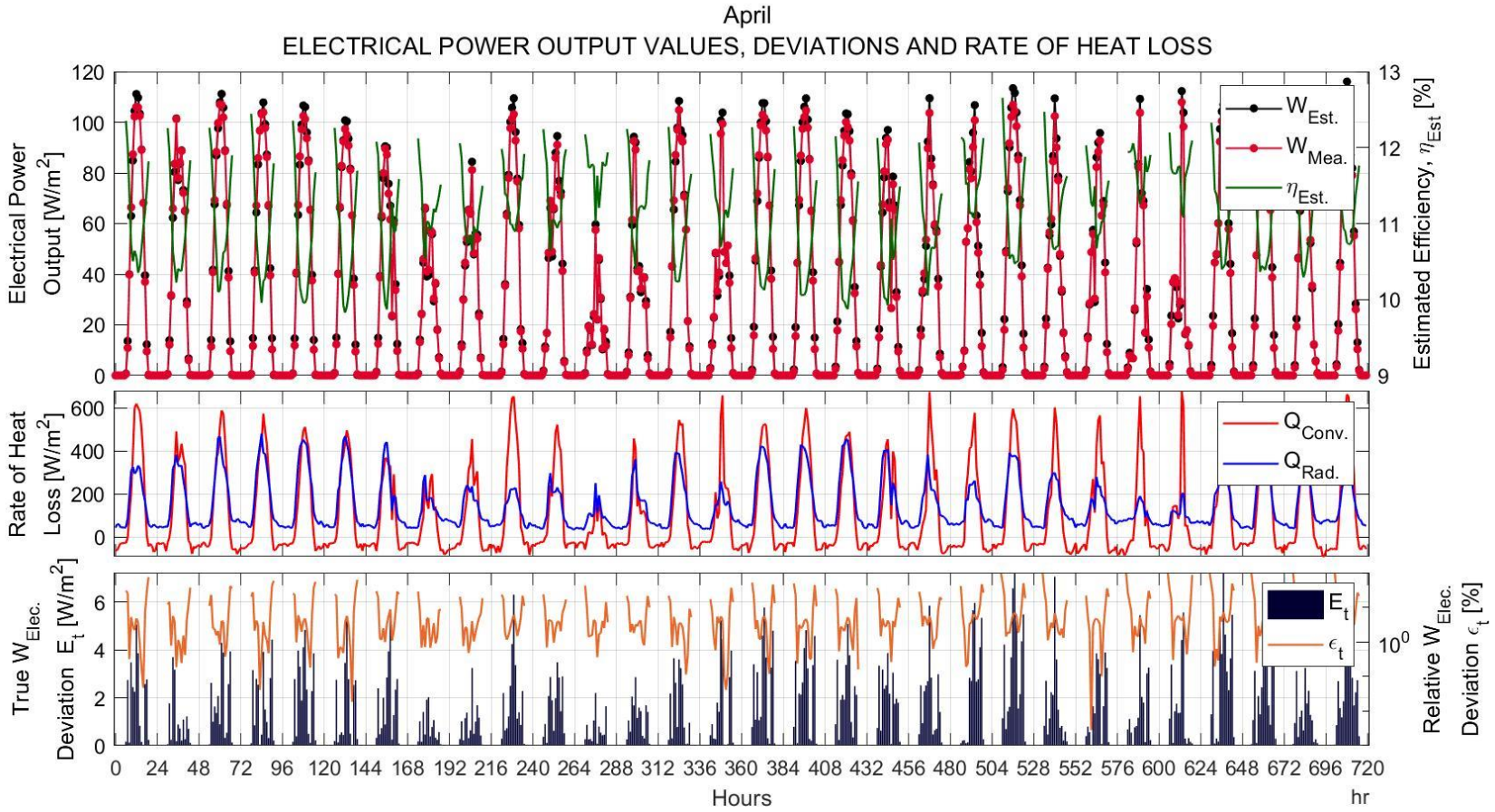

Figure A. 12: Estimated and measured module electrical power output and estimated efficiency (Graph 1), rate of convective and radiative heat transfer (Graph 2), deviations of estimated module electrical power output (Graph 3) for March

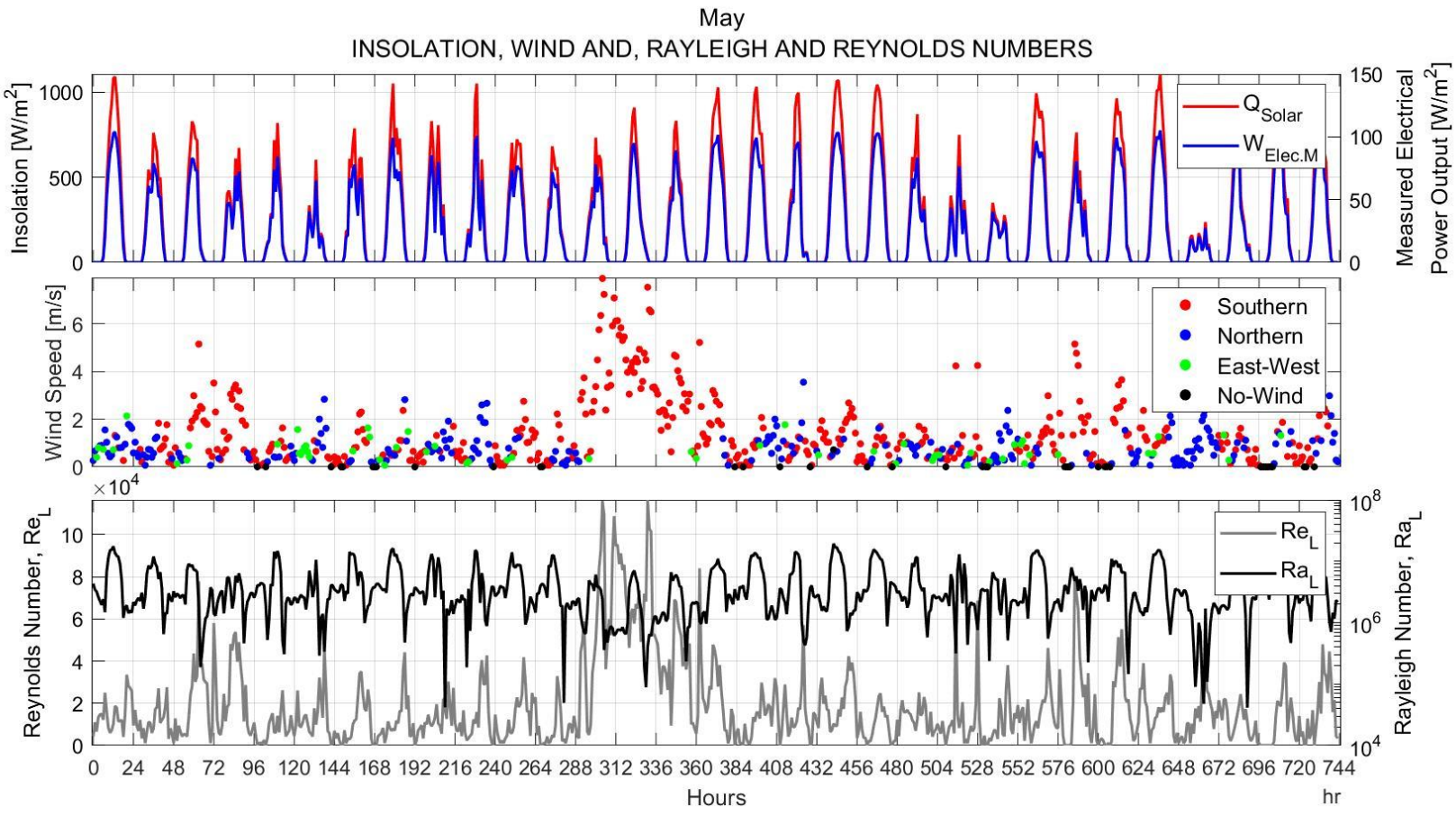

Figure A. 13: Solar irradiation and measured module electrical power output (Graph 1), wind speed and direction (Graph 2), Rayleigh and Reynolds numbers (Graph 3) for May

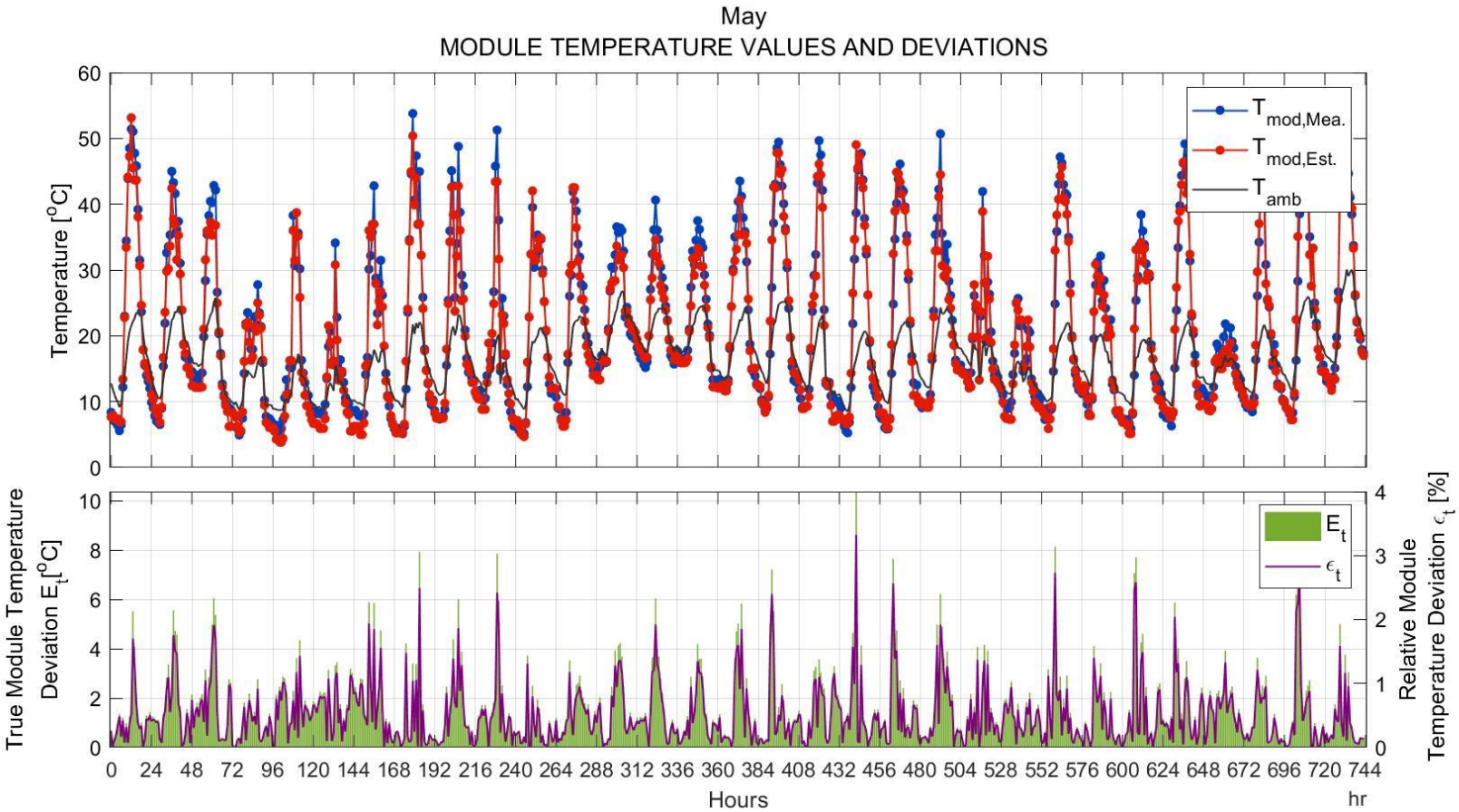

Figure A. 14: Estimated and measured module temperature, ambient, dew point and sky temperatures (Graph 1), deviations of estimated module temperature (Graph 2) for May

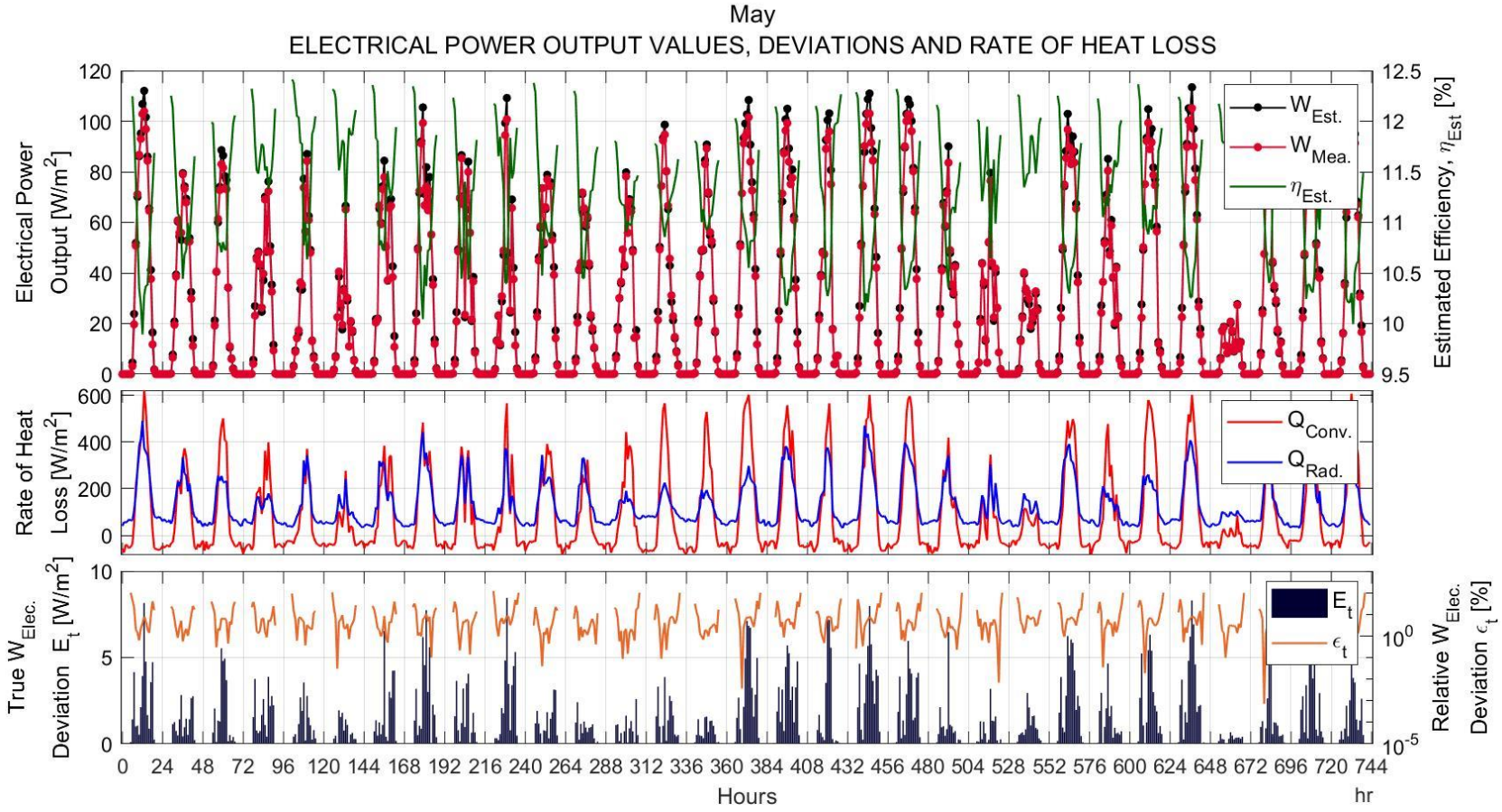

Figure A. 15: Estimated and measured module electrical power output and estimated efficiency (Graph 1), rate of convective and radiative heat transfer (Graph 2), deviations of estimated module electrical power output (Graph 3) for May

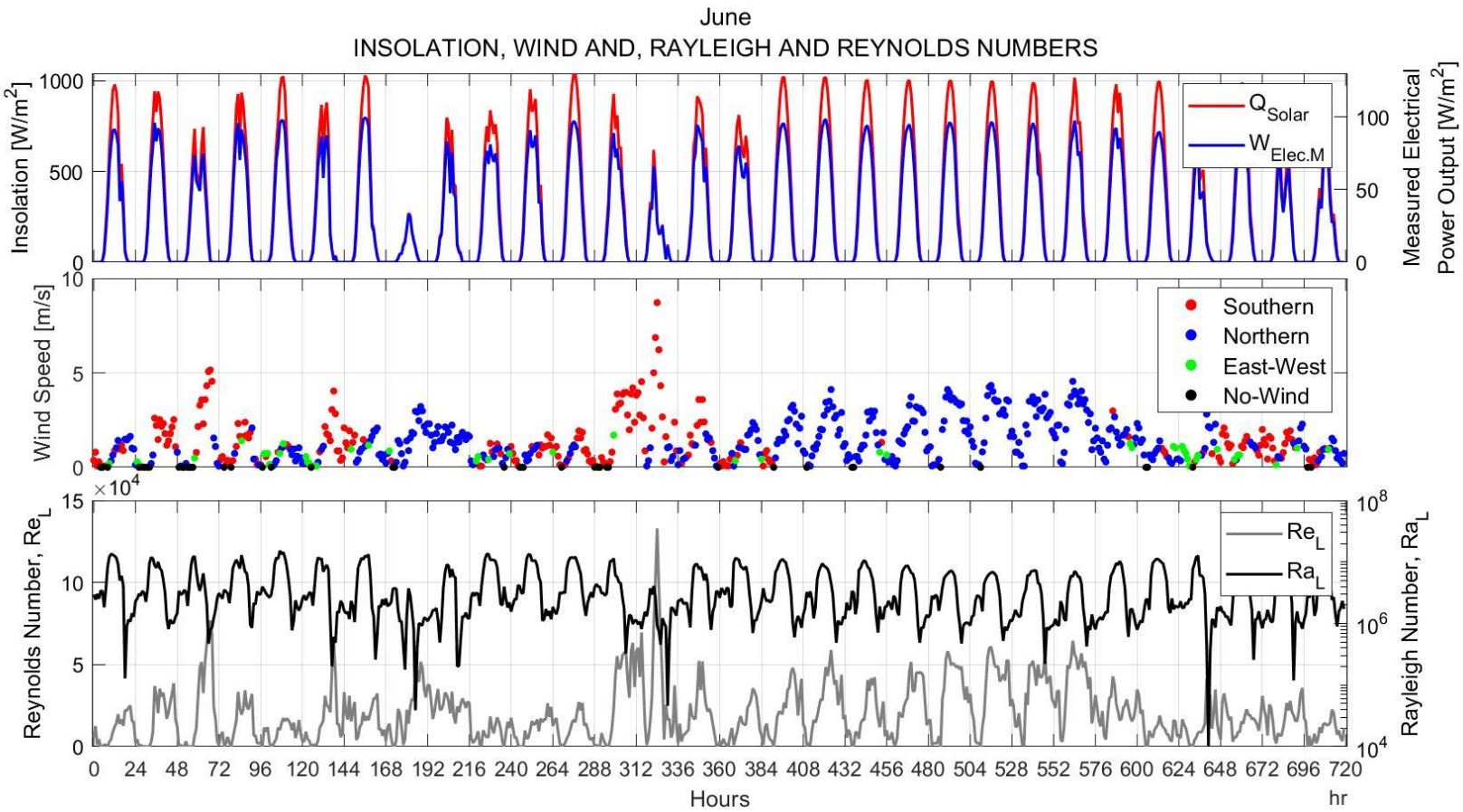

Figure A. 16: Solar irradiation and measured module electrical power output (Graph 1), wind speed and direction (Graph 2), Rayleigh and Reynolds numbers (Graph 3) for June

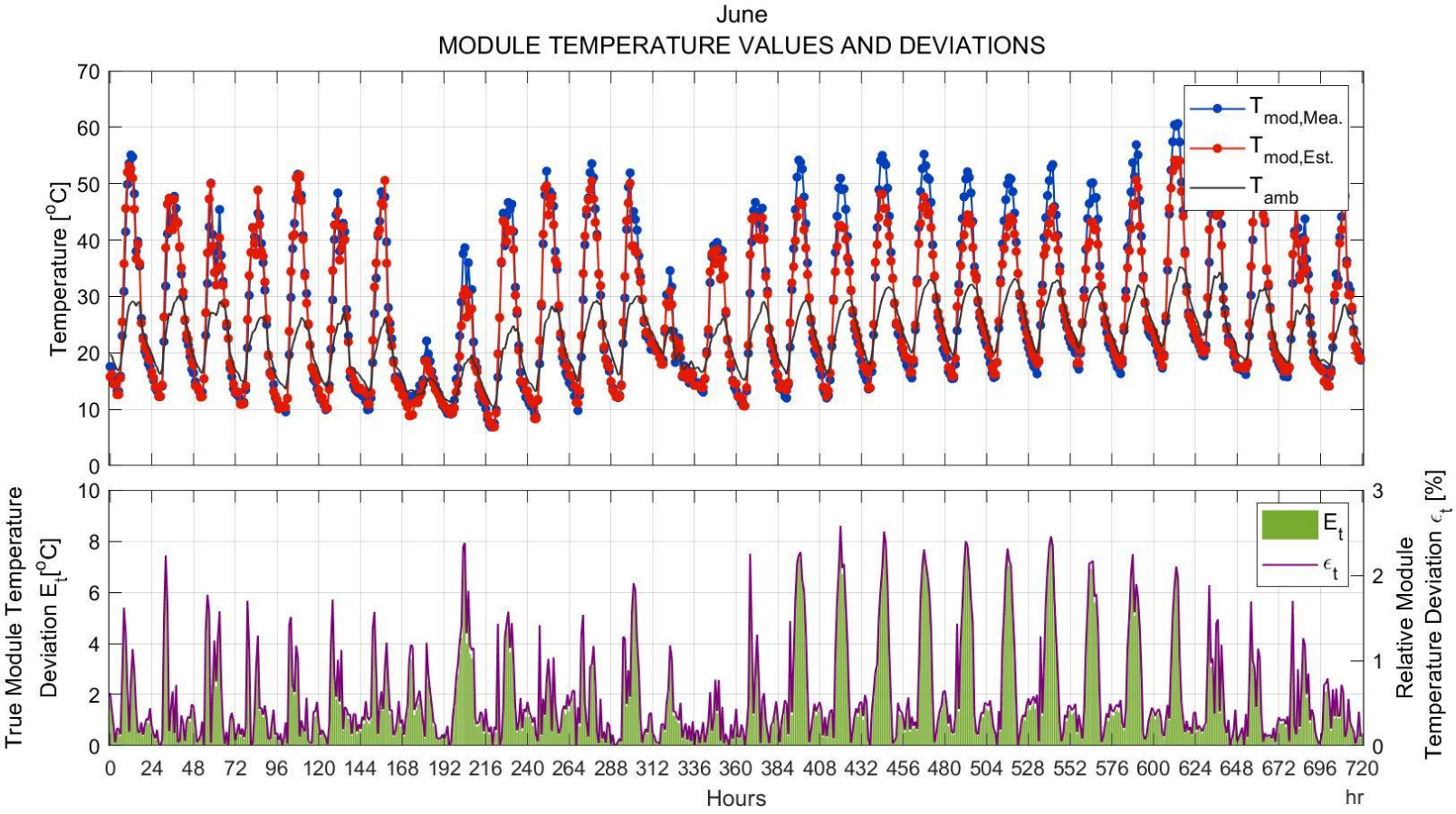

Figure A. 17: Estimated and measured module temperature, ambient, dew point and sky temperatures (Graph 1), deviations of estimated module temperature (Graph 2) for June

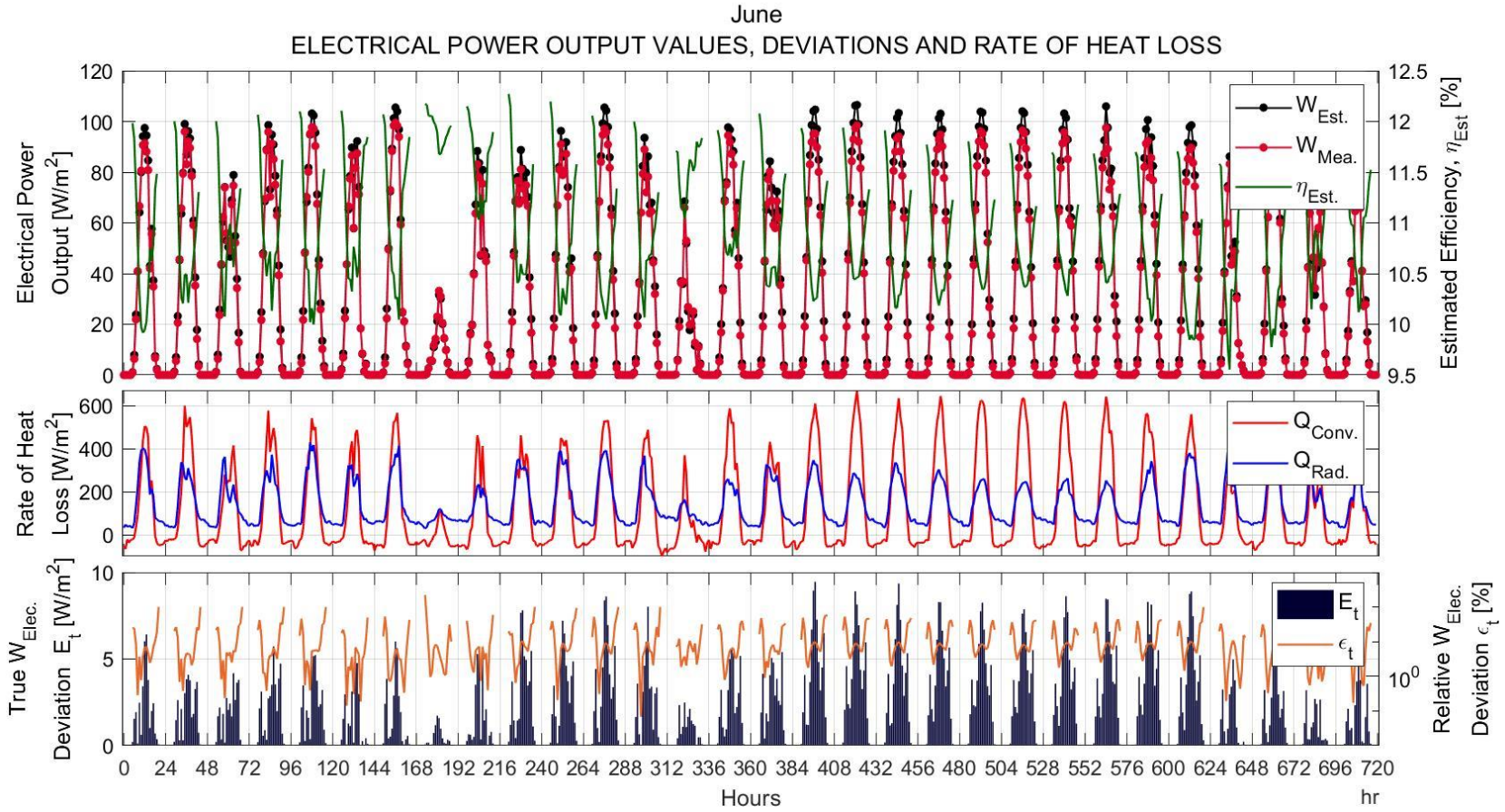

Figure A. 18: Estimated and measured module electrical power output and estimated efficiency (Graph 1), rate of convective and radiative heat transfer (Graph 2), deviations of estimated module electrical power output (Graph 3) for June

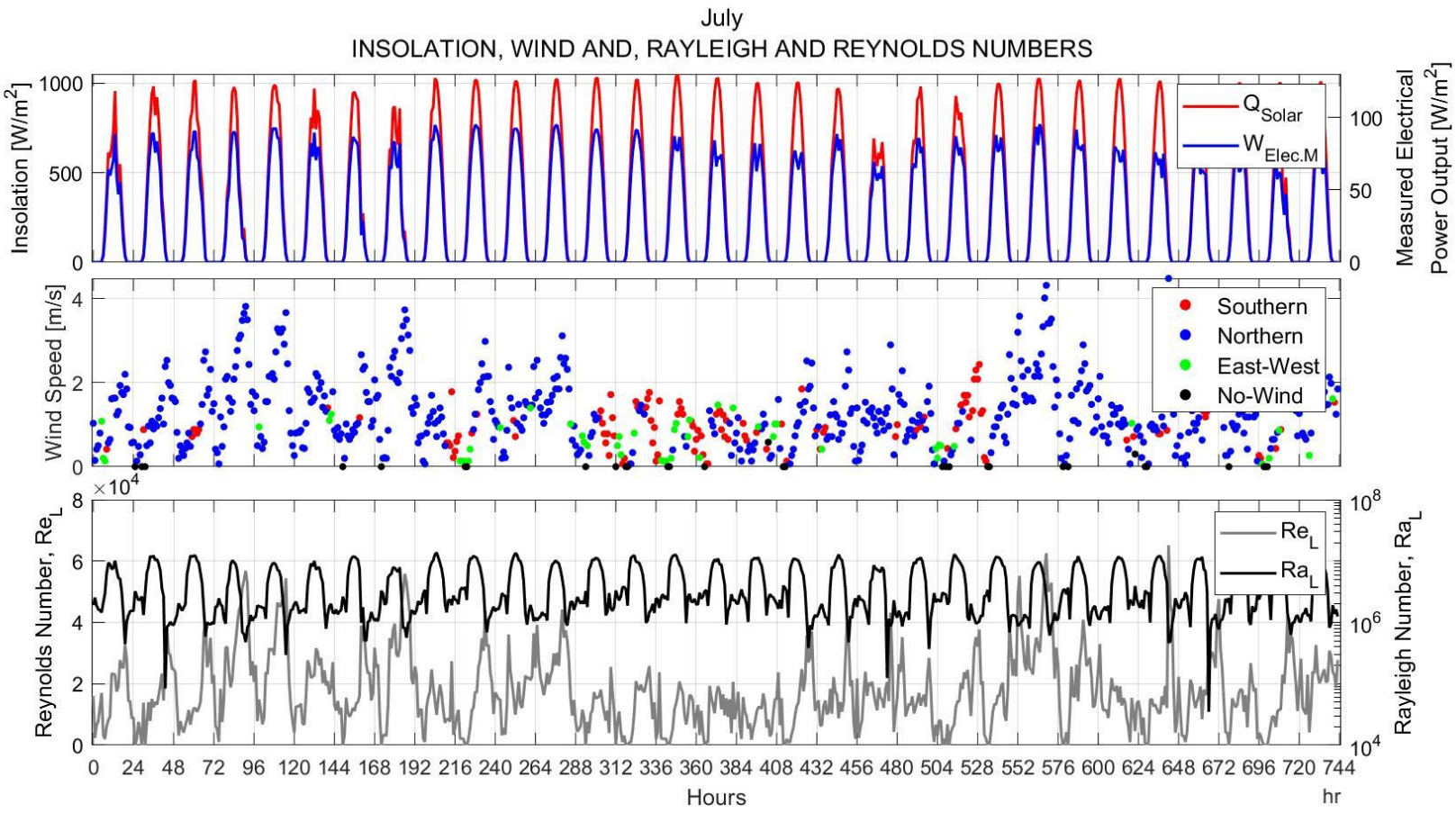

Figure A. 19: Solar irradiation and measured module electrical power output (Graph 1), wind speed and direction (Graph 2), Rayleigh and Reynolds numbers (Graph 3) for July

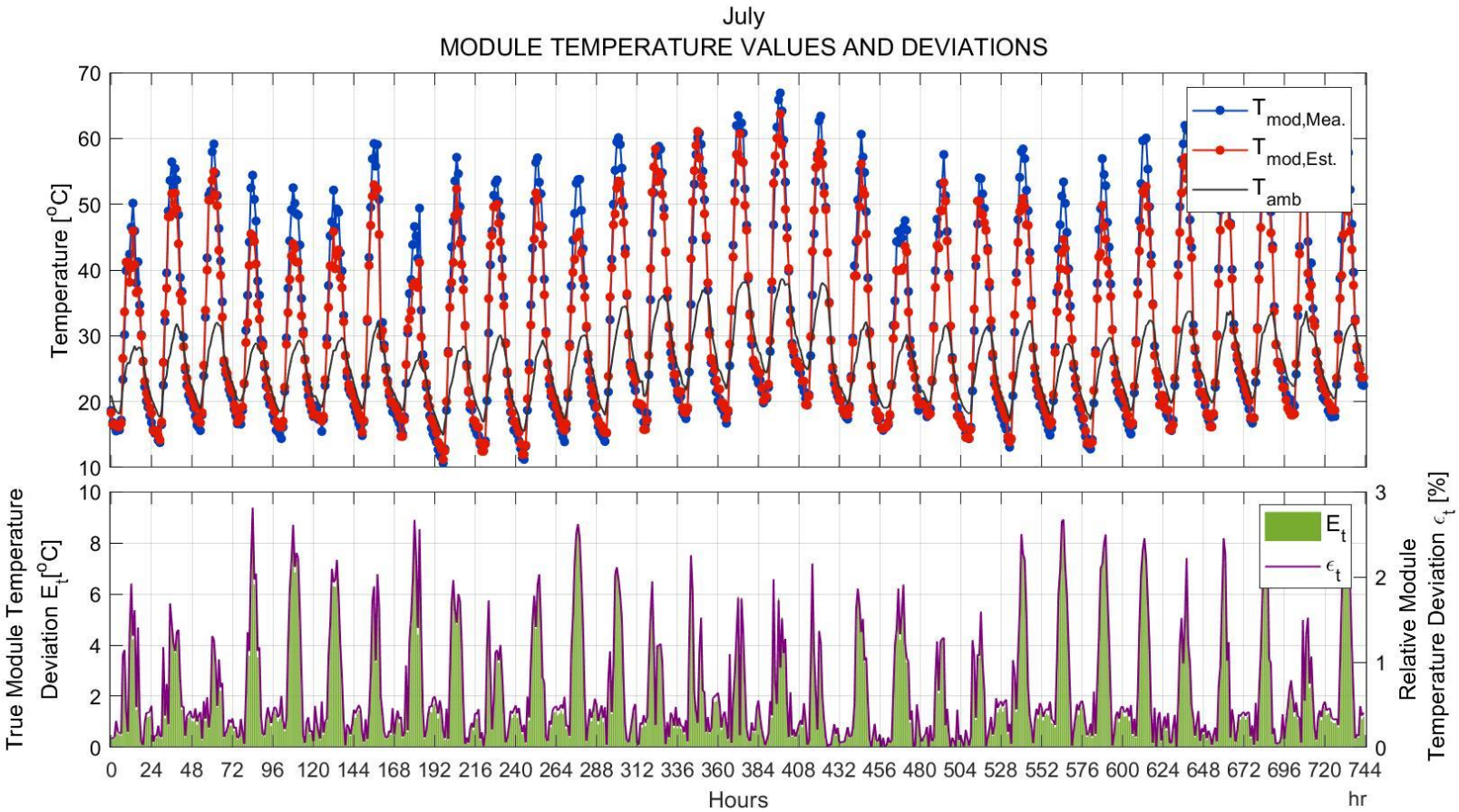

Figure A. 20: Estimated and measured module temperature, ambient, dew point and sky temperatures (Graph 1), deviations of estimated module temperature (Graph 2) for July

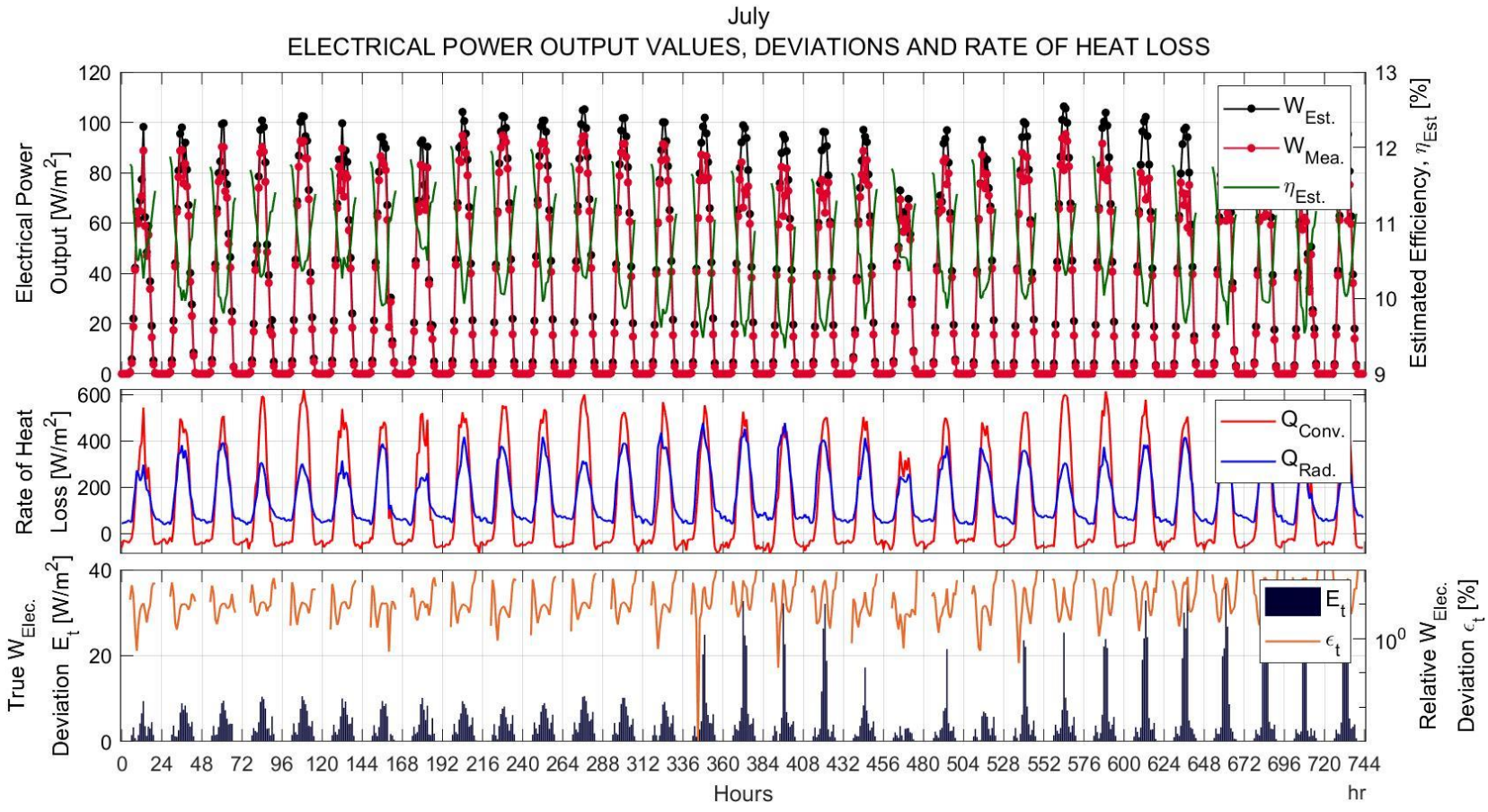

Figure A. 21: Estimated and measured module electrical power output and estimated efficiency (Graph 1), rate of convective and radiative heat transfer (Graph 2), deviations of estimated module electrical power output (Graph 3) for July

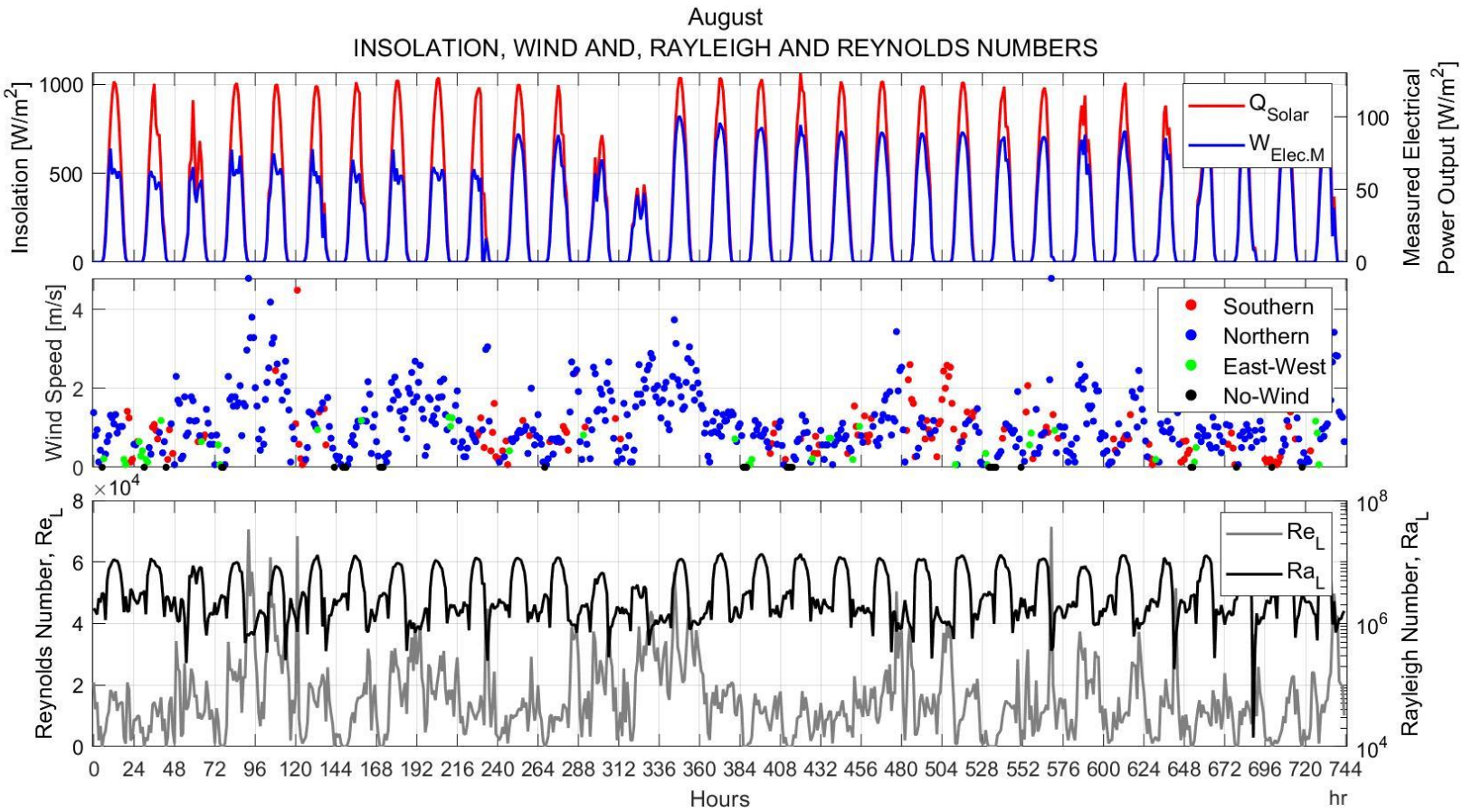

Figure A. 22: Solar irradiation and measured module electrical power output (Graph 1), wind speed and direction (Graph 2), Rayleigh and Reynolds numbers (Graph 3) for August

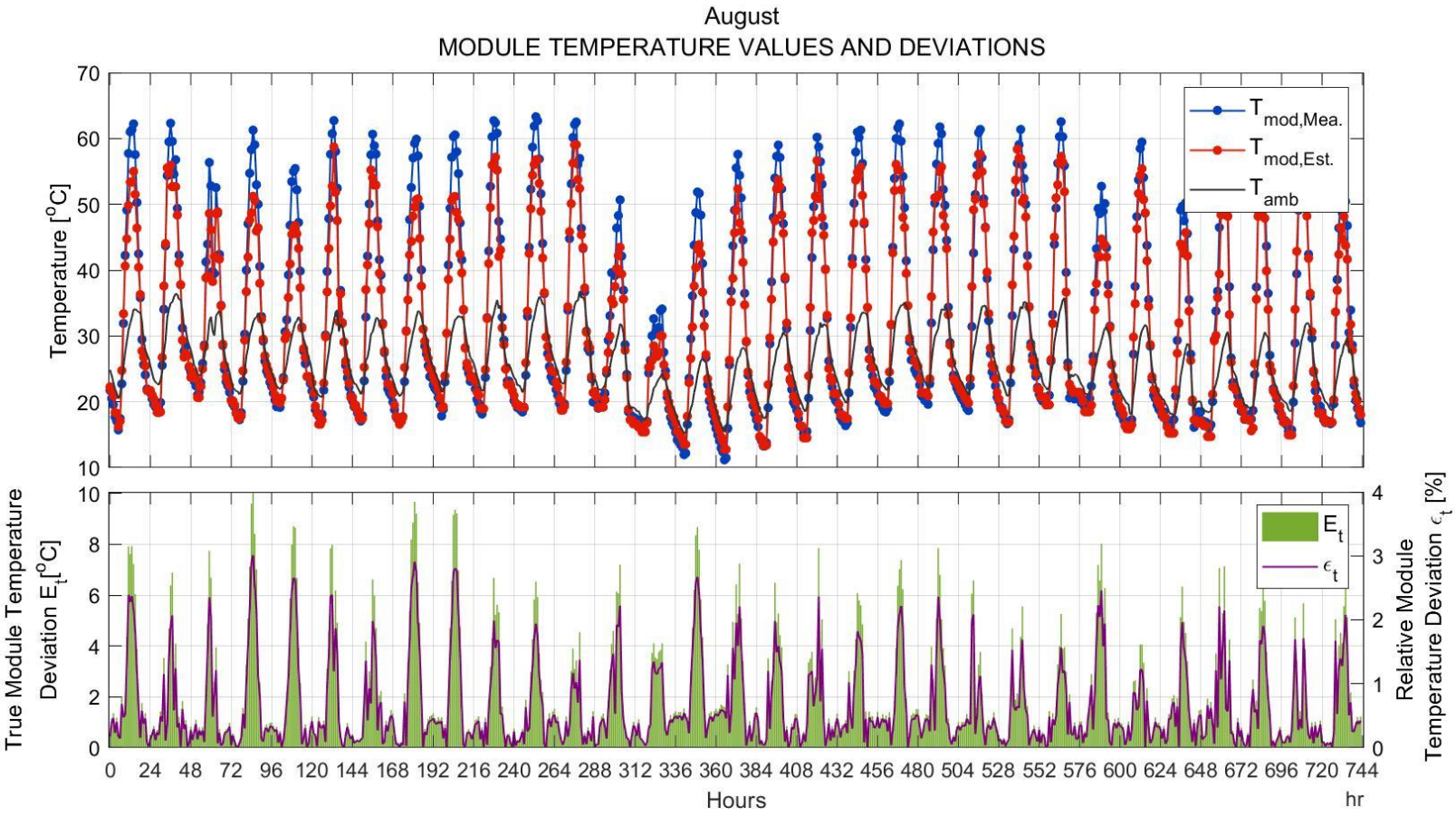

Figure A. 23: Estimated and measured module temperature, ambient, dew point and sky temperatures (Graph 1), deviations of estimated module temperature (Graph 2) for August

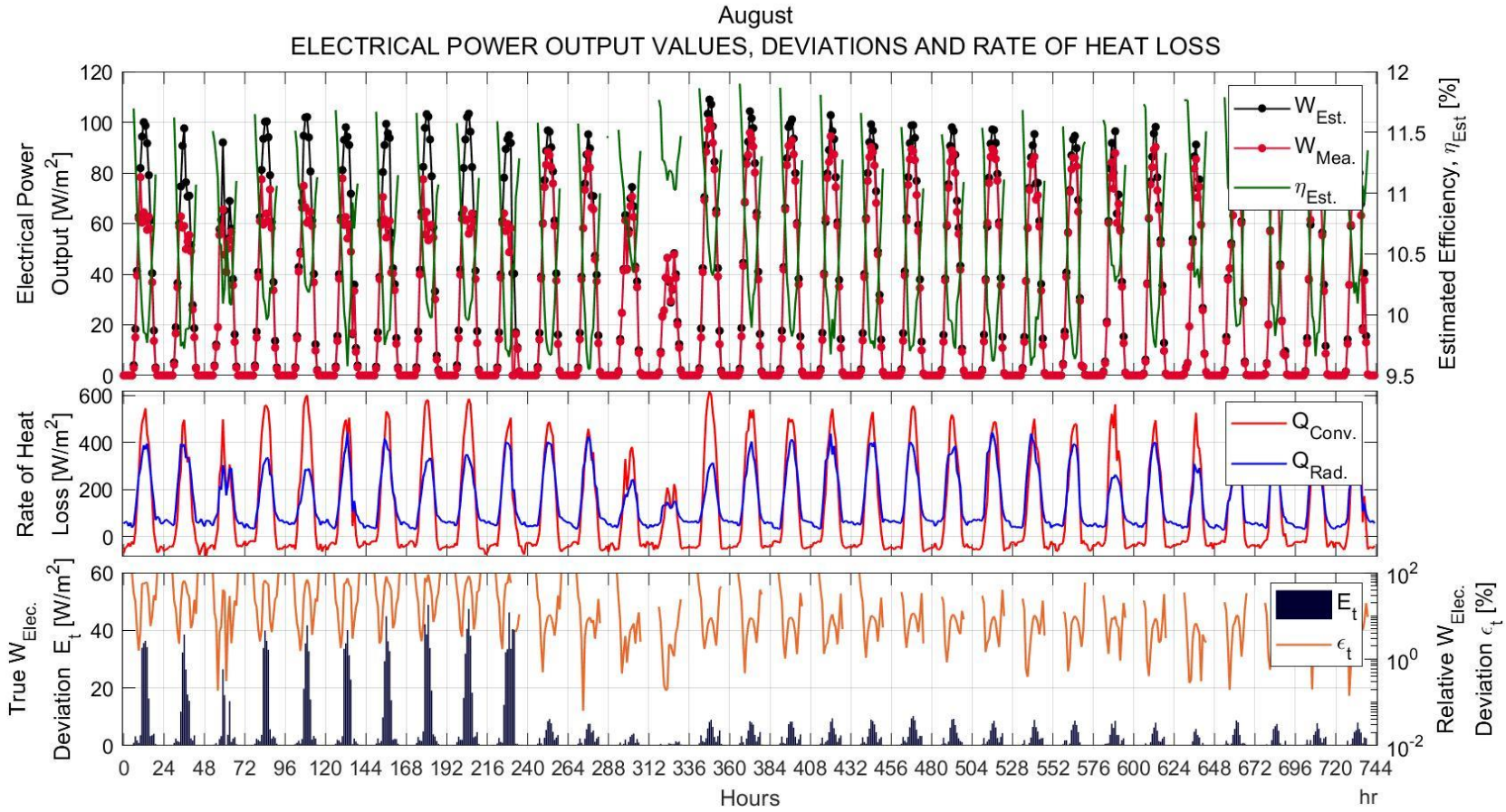

Figure A. 24: Estimated and measured module electrical power output and estimated efficiency (Graph 1), rate of convective and radiative heat transfer (Graph 2), deviations of estimated module electrical power output (Graph 3) for August

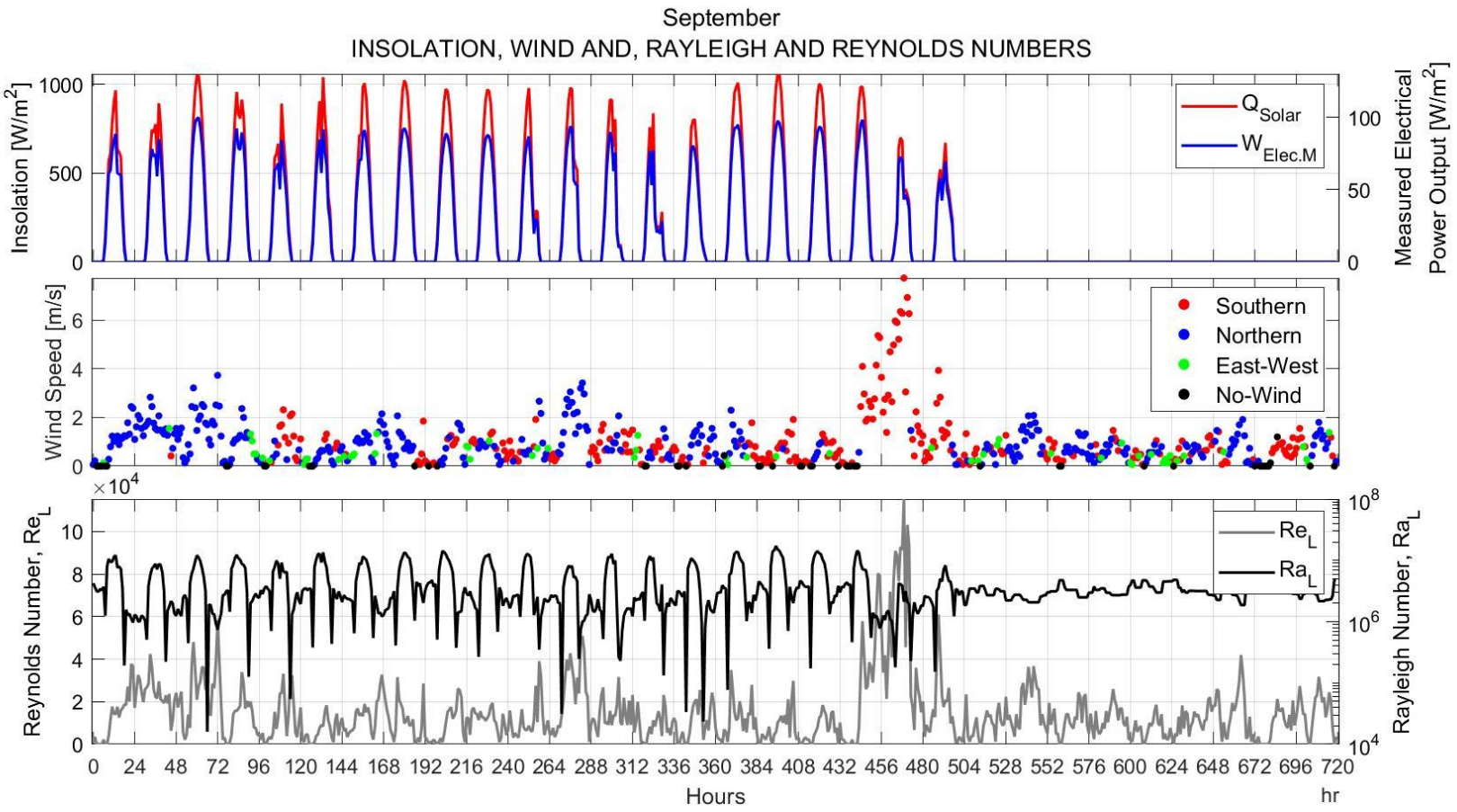

Figure A. 25: Solar irradiation and measured module electrical power output (Graph 1), wind speed and direction (Graph 2), Rayleigh and Reynolds numbers (Graph 3) for September

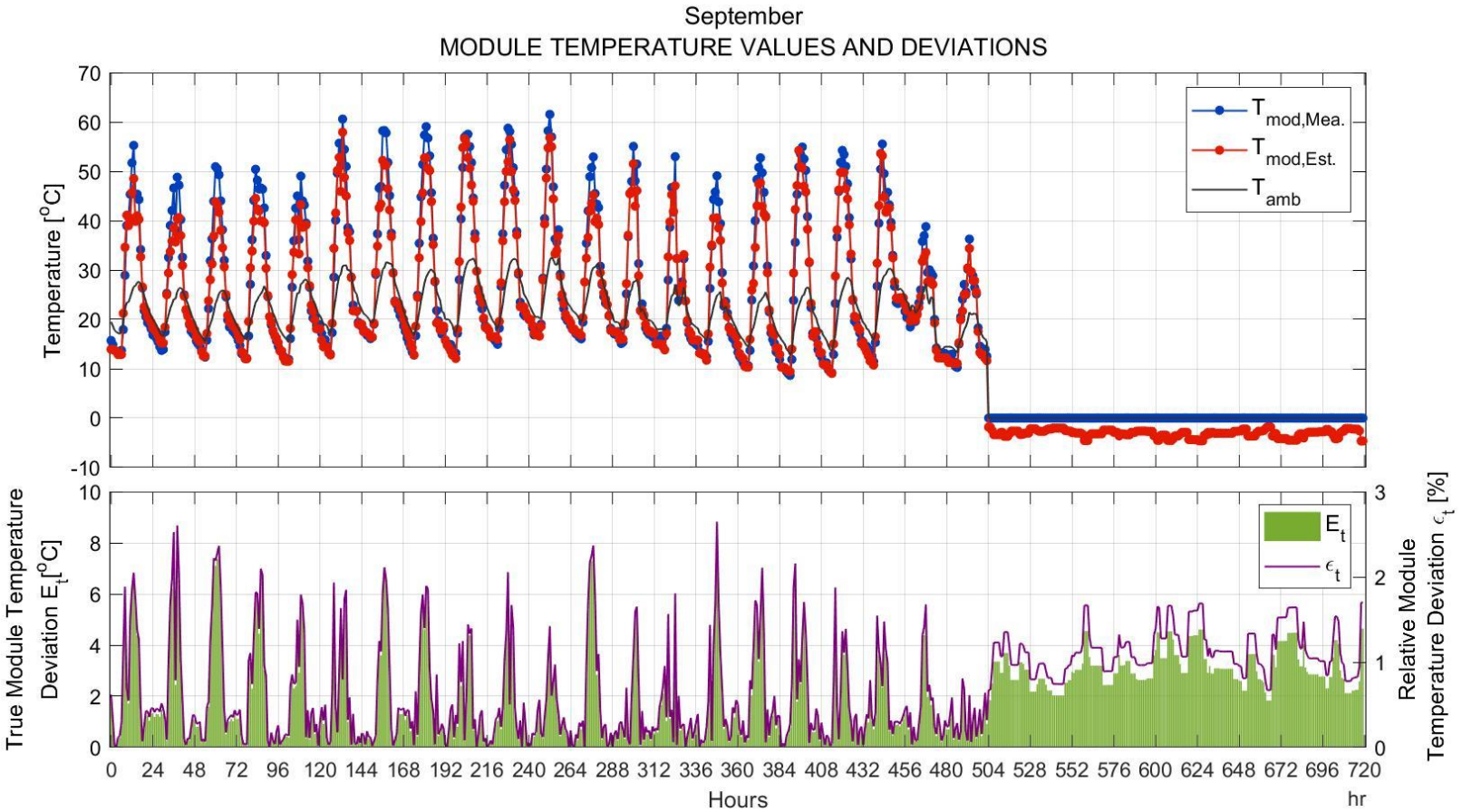

Figure A. 26: Estimated and measured module temperature, ambient, dew point and sky temperatures (Graph 1), deviations of estimated module temperature (Graph 2) for September

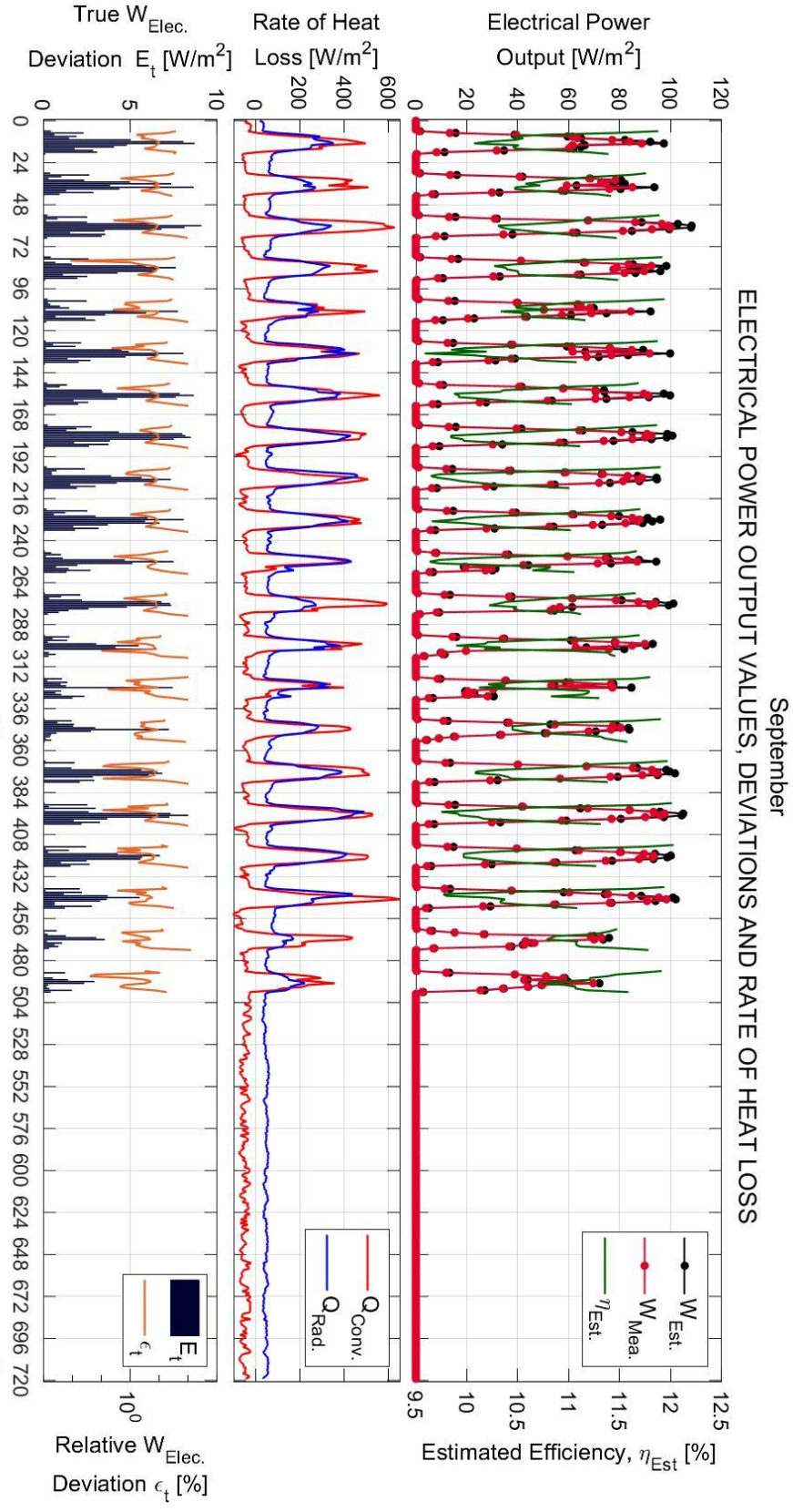

Figure A. 27: Estimated and measured module electrical power output and estimated efficiency (Graph 1), rate of convective and radiative heat transfer (Graph 2), deviations of estimated module electrical power output (Graph 3) for September

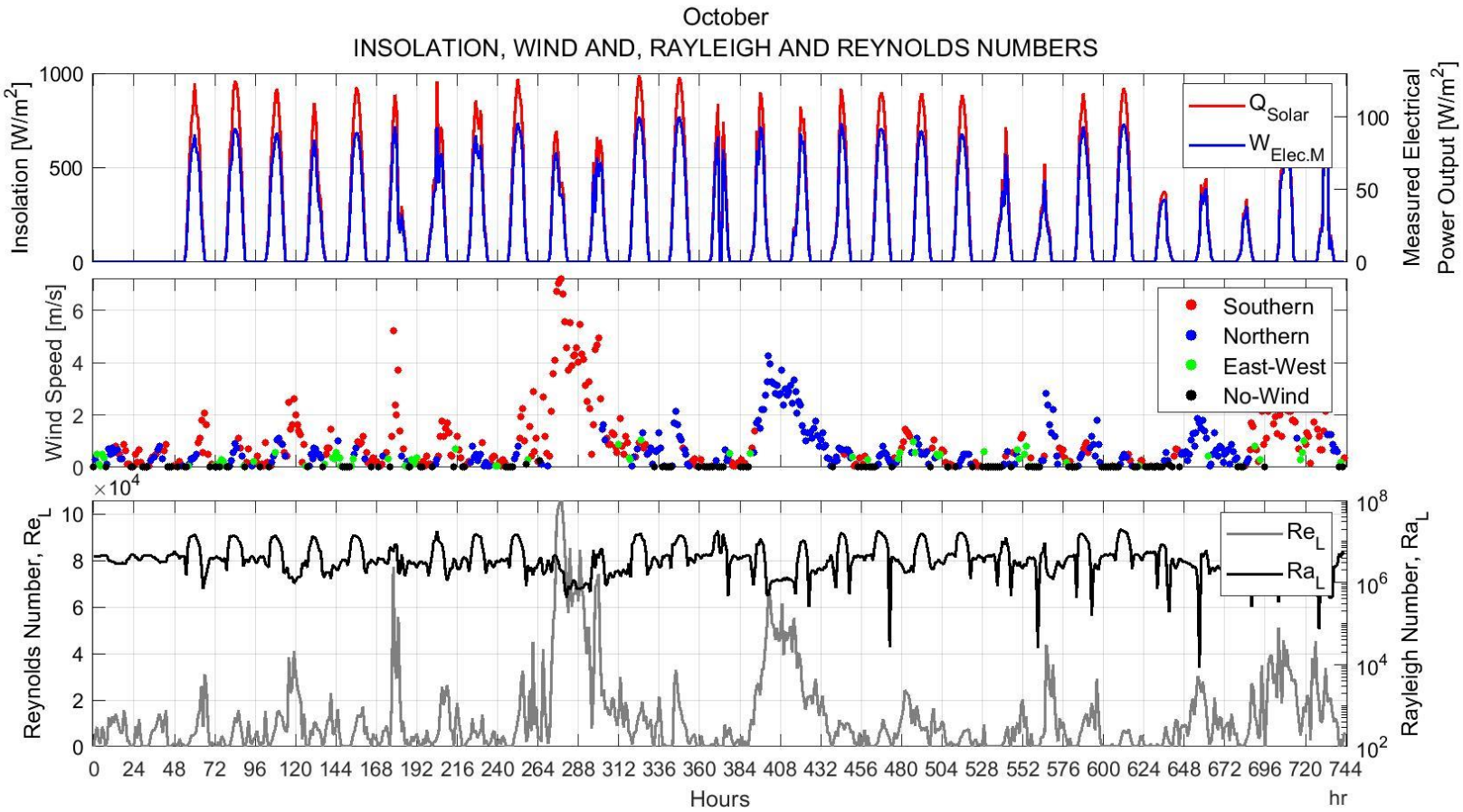

Figure A. 28: Solar irradiation and measured module electrical power output (Graph 1), wind speed and direction (Graph 2), Rayleigh and Reynolds numbers (Graph 3) for October

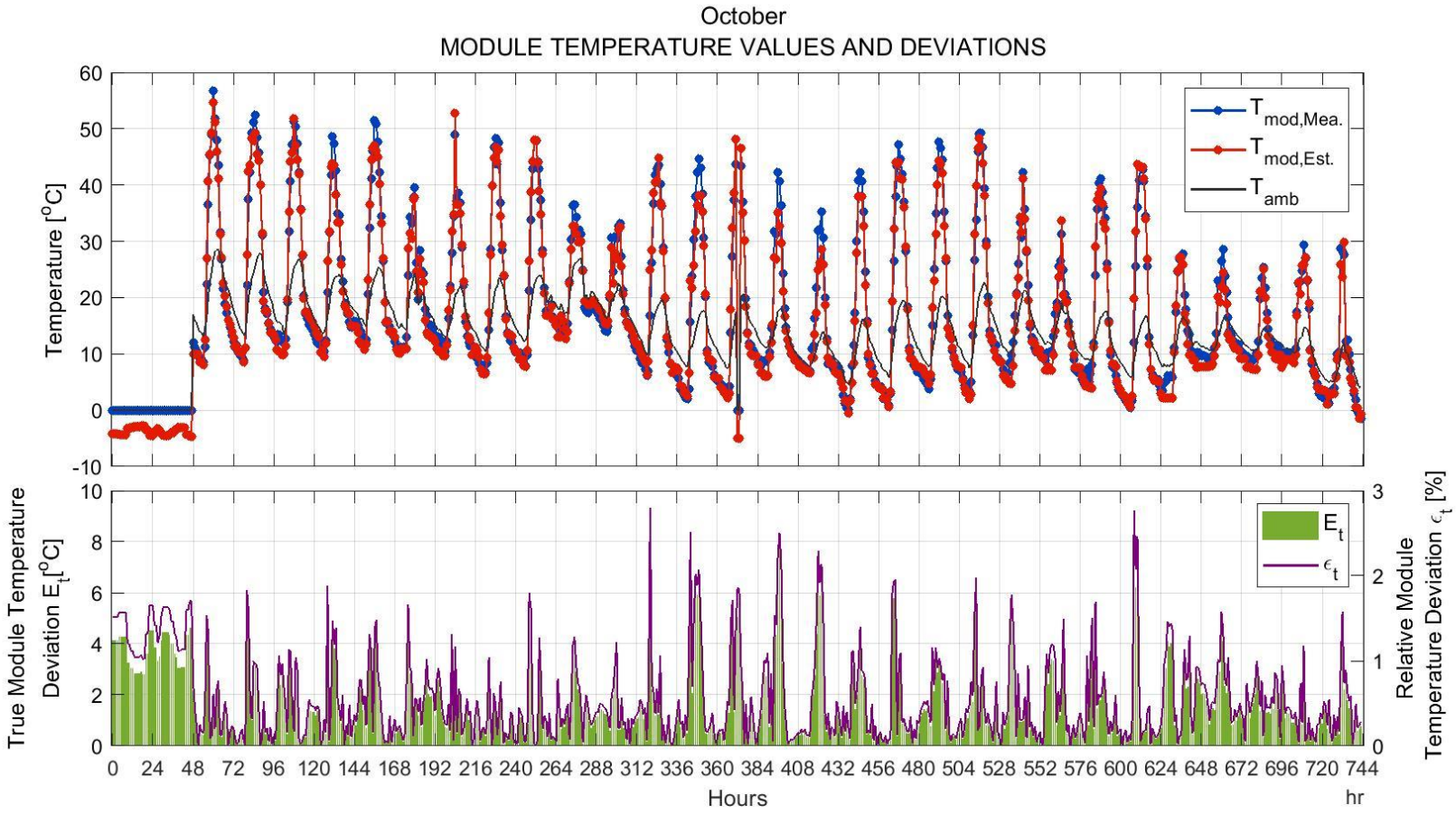

Figure A. 29: Estimated and measured module temperature, ambient, dew point and sky temperatures (Graph 1), deviations of estimated module temperature (Graph 2) for October

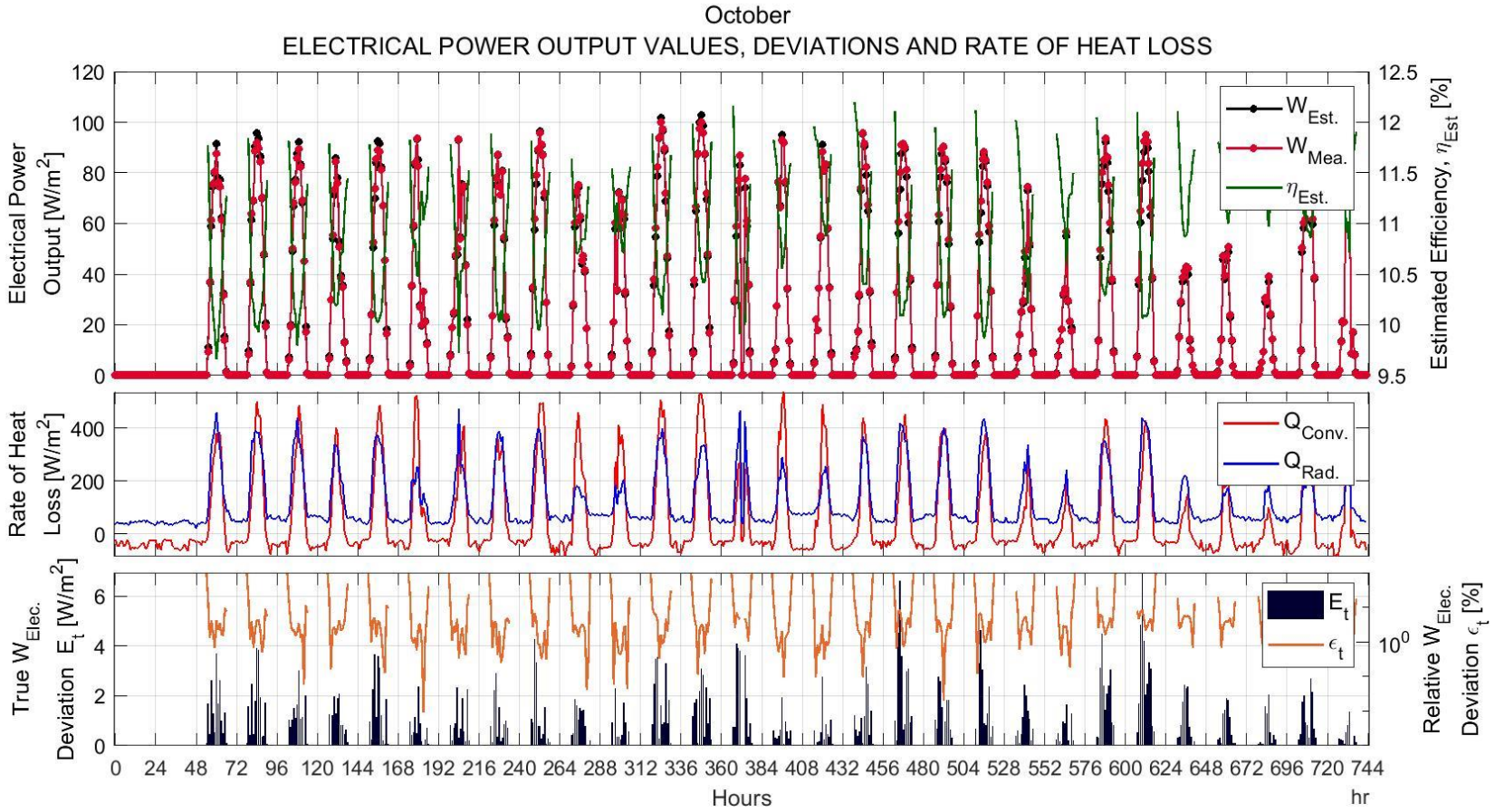

Figure A. 30: Estimated and measured module electrical power output and estimated efficiency (Graph 1), rate of convective and radiative heat transfer (Graph 2), deviations of estimated module electrical power output (Graph 3) for October

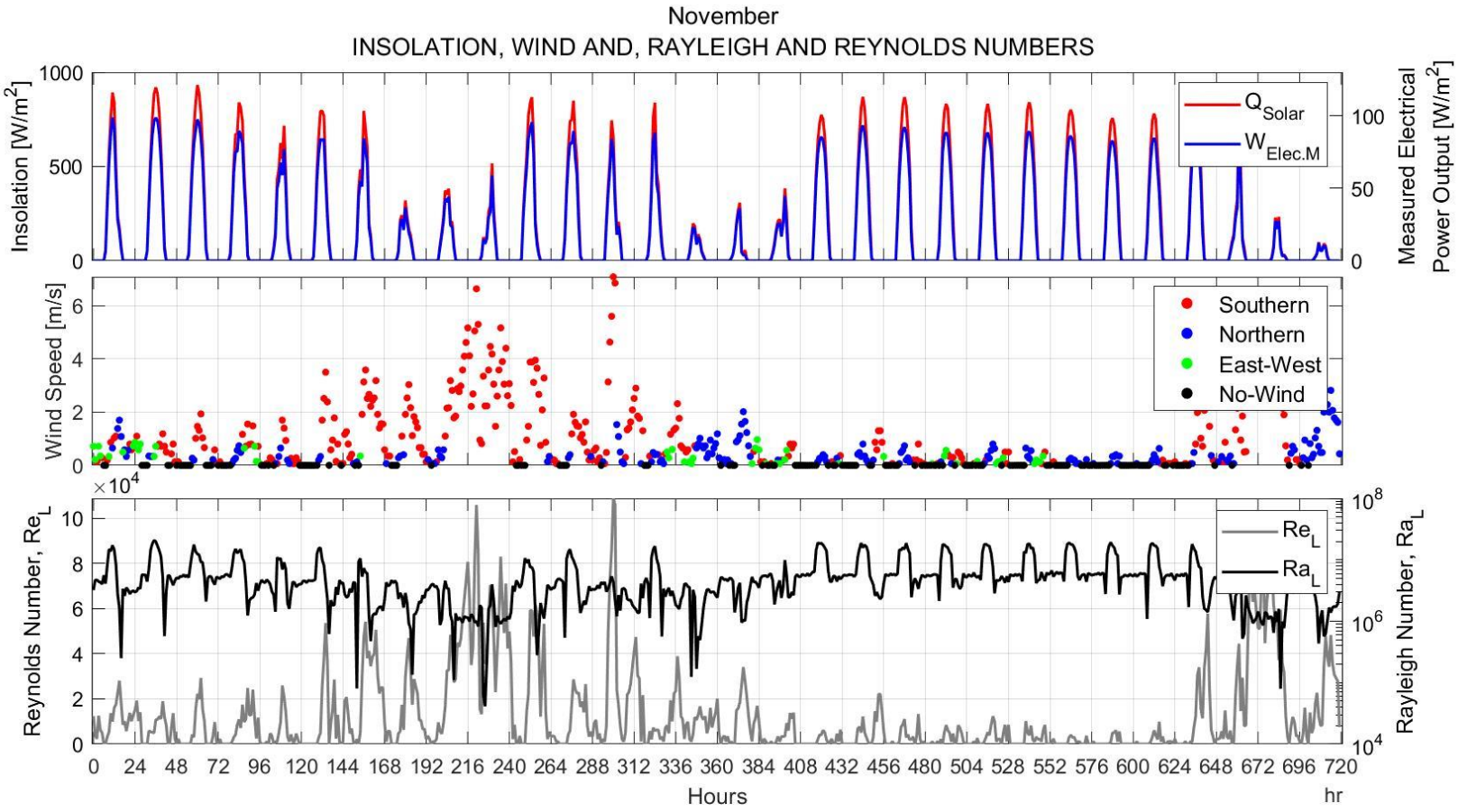

Figure A. 31: Solar irradiation and measured module electrical power output (Graph 1), wind speed and direction (Graph 2), Rayleigh and Reynolds numbers (Graph 3) for November

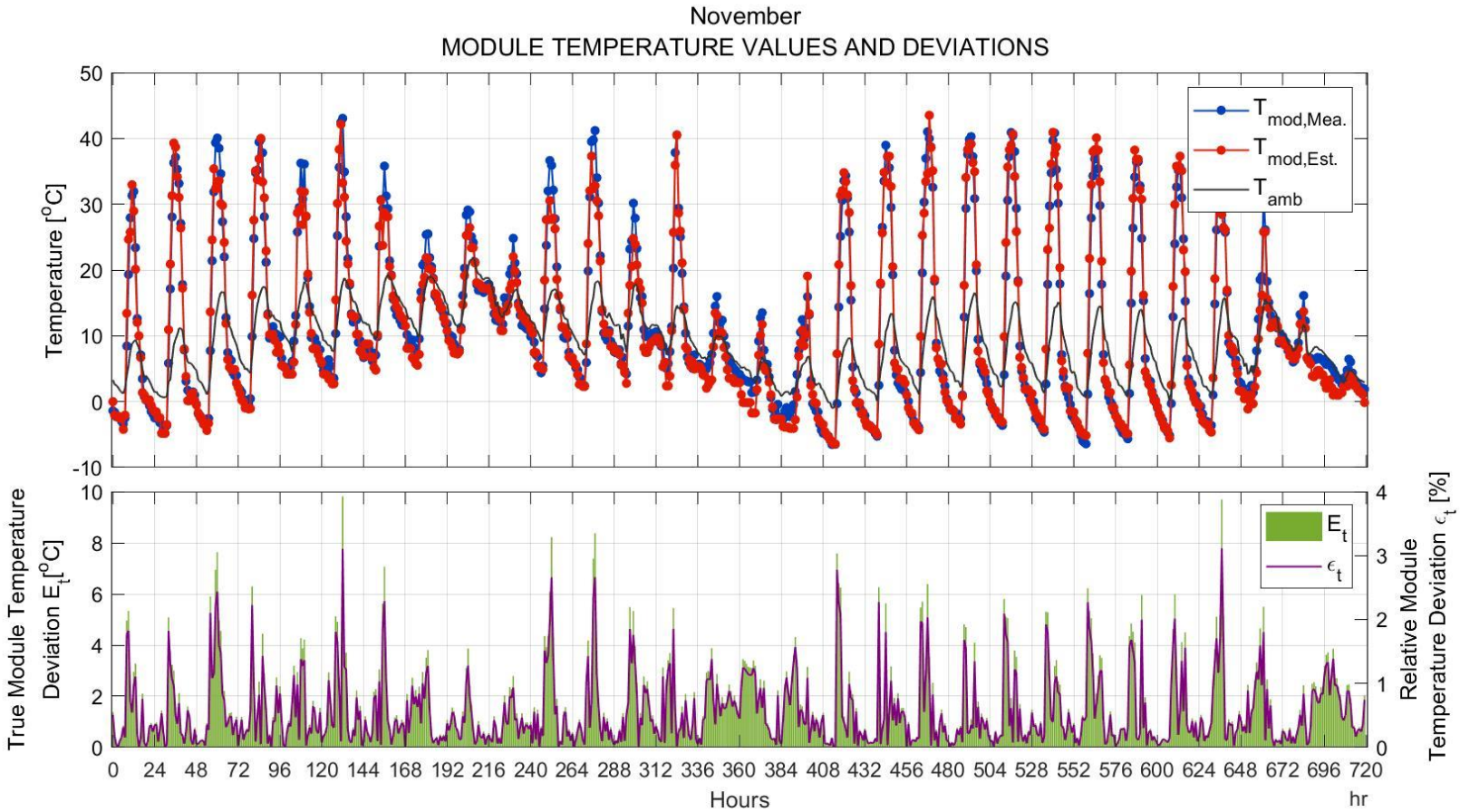

Figure A. 32: Estimated and measured module temperature, ambient, dew point and sky temperatures (Graph 1), deviations of estimated module temperature (Graph 2) for November

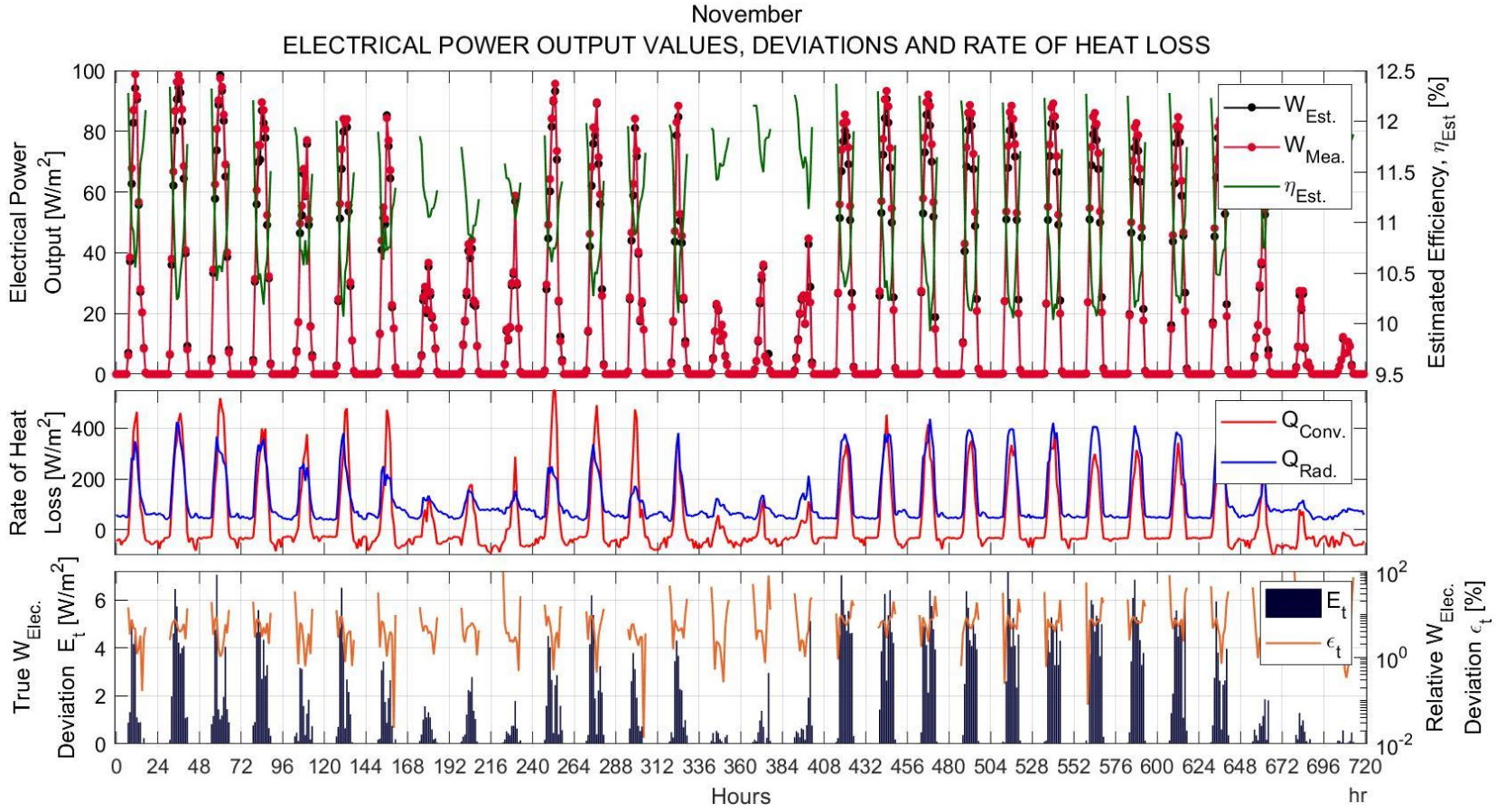

Figure A. 33: Estimated and measured module electrical power output and estimated efficiency (Graph 1), rate of convective and radiative heat transfer (Graph 2), deviations of estimated module electrical power output (Graph 3) for November

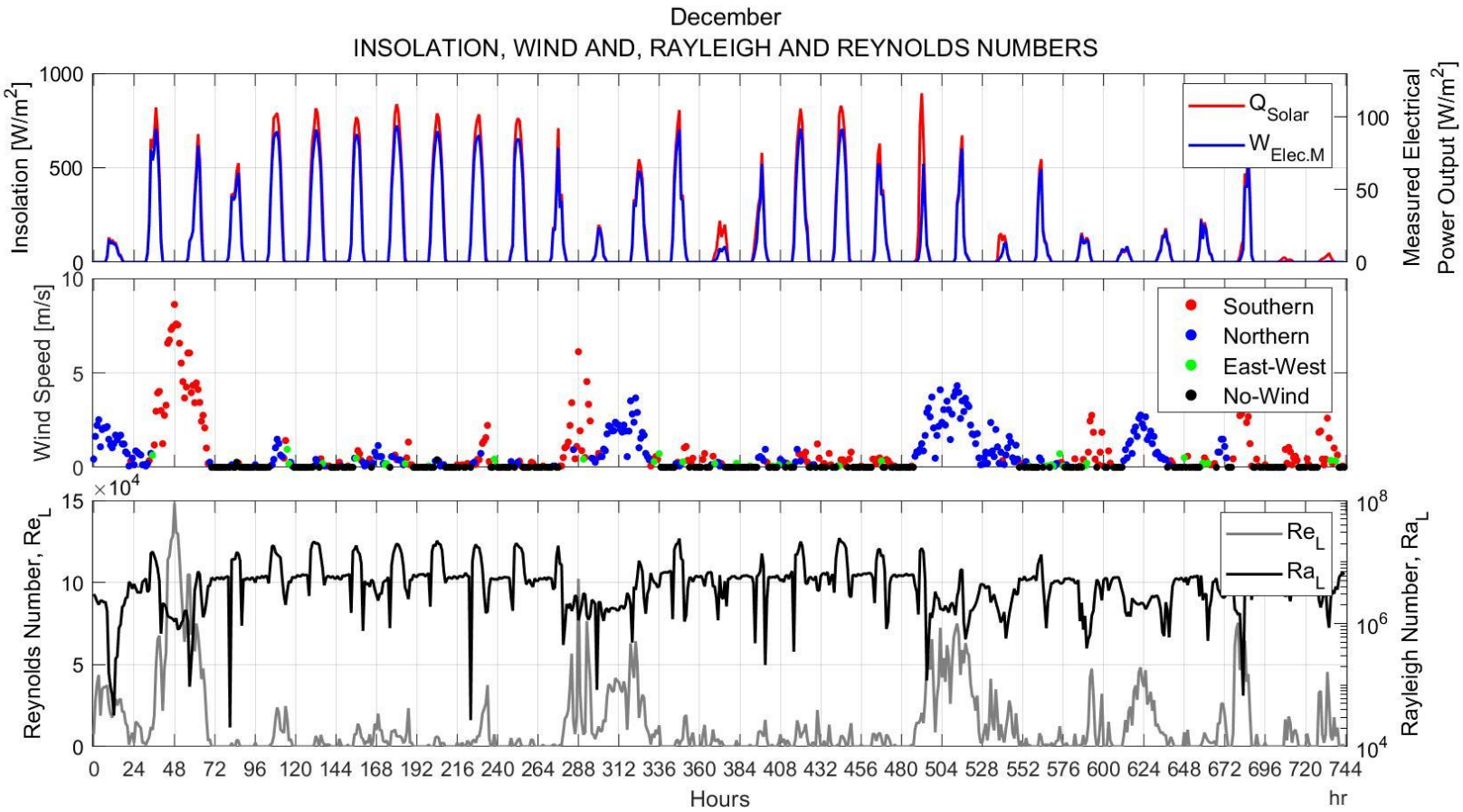

Figure A. 34: Solar irradiation and measured module electrical power output (Graph 1), wind speed and direction (Graph 2), Rayleigh and Reynolds numbers (Graph 3) for December

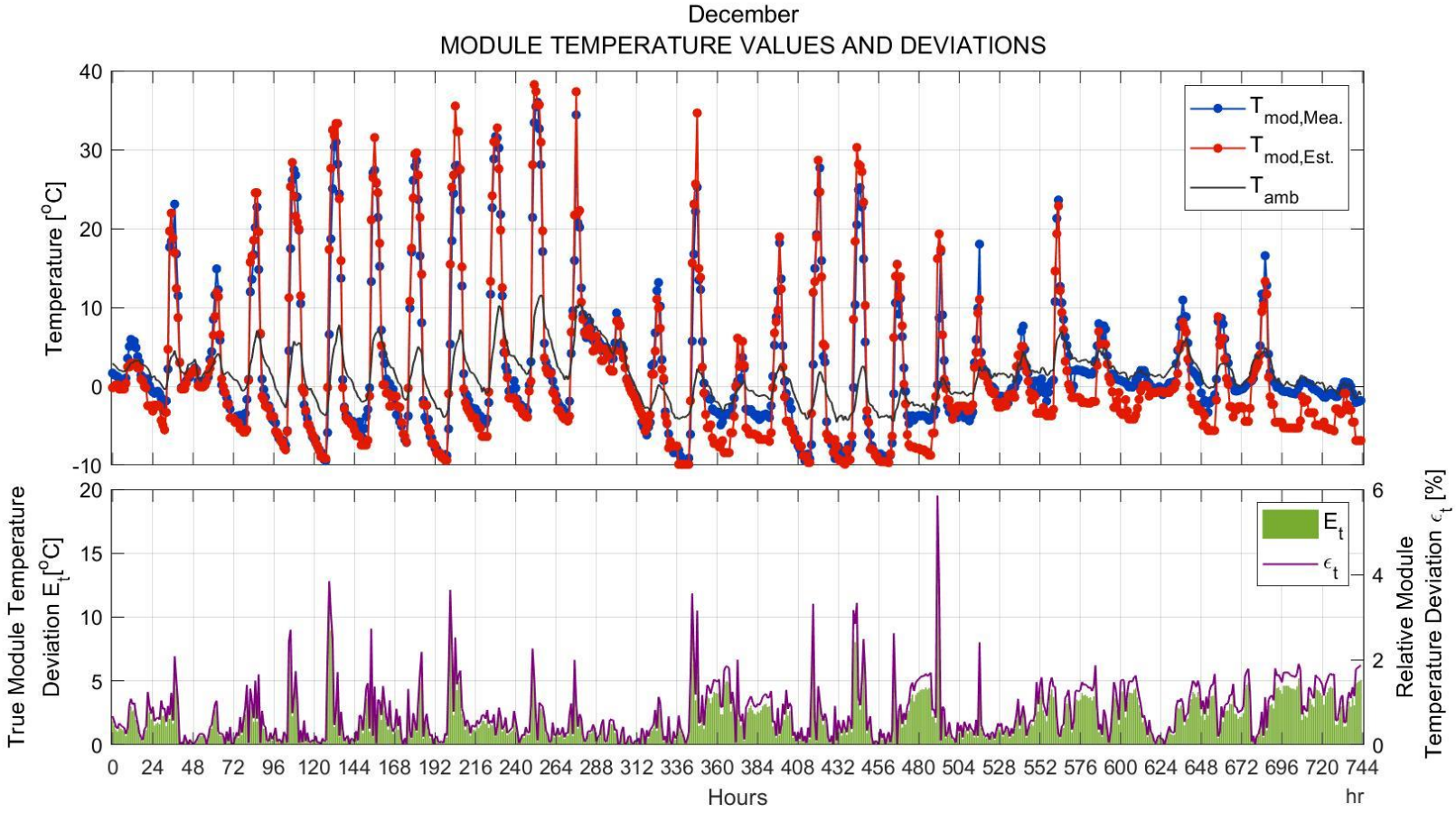

Figure A. 35: Estimated and measured module temperature, ambient, dew point and sky temperatures (Graph 1), deviations of estimated module temperature (Graph 2) for December

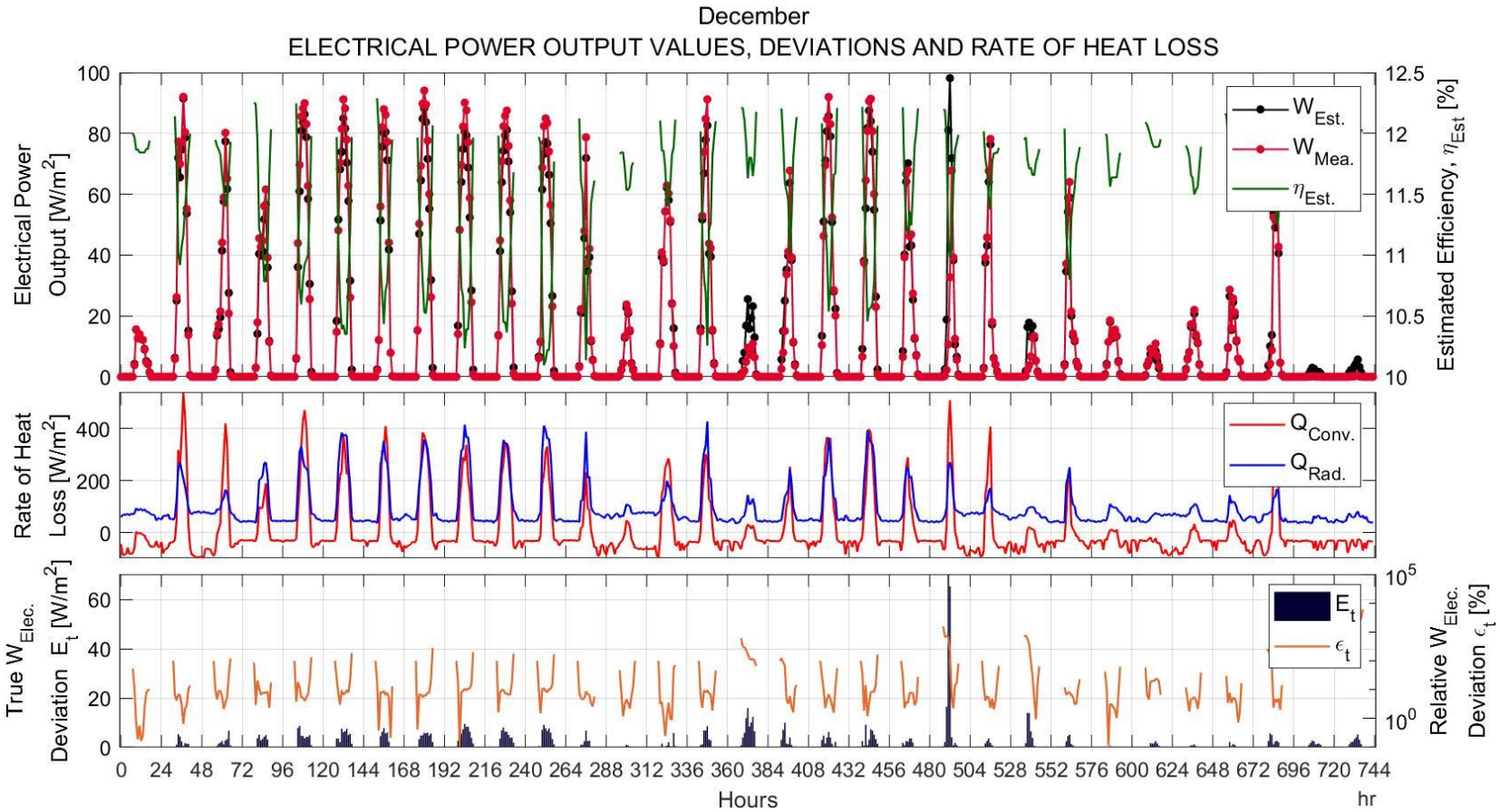

Figure A. 36: Estimated and measured module electrical power output and estimated efficiency (Graph 1), rate of convective and radiative heat transfer (Graph 2), deviations of estimated module electrical power output (Graph 3) for December